Ph.D. Dissertation

Modeling the Dissociation of Protonated Ions

Judit Sztáray

Supervisor:

László Drahos, Ph.D., Senior Research Scientist

Institute of Structural Chemistry, Chemical Research Center,

Hungarian Academy of Sciences

Chemistry Doctoral School

Head of the Doctoral School: *Prof. Dr. György Inzelt*

Theoretical and Physical Chemistry, Structural Chemistry Doctoral Programme

Head of the Doctoral Programme: *Prof. Dr. Péter Surján*

Eötvös Loránd University, Institute of Chemistry

Budapest, 2009

Acknowledgements

To ***Dr. László Drahos***, my advisor for his help in my research throughout this long journey.

To ***Dr. Károly Vékey,*** for the opportunity to do my doctoral research in the Institute of Structural Chemistry, Chemical Research Center, Hungarian Academy of Sciences and for the many excellent ideas over the many years working with him.

To ***Kálmán Újszászy***, who introduced me to and got me passionate about mass spectrometry and gave support and advice whenever I needed to turn to a friend.

To ***Prof. Dr. György Inzelt***, the head of the Chemistry Doctoral School, and to ***Prof. Dr. Péter Surján***, the head of the Doctoral Program.

To my family for their endless support and patience.

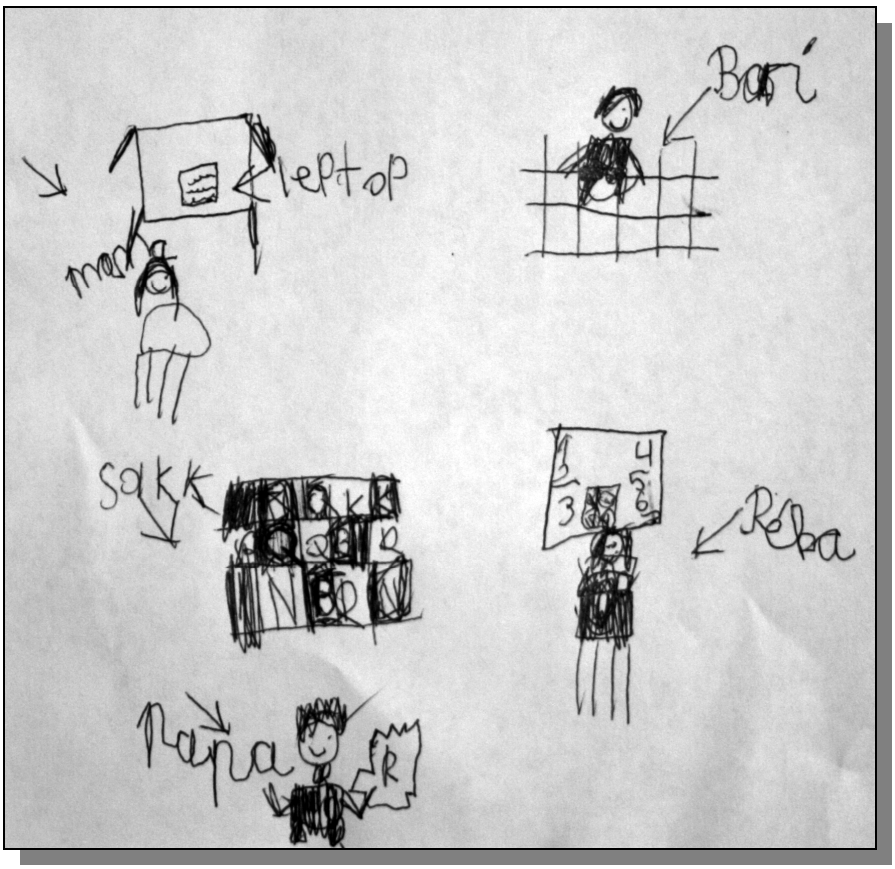

Table of Contents

List of Abbreviations

A – pre-exponential factor

AE – appearance energy

BD(E) – breakdown curve: fraction of the fragment ion's abundance

BIRD – blackbody infrared-radiative dissociation

CID – collision-induced dissociation

DOF – degrees of freedom

$E^{\#}$ – excess energy

E_a – activation energy

E_{coll} – collision energy

E_0 – critical energy

E_{int} – internal energy

ε_t – translational energy

EI – electron ionization

ESI – electrospray ionization

FAB – fast atom bombardment

FFR – field free region

FHBT – finite heat bath theory

FT-ICR – Fourier transform ion cyclotron resonance

$\Delta G^{\#}$ – Gibbs free energy of activation

Γ – Euler's gamma function

h – Planck constant

$\Delta H^{\ddagger}$ – enthalpy of activation

$\Delta_r H$ – reaction enthalpy

ICR – ion cyclotron resonance

IE – internal energy

IED – internal energy distribution

IRMPD – infrared multiphoton dissociation

k – rate constant

k_B – Boltzmann's constant

KER – kinetic energy release

<KER> – mean kinetic energy release

KERD – kinetic energy release distribution

KERS – kinetic energy recovery system

KIE – kinetic isotope effect

[M] – reactant concentration

MIKES – mass analyzed ion kinetic energy spectroscopy

MS/MS – tandem mass spectrometer / tandem mass spectrometry

N – number of molecules

OTS/PST – orbiting transition state / phase space theory

$\boldsymbol{p}_i$ – momenta

PA – proton affinity

$P(E_{\text{int}})$ – internal energy distribution function

$P(E_{\text{therm}})$ – thermal energy distribution function

PST – phase space theory

$\varrho(E)$ – density of states

$\boldsymbol{q}_i$ – positions

QQQ – triple quadrupole (mass spectrometer)

QET – quasi equilibrium theory

R – universal gas constant

REX – rapid energy exchange limit

RRK – Rice-Ramsperger-Kassel reaction rate theory

RRKM – Rice-Ramsperger-Kassel-Marcus reaction rate theory

$\Delta S^{\#}$ – entropy of activation

SID – surface induced dissociation

SY – survival yield

T – temperature

T_{char} – characteristic temperature

T_{eff} – effective temperature

TCID – threshold collision-induced dissociation

TPEPICO – threshold photoelectron photoion coincidence

TS – transition state

ν – frequency factor

ν_i – vibrational frequencies

ZPE – zero point energy

1. Introduction and Aims

Mass spectrometry is one of the most important analytical and structural research methods [1]. The constantly emerging, more and more versatile ionization, analysis and detection methods [2-4], along with considerable advances in the data analysis techniques allowed mass spectrometry to shift towards biochemistry and molecular biology [5-9]. While opening new horizons in bioanalytical chemistry and proteomics, mass spectrometry also retained its fundamental role in ion chemistry research [10-12]. By measuring ionization and appearance energies one can utilize mass spectrometry to derive thermochemical data for a wide array of systems [11, 13-15].

High-throughput mass spectrometry methods are limited by the inability to automate the interpretation of the recorded spectra [16-19]. The first step towards the automatization is a better understanding what is happening inside the mass spectrometer, such as the ionization and fragmentation processes, which requires intensive research on these fundamental processes. This can only be accomplished without a joint effort using both experiments and accurate modelings. In the past few years, a complex computational model was developed and programmed in the Mass Spectrometry Department of the Hungarian Academy of Sciences to describe the kinetic processes occurring in the mass spectrometer. The software based on the model (MassKinetics, http://www.chemres.hu/ms/masskinetics) is a useful tool for predicting the mass spectra from fundamental molecular and experimental parameters (e.g. vibrational frequencies, energetic data, experimental geometry, etc) [20].

The goals of my graduate research were (1) to gain a better understanding of the fundamental properties of dissociating ions, i.e. the initial state of the molecular ions, such as initial internal energy, effective temperature and also to be able to describe the processes through which these properties change. The ability to fully know and understand the details of these processes allows an accurate theoretical determination of basic features, such as reaction rates, ion internal energy distributions and ion intensities; (2) to model interesting features, like kinetic energy release (KER) and the kinetic isotope effect (KIE) of a few systems, such as protonated dimers and solvent clusters in order to get a better handle on these processes, as well; and (3) working on these fundamental problems and models systems, my goal was to test and further develop the MassKinetics program.

The studied systems can be categorized into four groups: a) the dissociations of protonated alkylamines were modeled and the internal energy distributions were determined in two different experimental conditions. The results helped to understand what effects the experimental conditions have on the results, namely the high-pressure and the low-pressure ion source, and to

study the theoretical aspects of kinetic energy release and the kinetic isotope effect.. b) Protonated benzylpyridines and protonated aromatic benzoic esters are often used to determine the energy profile of the mass spectrometer. That is why we chose to study these molecules to have a more thorough understanding of their dissociation. These molecules were also used to study the dependence of internal energy distribution on the instrumental parameters (e.g. cone voltage). c) Protonated methanol clusters proved to be a challenge due to their size and the unconventional, low-temperature experimental conditions; the kinetic energy release of these dissociations was modeled in order to get an insight into the mechanisms of these fragmentation processes. d) Finally, the most commonly used protonated oligopeptide, leucine enkephalin was investigated. Although several publications can be found about the dissociation parameters of the most studied fragmentation pathway, which produces the $\mathbf{b_4}^+$ ion; however, these literature data carry rather large uncertainties. Our aim was to use modeling to understand the reasons behind these deviations and to determine an overall Arrhenius dissociation parameter set with an acceptable error range.

Overall, my results show that with the knowledge of a few basic parameters and the experimental setup, the fate of the ions can be modeled and accurate ion intensities as well as other features of their dissociation can be predicted. These results bring the possibility of the automatic evaluation of any mass spectra into the near future.

I would like to emphasize that the experimental work that forms the basis of the theoretical modeling was done in various collaborations, while the modeling of the experimental results is the principal theme of my graduate research. Therefore, the Ph.D. thesis is structured from the modeling point of view: after the introduction, the fundamentals of the ion dissociation processes will be discussed along with the relevant methods that were used in the analysis of the experimental results. The parameters needed for the modeling calculations are discussed in a separate chapter, along with a summary of the experimental conditions. A short summary of the experimental results for each system is presented in this chapter as well, to have a better understanding of the modeling data, as these represent another set of input parameters for the modeling calculations. Since the emphasis of the work was on the mass spectrometric ion processes rather than the actual systems, the results are presented by the phenomena that was investigated, rather than by the individual systems. First, results on modeling the ion energy distributions at different stages of the dissociation processes of various model systems are discussed in detail. Second, results on modeling the kinetic energy release are presented for protonated alkylamine and protonated methanol cluster systems. In the third subchapter, results of the modeling calculation of kinetic isotope effect are presented for protonated alkylamine

systems. The results are concluded by a discussion of the re-evaluation of the previously published experimental data of protonated leucine enkephalin. For the most studied dissociation pathway of protonated leucine enkephalin, forming the $\mathbf{b}_4^+$ ion, the Arrhenius activation energy, the pre-exponential factor, the activation entropy, the Gibbs free energy as well as the critical energy could be determined with excellent accuracy and precision. The dissertation is concluded with a summary.

2. Mass Spectrometry – Experimental Techniques and Modeling Calculations

The ultimate goal of our modeling calculations is to accurately predict the mass spectra of a specific molecule. Although the evolution of the mass spectra is rather complex, it can be summarized in three main steps: 1. formation and/or excitation of the molecular ion in the gas phase; 2. unimolecular fragmentation of the molecular ion and 3. detection and identification of the product ions [21].

This chapter is divided into two parts: first, the definitions and theories related to the modeling of unimolecular ion dissociations will be presented and discussed; followed by the description of the various methods to model mass spectrometric experiments.

2. 1. Fundamentals of Unimolecular Ion Dissociation Modeling

2. 1. 1. Internal Energy Distributions (IED)

The internal energy (E_{int}) of the ions formed in a mass spectrometer has a profound influence on the appearance of the mass spectrum [21-23]. The relative intensities of the product ions, therefore, the ratio of the precursor and product ions are determined by the reaction rates of the unimolecular dissociations. The reaction rates are most strongly influenced by the internal energy of the precursor ions [21]. If ions have a high internal energy they will fragment to a large extent, producing a spectrum that typically shows a wide variety of abundant fragment ions. If, on the other hand, the internal energy is low, the ions will not fragment, or will produce only a few fragment ions of low abundance. This may be most easily demonstrated by comparing the mass spectra of a compound measured using 'soft' and 'hard' ionization techniques [1]. In Figures 2. 1, and 2. 2, the spectra of lysine demonstrate the effect of different internal energies deposited in hard ionization (electron ionization, EI) and soft ionization (electrospray, ESI).

These two figures are strikingly different in the amount of fragmentation; hence the deposited internal energy must be different as well. In the case of electron ionization, the ion is formed in vibrationally excited state (high internal energy), causing extensive fragmentation of the molecule. On the other hand, when using soft ionization, such as electrospray ionization technique, the ions are mainly formed in the vibrational ground state (low internal energy), therefore, very little fragmentation can take place [24].

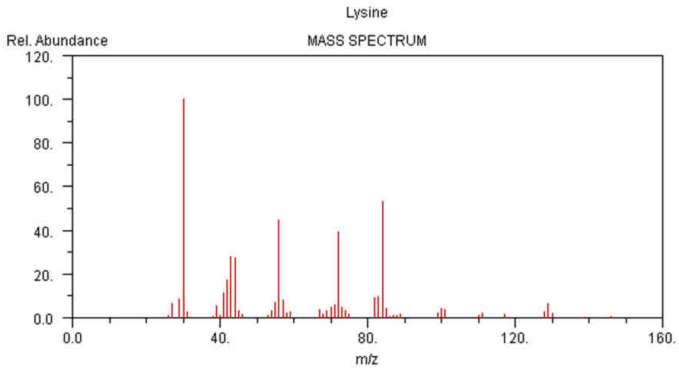

Figure 2. 1: *Electron ionization spectra of lysine (from http://webbook.nist.gov/chemistry)*

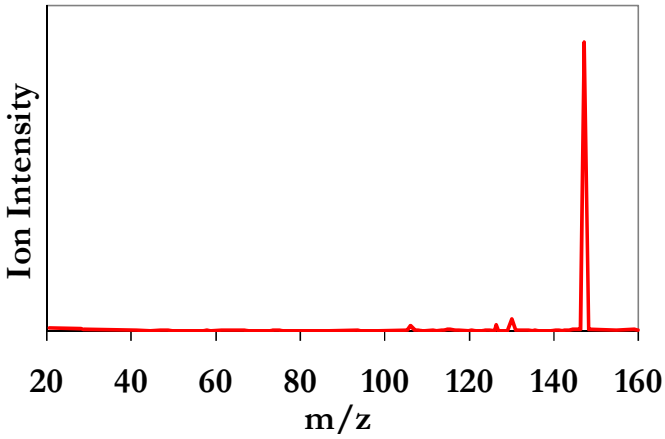

Figure 2. 2: *ESI spectra of protonated lysine (recorded on a Quattro Micro ESI-MS at 2 eV collision energy using collision-induced dissociation)*

In this thesis, the internal energy is defined as the sum of energies in vibrations and internal rotations of a molecule (or ion) above the zero point energy (ZPE) level [21]. The translation and overall rotation of the molecule (and the associated energies) are treated separately. The ion internal energy can come from four sources [21, 25]: 1. the internal energy of the molecule before ionization, 2. the energy supplied by the ionization method, 3. secondary excitation and 4. other modifying effects (such as collisional or radiation processes). The probability of a species having a particular internal energy range is described by the internal energy distribution function, $P(E_{int})$.

While the ions inside the mass spectrometer are not strictly in thermal equilibrium, in most ion sources, the ions are formed at a certain source temperature. Furthermore, in several modern mass spectrometry experiments, ions are formed at relatively high source pressure (1 – 10 bar), at which numerous collisions occur and the ions may be stored and thermalized at various, usually well characterized temperatures later. This means that it is reasonable to assume that the internal

energy distribution is similar to a thermal distribution, and therefore, it is useful to discuss briefly the thermal energy and the thermal energy distribution, and its calculation.

When applying the harmonic oscillator's quantized formalism, the average vibrational thermal energy of a molecule is [26]:

$$E_{\text{therm}} = \sum_{i=1}^{s} \frac{h\nu_i}{\exp\left(\frac{h\nu_i}{k_B T}\right) - 1} \tag{1}$$

where h is the Planck constant, ν_i are the vibrational frequencies, k_B is the Boltzmann constant, and T is the absolute temperature.

The thermal energy distribution ($P(E_{\text{therm}})$) can be calculated with the following expression [27]:

$$P(E;T) = \frac{\rho(E)\exp\left(-\frac{E}{k_B T}\right)}{\int_0^{\infty} \rho(E)\exp\left(-\frac{E}{k_B T}\right)} \tag{2}$$

where $\rho(E)$ is the density of states at energy level E.

2. 1. 2. Reaction Rates

Accurate ion intensities of a mass spectrum can only be calculated with precise reaction rates. Below, the theory of the applied reaction rate formalism is discussed.

A unimolecular reaction is an elementary reaction where a single species (a molecule or an ion) produces one or more products (isomerization or dissociation), respectively:

$$\text{M} \longrightarrow \text{Product(s)} \tag{3}$$

Unimolecular elemental reactions follow first order kinetics, where the negative of the time derivative of the reactant concentration ([M]) is proportional to the reactant concentration:

$$-\frac{d[M]}{dt} = k[M] \tag{4}$$

The time dependent concentration of [M] is calculated by integrating equation (4):

$$[M] = [M]_0 \cdot e^{-kt} \tag{5}$$

where k is the reaction rate constant with unit of reciprocal time, $[M]_0$ is the concentration of species M at time $t = 0$.

The reaction rate constant, despite its name, depends on the temperature (or internal energy). Reaction rate theories usually relate to thermal processes, where molecules are constantly energized and deactivated by collisions with other molecules. Ions produced in a mass

spectrometer are typically energized in a single event (e.g. ionization or collision) and are not in equilibrium with their environment. Hence, the microcanonical formalism is required when applying statistical rate theories to mass spectrometry. The connection between the canonical rate constant, $k(T)$, and the microcanonical rate constant, $k(E)$, involves an integration over the thermal energy distribution:

$$k(T) = \int_{E_0}^{\infty} P(E;T)k(E)dE \tag{6}$$

where E_0 is the critical energy and $P(E,T)$ is the internal energy distribution at a certain temperature, T. Many systems of chemical interest can be described by a thermal distribution; therefore, the $k(T)$ function is of more interest than $k(E)$ [25].

2. 1. 2. 1. The Arrhenius Equation

For thermal dissociations, the temperature dependence of the thermal dissociation rates can be summarized in the well-known Arrhenius equation [28, 29]:

$$k(T) = A\exp\left(-\frac{E_a}{RT}\right) \tag{7}$$

where A is the pre-exponential factor and E_a is the activation energy. The relationship between the critical energy and the activation energy is described in the Tolman theorem [30] that can be expressed with the following formula as discussed in *Laskin*'s paper [31] and other books [32, 33]:

$$E_a = E_0 + < E^{\ddagger} > - < E > + k_B T \tag{8}$$

or

$$E_a = \Delta H^{\ddagger} + k_B T \tag{9}$$

where k_B is the Boltzmann's constant; $<E^{\ddagger}>$ and $<E>$ are the average internal energy of the transition state (TS) and of the reactant molecules evaluated at temperature T, respectively and $\Delta H^{\ddagger}$ is the activation enthalpy of the reaction.

Laskin carried out a detailed analysis of the Tolman theorem using leucine enkephalin as the model compound [31]. It was demonstrated that the nature of the reaction, and therefore, the transition state determines the correction factor between E_a and E_0: in the case of a tight transition state (small log$A$), the correction part is negative and E_a is lower than E_0, while in the case of a loose TS, the correction factor is positive, therefore E_a is higher than E_0.

The physical meaning of the pre-exponential factor can be given by *Eyring*'s absolute reaction rate theory [34], where the reaction rate in a thermal system is given by the following formula [33]:

$$k(T) = \frac{k_B T}{h} \frac{Q^{\ddagger}}{Q} \exp\left(-\frac{E_a}{RT}\right) \tag{10}$$

or

$$k(T) = \frac{k_B T}{h} \exp\left(\frac{\Delta S^{\ddagger}}{R}\right) \exp\left(-\frac{E_a}{RT}\right) \tag{11}$$

From Equations (7), and (11), the following formula for the pre-exponential factor can be derived:

$$A = \frac{k_B T}{h} \exp\left(\frac{\Delta S^{\ddagger}}{R}\right) \tag{12}$$

This shows a direct correlation between the pre-exponential factor and the activation entropy.

However, to accurately model any non-thermal process in the mass spectrometer, the function *k(E)* is needed [32]. A brief summary of the microcanonical formalism will be given here as it is implemented in the MassKinetics program to accurately calculate the energy dependence of the reaction rates.

2. 1. 2. 2. RRKM/Quasi Equilibrium Theory (QET)

The mechanism of unimolecular reactions were the scope of intensive research, and one of the first quantitative descriptions was given by *Lindeman* [35], who proposed a mechanism involving both bi- and unimolecular steps. Here, the systems are described by an equilibrium temperature and, therefore, a canonical rate constant, *k*(*T*). After the semi-quantitative RRK theory [36, 37], the RRKM theory was developed by *Rice*, *Ramsperger*, *Kassel* and *Marcus* [38, 39], to overcome some of the limitation and assumptions of the former theories resulting in a quantitative description of the *k*(*E*) function. At the same time, the quasi-equilibrium theory (QET) was developed independently by *Wallentein*, *Wahrhaftig*, *Rosenstock* and *Eyring* for describing systems in non-equilibrium states, such as under mass spectrometric conditions [40]. Despite the two different derivations, the final equation for calculating the reaction rate as a function of the energy is the same. Here, RRKM theory is presented based on *Baer and Hase*'s book [32] that uses the classical transition state theory by *Wigner* [41].

A possible representation of a unimolecular reaction is a flux in the phase space. A molecule with a total of *m* internal degrees of freedom can be described by the motion of *m* positions (**q**) and *m*

momenta (**p**), therefore, the system is described with $2m$ coordinates. At constant energy, this is reduced to a $2m-1$ dimensional hypersurface. If this fixed energy, E, is greater than the dissociation energy, E_0, the system is capable of dissociating, by crossing the critical surface, or the transition state. This is a $2m-2$ dimensional surface that divides the reactants and the products, and is located such in a way that if a trajectory passes through, it will proceed toward the reaction products without returning. For reactions with a reverse activation barrier, the critical surface is located at the saddle point. For reactions with no or small reverse activation barrier, the location of this critical surface depends on the total energy.

The reaction rate is, therefore, the total flux of reactants passing through the critical surface. The dissociation takes place along a one-dimensional reaction coordinate, which is the minimum energy path. Assuming that this coordinate is perpendicular to the rest of the coordinates at the transition state, the system is separable and the spatial and conjugate momentum assigned to the TS are designated as $q^‡$ and $p^‡$. Furthermore, assuming that the total phase space is populated statistically, the ratio of molecules near the critical coordinate to the total molecules can be determined as:

$$\frac{dN\left(q^‡, p^‡\right)}{N} = \frac{dq^‡ dp^‡ \int_{H=E-\varepsilon_t-E_0} \cdots \int dq_1^‡ \cdots dq_{n-1}^‡ dp_1^‡ \cdots dp_{n-1}^‡}{\int_{H=E} \cdots \int dq_1 \cdots dq_n dp_1 \cdots dp_n} \tag{13}$$

where E_0 is the activation energy, and ε_t is the translational energy associated with the momentum $p^‡$ in the reaction coordinate.

The reaction rate is then the time derivative of the molecules near the critical surface, i.e. the flux of molecules passing through the critical region:

$$\text{Flux} = \text{reaction rate} = \frac{dN\left(q^‡, p^‡\right)}{dt} \tag{14}$$

Having assumed the reaction coordinate being perpendicular and therefore separable from all other coordinates, this time derivative only contains the $dq^‡$ and $dp^‡$ terms. Applying $dq^‡/dt = p^‡/\mu^‡$, where μ is the reduced mass of the two separating fragments, the following formula can be derived from Eq. (13):

$$\frac{dN\left(q^‡, p^‡\right)}{dt} = \frac{N\frac{p^‡ dp^‡}{\mu^‡} dq^‡ dp^‡ \int_{H=E-\varepsilon_t-E_0} \cdots \int dq_1^‡ \cdots dq_{n-1}^‡ dp_1^‡ \cdots dp_{n-1}^‡}{\int_{H=E} \cdots \int dq_1 \cdots dq_n dp_1 \cdots dp_n} \tag{15}$$

The energy in the reaction coordinate can be substituted with $\varepsilon_t = p^{‡2}/\mu^‡$, the time derivative of this is $d\varepsilon_t = p^‡ dp^‡/\mu^‡$, therefore the expression has the following form:

$$\frac{dN\left(q^{\ddagger},p^{\ddagger}\right)}{dt}=\frac{Nd\varepsilon_t^{\ddagger}\int_{H=E-\varepsilon_t-E_0}\cdots\cdots\int dq_1^{\ddagger}\cdots dq_{n-1}^{\ddagger}dp_1^{\ddagger}\cdots dp_{n-1}^{\ddagger}}{\int_{H=E}\cdots\int dq_1\cdots dq_n dp_1\cdots dp_n} \tag{16}$$

This is the reaction rate in terms of N, the number of molecules, multiplied by the rate constant, $k(E, \varepsilon_t)$. This latter can be expressed by the ratio of two phase space areas, using the density of states: the denominator is the density of states multiplied by the factor h^n, while the numerator is an integral over one less dimension, so there it is h^{n-1}. The rate constant, $k(E, \varepsilon_t)$ becomes:

$$k\left(E,\varepsilon_t\right)=\frac{\rho^{\ddagger}\left(E-E_0-\varepsilon_t\right)}{h\rho\left(E\right)}, \tag{17}$$

where h is the Planck constant. This formula expresses the rate constant in terms of the total energy, E, and the translational energy of the departing fragments at the transition state, ε_t.
This above expression is valid for one particular pass through the transition region, with a certain available energy. However, the total dissociation rate can be expressed by integrating over all the different translational energies in the transition state:

$$k\left(E\right)=\frac{\int_0^{E-E_0}\rho^{\ddagger}\left(E-E_0-\varepsilon_t\right)d\varepsilon_t}{h\rho\left(E\right)}=\frac{N^{\ddagger}\left(E-E_0\right)}{h\rho\left(E\right)} \tag{18}$$

where $N^{\ddagger}(E - E_0)$ is the sum of states at the transition state from 0 to $E - E_0$, and $\rho(E)$ is the density of states. During the derivation of this formula the rotations were neglected, and the reaction symmetry can be accounted for by a simple multiplication.

Some of the fundamental assumptions of RRKM theory are: the molecules populate all of the phase space statistically throughout their dissociation; all of the molecules that are in the critical space lead to products and, that the transition state coordinates are perpendicular to all other coordinates and, therefore, can be separated from them. However, for a more detailed discussion of these assumptions, and their validity, the reader is referred to dedicated publications [32].

As mentioned above, QET was developed at the same time as RRKM theory, and it was focusing on non-thermal systems, such as mass spectrometers. The fundamental assumptions of the QET are the following (compared to the ones of RRKM) [40]:
a) the time required for dissociation is long compared with the time of the interaction(s) leading to excitation; b) the rate of dissociation is slow relative to the rate of distribution of the internal energy over all degrees of freedom; c) an ion in the mass spectrometer represents an isolated system in a state of internal equilibrium, i.e. there is no energy exchange with the environment

and the energy within the ion distributed statistically over the internal oscillators; d) fragmentation products are formed by a series of competitive and consecutive unimolecular reactions. While assumption a), c) and d) are usually valid in most mass spectrometric experiments, the time of the reactions is known less accurately therefore assumption b) is still under heavy debate in the scientific community and much research is done to address this problem [25, 42, 43].

2. 1. 3. Description of the Transition State (TS)

2. 1. 3. 1. Frequency Factor

When calculating the energy dependent reaction rates derived above, the sum- and the density of states are needed. The detailed discussion on the various ways of calculating the sum and density of states can be found in various books and reviews [32, 33]. In general, to calculate these values one needs the frequency set of the molecular ion and of the transition state.

The frequency sets can be determined in two ways: experimentally and theoretically; while experimental determination works for the reactant, the vibrational frequencies of the transition state – except for systems with only a few atoms – can only be determined using quantum chemical calculations, which is a daunting task if accurate vibrational frequencies are needed. Therefore they are often estimated: many applications are not sensitive to the accuracy of these vibrational frequencies, so knowing only the type of the transition state is sufficient for a successful modeling. In that case, the complete vibrational frequency set can be replaced with a single, so-called frequency factor, and the natural logarithm of it is the pre-exponential factor. This latter was briefly mentioned above at the introduction of the Arrhenius parameter; it can be determined experimentally using the Arrhenius equation, as will be demonstrated below [31]. It can also be estimated if the type of the dissociation is known: dissociations are usually categorized into two main classes based on their transition states: direct bond cleavages and rearrangements [10, 44] and it can be characterized by the pre-exponential factor, frequency factor (ν) and the activation entropy ($\Delta S^{\ddagger}$). The transition state of direct cleavage is defined as a "loose" complex: the structure and geometry are close to those of the products and hence it is also called "late" transition state. These transition states have high frequency factors ($\nu = 10^{13} - 10^{15}$ s^{-1}) and high pre-exponential factors ($\log A = 13 - 15$), as well as positive activation entropy values ($\Delta S^{\ddagger} > 0$). Contrary to direct bond cleavage, rearrangement reactions usually have a higher critical energy and a higher reaction rate constant as well as a negative activation entropy value ($\Delta S^{\ddagger} < 0$). Rearrangement reactions usually proceed via tight transition states, many times

forming a cyclic transition structure. Since this TS is typically far from the structure of the products, it is also called early transition state. The frequency factor is low ($\nu = 10^6 – 10^{12}$ s^{-1}) and so is the pre-exponential factor, ($\log A = 6 – 12$). Based on these general considerations, when the transition state cannot be localized (cannot be optimized using quantum chemical calculations) and therefore the exact geometry and the vibrational frequency set are not known, an average pre-exponential factor is used based on their dissociation type: low if it is assumed to be a rearrangement and high pre-exponential factor is used in the RRKM modeling if it is assumed to be a direct dissociation [21].

2. 1. 3. 2. Critical Energy

To apply RRKM theory in the modeling calculations the critical energy of the examined dissociation is also needed: that is the difference in the zero-Kelvin heat of formation of the activated complex and that of the ground state. In many cases, it is incorrectly used as a synonym to the activation energy, which is defined in case of thermal systems as the difference in internal energy of the transition states and the average thermal energy of the reactant. The connection between the two energies is given by the Tolman equation, see above (Eq. (8)) [30]. Calculating the critical energy from the Arrhenius activation energy requires the knowledge of partition functions of the TS and of the excited molecule that are correlated with the activation entropy and statistical theory is needed to accurately convert one to the other [10]. In general, however, the following relations can be stated: if the activation entropy is positive – i.e. the dissociation proceeding via loose TS and $\log A$ is high – the E_a is higher than E_0. While for reactions proceeding via tight TS, i.e. negative activation entropy and low $\log A$, the E_a will be lower than E_0.

The critical energy can also be calculated using quantum chemical methods [45]; however, in the case of a reaction with a reverse barrier, this requires the knowledge of the geometry of the transition state, which is often not easily attainable. In the case of a loose transition state, however, there is either no activation barrier of the reverse reaction or it is so small that it can be neglected, and therefore the critical energy can be defined as the difference of the zero point corrected energies of all the products and the molecular ions.

The critical energy can also be estimated using an equation developed by *Pope* and coworkers [46]. The reaction enthalpy, which can be measured, is expressed with the following equation:

$$\Delta H^T_{számított} = \Delta E^0_e + \Delta\left(\Delta E_e\right)^T + \Delta E^0_v + \Delta\left(\Delta E_v\right)^T + \Delta E^T_r + \Delta E^T_t + \Delta PV \quad (19)$$

where

ΔE_e^0 is the difference in electronic energy of the reactant and the products at 0 K

$\Delta(\Delta E_e)^T$ is the difference in ΔE_es calculated at temperature T and 0 K (this can be neglected for most of the cases)

ΔE_v^0 is the difference in the zero point energy of the reactant and products

$\Delta(\Delta E_v)^T$ is the difference in the vibrational energy calculated at temperature T and 0 K

ΔE_r^T is the difference in the rotational energy of the reactant and the products at temperature T (In the classical treatment this equals to $-½RT$ for every rotational degrees of freedom that changes to translation in the reaction; a good approximation at room temperature)

ΔE_t^T is the difference in the translational energy of the reactant and the products at temperature T (can be calculated using the change in translational degrees of freedom and $-½RT$)

ΔPV „pressure-volume work", for ideal gases it is ΔnRT, where Δn is the change in moles during the reaction

When the reverse reaction has no activation energy barrier – this is most often the case in mass spectrometry – the critical energy can be calculated as the sum of the electron energy difference and the zero point vibrational energy: $E_0 = \Delta E_e + \Delta E_v$. Therefore the critical energy can be determined from the standard enthalpy, which can be measured easily, using the following equation:

$$E_0 = \Delta H^T - \Delta(\Delta E_v)^T - \frac{f + l + 2n}{2} RT \qquad (20)$$

where f is the change in the rotations, l is the change in the translations during the reaction, n is the change in the moles during the reaction.

2. 1. 3. 3. Kinetic Shift

The time window of the experiment, the internal energy dependent reaction rates (therefore, ion lifetimes) together determine the observed ion ratios in the mass spectrum [32]. The time-scale of a typical gas phase ion experiment can vary from 10^{-7} s to several seconds depending on the experimental conditions and it can also depend on the size of the molecule. In the case of a magnetic sector type instrument, ions are considered metastable with typical lifetimes of 10^{-6} – 10^{-4} s [47], whereas metastable ions in a quadrupole or ion trap are the ones with lifetimes longer than 10^{-4} s [24]. The shorter the time-scale of the experiment, the higher the ion internal

energy has to be for the fragmentation to have enough energy to overcome the activation barrier to dissociate to a product ion that is observable within the time-frame of the experiment.

Knowing the reaction rate constants and the resident times in the instruments, the ion ratios can be calculated as a function of the internal energy. The internal energy that is required to observe a particular (precursor or fragment) ion, is called the (ambient) appearance energy (*AE*) [48]. This value is typically in the order of a few electron volts for small or medium sized molecules, but it can be 10 – 20 eV for larger molecules.

Because of the finite unimolecular dissociation rates, the time scale of the experiment may be too short to observe dissociation even when the molecule or ion has enough energy to dissociate. This is especially true for larger molecules, because the rate constant decreases dramatically with increasing degrees of freedom (DOF) [49]. The difference between the internal energy necessary to fragment molecules at observable rates (the appearance energy) and the critical energy is called the kinetic shift [48]. This also means that different instruments may have widely different kinetic shifts.

The effect of the kinetic shift is perhaps the most striking when one looks at a breakdown diagram, i.e. the relative ion abundances as a function of the ion internal energy [21, 48, 50]. Due to the kinetic shift, the crossover point of the molecular and the fragment ion curves shifts to higher energies than expected, requiring more energy to detect the fragmentation. The breakdown curves can be calculated using statistical reaction rate theories or experimentally by recording the product ions and the precursor ion as a function of the internal energy. Breakdown curves can also be shown as the ion ratios as a function of collision energy when collision-induced dissociation is used in the experimental setup, and with the knowledge of the collisional energy transfer function and the initial internal energy, the internal energy of the fragmenting ion can be calculated.

2. 1. 4. Modeling Secondary Excitations: MassKinetics

Soft ionization techniques are used to avoid or minimize fragmentation and to ionize samples, which have low or no vapor pressure, without decomposition [49, 51]. The most commonly used soft ionization technique is electrospray ionization (ESI), which result in protonated molecular ions below the critical energy [24]. Various excitation methods can be coupled to ESI to increase the ions' internal energy in order to control the amount of fragmentation or to investigate the internal energy dependence of the fragmentation behavior. These methods are also called secondary excitations [21]. The most common technique of these is the collisional induced dissociation (CID) activation method [4, 6, 52], where the ions of interest are collided with

neutral gases (N_2, Ar, He) at finely controlled kinetic energies. During the collision, part of the ion's translational energy becomes internal energy, therefore the internal energy increases. The energy transfer processes together with the excitation and fragmentation can be modeled by the so called master equation technique, which is a complex differential equation system that describes the internal energy change as the function of the internal energy distribution and the energy transfer probabilities [3, 53-56]. The calculations are based on the RRKM theory and are so time-consuming that several assumptions have to be made when applied to larger systems.

The energy transferred to the molecular ion during the collision is usually described not with a single energy value, rather than a transfer function. This collisional energy transfer function usually approximated by either *Armentrout*'s distribution [57], which is determined experimentally; *Hase*'s distribution [58], which is obtained from trajectory calculations; or a simple exponential distribution [59]. The determination of the accurate functions requires complex experimental and theoretical work, and is under detailed investigation by leading research groups in fundamental mass spectrometry [3, 60-62].

MassKinetics is an RRKM-based program for modeling mass spectrometric processes, which has been developed in our group by implementing most major mass spectrometry theories [20]. The program can compute reaction rates, energy exchange processes in the gas phase and can calculate product ion abundances as the ions move through various parts of a mass spectrometer. In MassKinetics, ions are characterized by their internal and kinetic energies, which define the "state" of an ion. Essential features of the MassKinetics model are the use of internal (and, if necessary, kinetic) energy distributions and the use of probabilities to describe transitions between different states. Reaction rate calculations are based on the transition state theory in its Rice–Ramsperger–Kassel–Marcus (RRKM) formulation. Energy exchange processes and fragmentations take place in the same time frame, which is taken into account using the master-equation formalism. The kinetic and/or internal energies of the ions in the gas phase may change due to (a) acceleration in electromagnetic fields (b) radiative energy exchange (photon absorption and emission) (c) collisional energy exchange and (d) energy partitioning in chemical reactions, which are all taken into account. Note that among these, collisional energy exchange may be described using different collision models. While the mathematical description of these physical processes is quite complex, it has the immense advantage that ion abundances can be calculated accurately using very few empirical or adjustable parameters [20].

The modeling process can be summarized in a flowchart [63]:

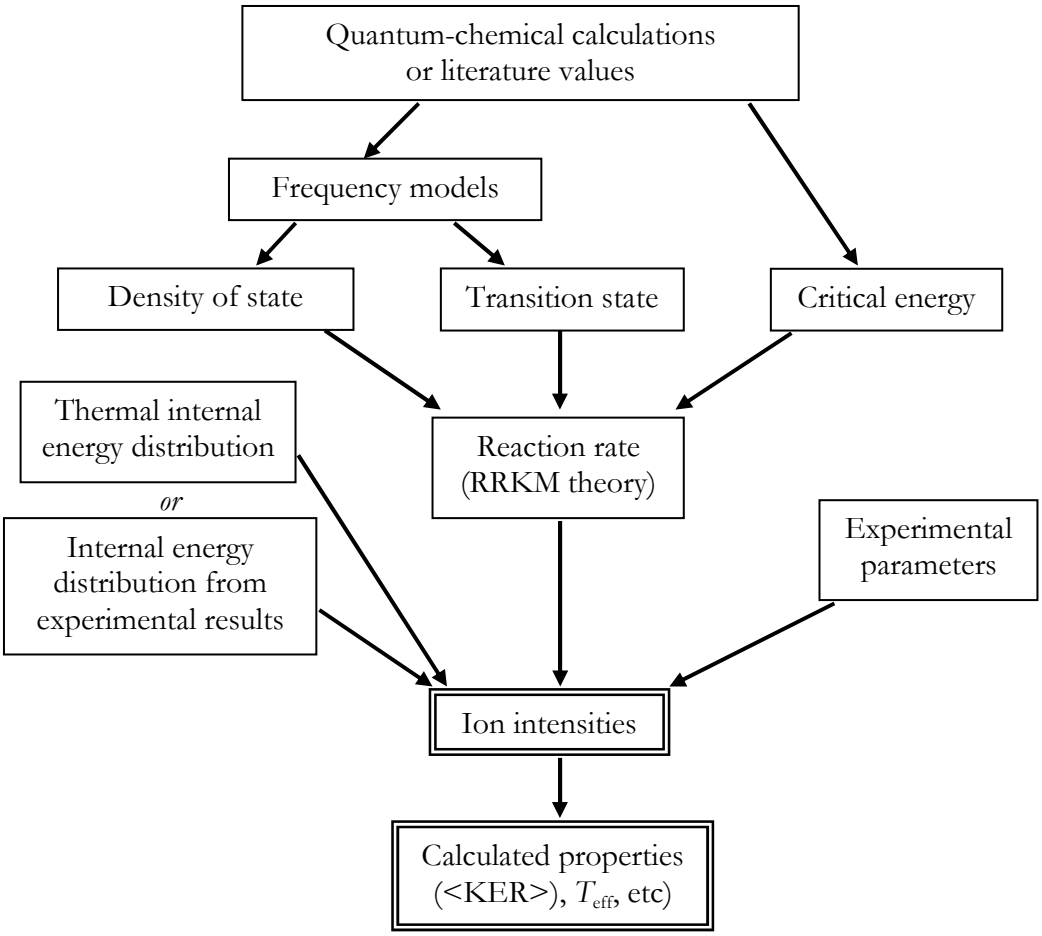

2. 2. Experimental Methods to Address the Fundamentals of MS Processes

2. 2. 1. Methods to Characterize Internal Energy Distributions

In all MassKinetics calculations, initial internal energies are needed to characterize the molecular ions. At the simplest level, an average internal energy value can be used for the modeling. However, in reality the ions are usually produced with a wide distribution of internal energies, rather than a single internal energy value [21]. As a result, ions from a high-energy part of the energy distribution can already decompose in the ion source, while ions with low internal energy (also described as "cold" ions) can reach the detector without any fragmentation. Ions in the intermediate part of the energy distribution can leave the ion source and decompose on their way to the detector, mainly in the field free region (FFR). These are referred to as the metastable ions [64].

The determination of an internal energy distribution is challenging since there are only a few, specialized instruments that can produce an ion with a well defined energy distribution. However, there are at least three different methods developed recently that allows solving this problem with conventional mass spectrometers.

2. 2. 1. 1 Thermometer Molecule Method

The thermometer molecule method [22] is based on certain ions, such as $W(CO)_6^+$ that undergo consecutive fragmentations, loosing simple neutral fragments (CO in this case) in each step. Since the critical energy of each step is well known, the observed fragments correspond to an upper and lower limit in the internal energy that the molecular ion originally possessed and, therefore, the internal energy distribution can be determined to a reasonable accuracy. The method is illustrated in Figure 2. 3 taken from [22]. The disadvantages of this simple technique are that only molecules with well defined thermochemistry and with similar, consecutive fragmentation pathways can be used, the resolution of the curves is limited and the above mentioned kinetic shift is not taken into account.

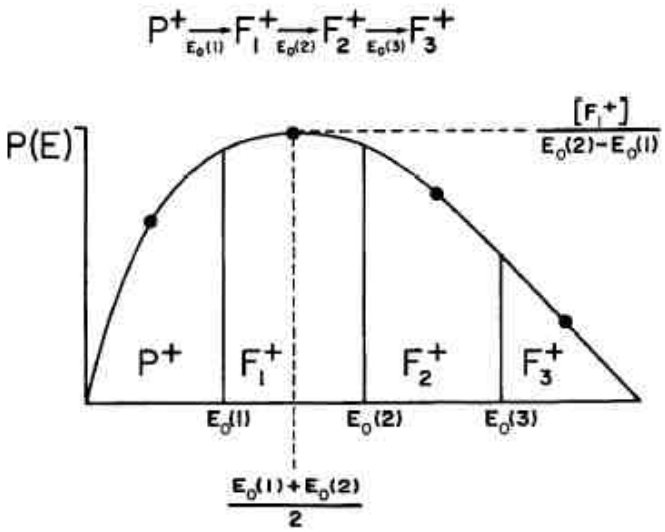

Figure 2. 3: *Diagram of the thermometer molecule method: P(E) solid line is the internal energy distribution, P^+ - molecular (precursor) ion, F_1^+, F_2^+ and F_3^+ are the fragment ions and $E_0(1)$, $E_0(2)$ and $E_0(3)$ are the critical energy of the corresponding dissociations [22].*

2. 2. 1. 2. Deconvolution Method

Overcoming some of the disadvantages of the thermometer molecule method, the deconvolution method has been developed by *Vékey* et al. [65, 66]. Instead of the energy ranges between the known critical energies, energy ranges obtained from the actual experimental breakdown curves are used. The energy distribution is then determined in a similar manner as in the thermometer method. Because the kinetic shift is implicitly taken into account by the experimental breakdown curve, this method provides more accurate energy distribution.

2. 2. 1. 3. Survival Yield Method

The most recently developed method, the survival yield method [67, 68], employs homologous or similar molecules with a simple fragmentation mechanism (one fragment ion with the loss of a neutral molecule) and known critical energies, and assumed to have the same internal energy distribution. Since the dissociation is a simple bond cleavage, it is assumed that no reverse activation barrier exists, therefore the activation energy equals to the reaction enthalpy change. The reaction enthalpy change can either be measured, taken from the literature, or be calculated using results from simple quantum chemical calculations. The survival yield (SY) of the molecular ion is determined from the measured intensities:

$$Y = \frac{I(M^+)}{I(M^+) + I(F^+)} \tag{21}$$

where $I(M^+)$ is the intensity of the molecular ion and $I(F)^+$ is the intensity of the fragment ions. The SY is then plotted as a function of the critical energy, and the derivative of the resulting curve gives the internal energy distribution.

The advantages of the survival yield method are that internal energy distributions of soft ionization techniques (such as ESI) can be determined, and that it does not require complicated instrumentation [68, 69]. The disadvantage of the SY method is that it does not take the kinetic shift into account, therefore, the internal energy and the internal energy distribution is underestimated for slow dissociations. However, this latter concern can be solved by plotting the survival yield against the appearance energy rather than the critical energy [70, 71].

2. 2. 1. 4. Threshold Photoelectron Photoion Coincidence (TPEPICO) Spectrometry

Analogously to the SY method, the entire ion internal energy distribution can be directly obtained from the TPEPICO breakdown diagram [72]. In this technique, the internal energy of the precursor ions comes directly from the photon energy of the photoionization process by a simple subtraction of the adiabatic ionization energy. In the case of a fast dissociation, the breakdown curve is simply the integral of the ion energy distribution as:

$$BD(E) = \int_{E-E_0}^{+\infty} P(x)\mathrm{d}x, \tag{22}$$

where BD(E) is the fraction of the fragment ion's abundance, and $P(x)$ is the ion internal energy distribution. Therefore, the ion energy distribution can be obtained directly by the first derivative

of the breakdown curve with respect to the photon energy. The drawback of this technique is that TPEPICO is limited to relatively small systems.

2. 2. 2. Methods to Determine Arrhenius Dissociation Parameters

As it was stated above, knowing the accurate critical energy and/or activation energy and the pre-exponential factor plays a crucial role in the success of the modeling. Part of my Ph.D. research was a reevaluation study of the published Arrhenius dissociation parameters of protonated leucine enkephalin, to obtain a data set that is accurate enough for modeling purposes [73]. Therefore, I would like to give a short introduction to the various experimental techniques that are used to determine energetics data of unimolecular dissociations with the help of protonated leucine enkephalin, the most commonly used standard in mass spectrometry. Certainly, it is not intended to be a complete list of all the possible experimental techniques, rather to give a better understanding of the experimental data that was used in my Ph.D. research.

For protonated leucine enkephalin, there were seven papers published in the past few years, each one involving a novel technique to determine the activation energy and the pre-exponential factor of the most commonly studied dissociation, the $MH^+ \rightarrow \mathbf{b_4}^+$ fragmentation channel of protonated leucine enkephalin [31, 54, 74-79]. Instead of grouping these publications based on the techniques, the chronological order was kept so that the development of the techniques can be illustrated.

The Arrhenius parameters and reaction-rate data of leucine enkephalin were determined for the first time by measuring the thermal decomposition of protonated leucine enkephalin ions using a heated tube reactor at 600 – 680 K coupled to a mass spectrometer detector [80]. Special attention was given to see if the ion population was effectively thermalized, so that accurate temperature dependence could be detected. Ion intensities were measured at different temperatures, from which kinetic data could be extracted.

The activation energy of protonated leucine enkephalin fragmentation has also been determined by evaluating surface induced dissociation (SID) and thermal decomposition results with RRKM theory [76]. Fragmentation efficiency curves were measured, and from a knowledge of the mean internal energy deposited (using 13 % energy transfer efficiency in thermal dissociation), the amount of internal energy increase was determined as a function of the collision energy and kinetic data could be determined from the efficiency curves.

Williams and coworkers developed an elegant new concept to perform thermal activation and dissociation in a Fourier transform ion cyclotron resonance (FT-ICR) instrument, called

'blackbody infrared radiative dissociation', BIRD [77]. In this technique, the ICR cell of the mass spectrometer is kept at a certain temperature, and energy exchange and thermal equilibration occurs not by collisions, but by the absorption/emission of infrared photons. Fragment ion intensities are measured as a function of reaction time (in the order of seconds); and rate constants are determined this way. These rate constants are, in turn, measured as a function of temperature. The results are evaluated with a conventional Arrhenius plot to yield the activation energy and the pre-exponential factor. The main assumption used in the evaluation of BIRD results is that the rapid energy exchange (REX) limit is reached [49]; which is a prerequisite to use the Arrhenius equation to evaluate the results.

An analogous approach has been developed by *McLuckey* and coworkers with a quadrupole ion-trap instrument [75]. In this case, the temperature of the dissociating ions was controlled by the temperature of the helium bath gas and REX limit was assumed due to the sufficient number of collisions. Temperature-dependent dissociation rates of the $MH^+ \rightarrow \mathbf{b_4}^+$ ion process have been measured.

Another approach pioneered by *Williams* and coworkers used the infrared multiphoton dissociation (IRMPD) technique to determine the photodissociation kinetics of protonated leucine enkephalin with a continuous-wave CO_2 laser and FT-ICR [54]. First-order kinetics was fitted to the experimental data, and a master-equation simulation was performed in order to extract energetics information. Advantage of this technique is that laser IRMPD can access higher internal energies; however, no precise data could be determined with this technique only a very broad range for the E_a and A values. Therefore this data was not used in our analysis.

A different method, derived by *DePauw* and coworkers uses changes in the resonant-activation amplitude in a quadrupole ion-trap [78]. Based on the results of *McLuckey*, they have achieved thermal-like conditions with resonant activation and established a linear relationship between the effective temperature (i.e., the mean internal energy) and the activation amplitude. Based on this correlation, a unique calibration curve was derived that can be used to determine energetics parameters. This approach is promising because experiments are relatively simple to perform and (after the calibration process) straightforward to evaluate. However, because this approach involves various assumptions and a calibration process, the possibility of significant systematic errors must be considered.

The most recent attempt to determine the activation parameters for leucine enkephalin was published by *Laskin* [31], and is based on time- and energy-resolved surface induced dissociation (SID) studies performed with a FT-ICR instrument. Fragmentation-efficiency curves were recorded, and analysis involving RRKM theory was preformed.

A table summarizing these results is presented in the Experiments and Calculations section along with some general remarks of the published Arrhenius dissociation data and the raw kinetics data that was used in the re-analysis work.

2. 2. 3. Kinetic Method

The kinetic method that was developed by *Cooks* in the 1970's [81-83] allows one to determine thermochemical data (such as proton affinity, ionization energy, etc.) using the reaction rates of competitive dissociations. It does not require complicated instrumentations, and is sufficiently straightforward to use on a wide variety of systems to become a very popular technique. One of the most common uses of the kinetic method is to determine proton affinities by using protonated dimers, $B_1B_2H^+$, consisting of two monomer bases. Such systems can dissociate in two different ways, producing B_1H^+ or B_2H^+ ions:

$$B_1 \text{ ----- } H^+ \text{----- } B_2 \begin{array}{l} \xrightarrow{k_1} B_1H^+ + B_2 \\ \xrightarrow{k_2} B_2H^+ + B_1 \end{array} \qquad (23)$$

where k_1 and k_2 are the reaction rate constants. The potential energy diagram of the two dissociations is shown in Figure 2. 4 [84].

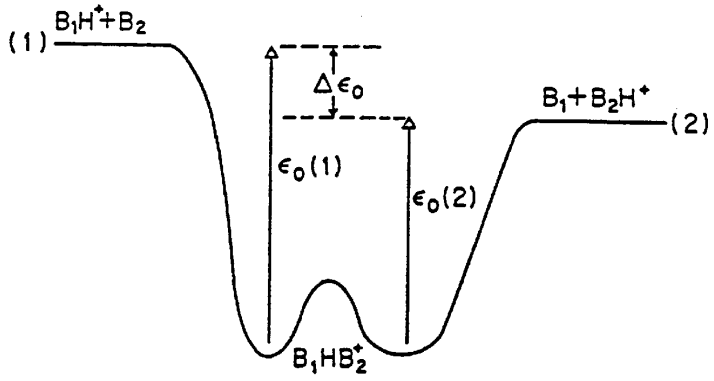

Figure 2. 4: *The potential energy diagram of the dissociation of a protonated dimer, B_1B_2H. The two different pathways are shown with $E_0(1)$ and $E_0(2)$ critical energies, producing B_1H^+ or B_2H^+ ions [82].*

The two minima and the assumption that there is no reverse activation barrier are in accordance with the quantum chemical calculations and experimental findings [84].
Therefore the difference in the critical energies is:

$$\begin{aligned} \Delta E_0 = E_0(1) - E_0(2) &= \Delta H_f(B_1H^+) + \Delta H_f(B_2) - \Delta H_f(B_1) - \Delta H_f(B_2H^+) \\ &= \Delta H_f(B_1H^+) - \Delta H_f(B_1) - [\Delta H_f(B_2H^+) - \Delta H_f(B_2)] \end{aligned} \qquad (24)$$

The proton affinities of the two bases are:

$$PA(B_1) = \Delta H_f(B_1H^+) - \Delta H_f(B_1) - \Delta H_f(H^+) \quad (25)$$

$$PA(B_2) = \Delta H_f(B_2H^+) - \Delta H_f(B_2) - \Delta H_f(H^+) \quad (26)$$

therefore,

$$\Delta E_0 \cong PA(B_2) - PA(B_1) = \Delta PA \quad (27)$$

The logarithm of the reaction rate according to the Arrhenius equation is the following:

$$\ln(k_1) = \ln(A_1) - \frac{E_0(1)}{k_B T}, \text{ and } \ln(k_2) = \ln(A_2) - \frac{E_0(2)}{k_B T} \quad (28)$$

If the two transition states are sufficiently similar that the pre-exponential factor can be taken as equal, the logarithm of the ratio of the two dissociation rate constants is the following:

$$\ln \frac{k_1}{k_2} = \frac{E_0(1) - E_0(2)}{k_B T} \approx \frac{\Delta PA}{k_B T} \quad (29)$$

The central formula of the kinetic method is therefore:

$$\ln \frac{[B_1H^+]}{[B_2H^+]} \approx \ln \frac{k_1}{k_2} \approx \frac{\Delta(\Delta GB)}{RT_{eff}} \approx \frac{\Delta PA}{RT_{eff}}, \quad (30)$$

because the $[B_1H^+]/[B_2H^+]$ ratio (the intensity ratio in the mass spectra) is equal to the ratio of the reaction rates.

2. 2. 4. Kinetic Isotope Effect (KIE)

The effect of isotopic substitution (usually hydrogen to deuterium) on a rate constant is referred to as the kinetic isotope effect (KIE), and can be expressed with the following formula [85, 86]:

$$KIE = k_H/k_D \quad (31)$$

where k_H and k_D represent the rate constants of the original and the deuterated molecule or ion. In the case of a substitution that is directly involved in a chemical bond breakage or bond formation during the particular process of interest, the effect is referred to as the primary isotope effect [87-89]. This is a larger change in the reaction rate than the secondary isotope effect, where the isotope substitution is on a part of the molecule that is not directly involved in the bond breaking or bond formation. The larger the change in the reduced mass upon isotopic substitution, the greater the kinetic isotope effect. Since the vibrational modes involving heavier atoms have lower frequencies, they have lower zero point vibrational energies (ZPE), therefore more energy is needed to break these bonds. This results in a higher activation energy and, hence, lower reaction rate. For example, in the case of changing a hydrogen to a deuterium atom, 6 – 10 times faster reaction rates can be observed for reactions involving loose transition states.

The difference in the zero point vibrational energies can be determined to an acceptable accuracy by quantum chemical calculations. If the various vibrational levels are also known for the two isotopic forms, the KIE can be calculated in thermal systems, as well.

In the case of tight transition states, the value of the KIE can even be $k_H/k_D < 1$, but this ratio becomes larger than one as the transition state becomes looser. For reactions involving the reversible exchange of the isotopes between the molecular species, the kinetic isotope effect is given by the equilibrium constants [90].

A special case of the KIE is the intermolecular isotope effect, where an isotopically labeled ion has two possible dissociation pathways involving the two isotopes. Since the reaction occurs from a common precursor, the size of the kinetic isotope effect can be determined from the relative abundances of the product ions in their mass spectra. This is, in fact, a special case of the kinetic method discussed above [87, 91-93].

2. 2. 5. Kinetic Energy Release (KER)

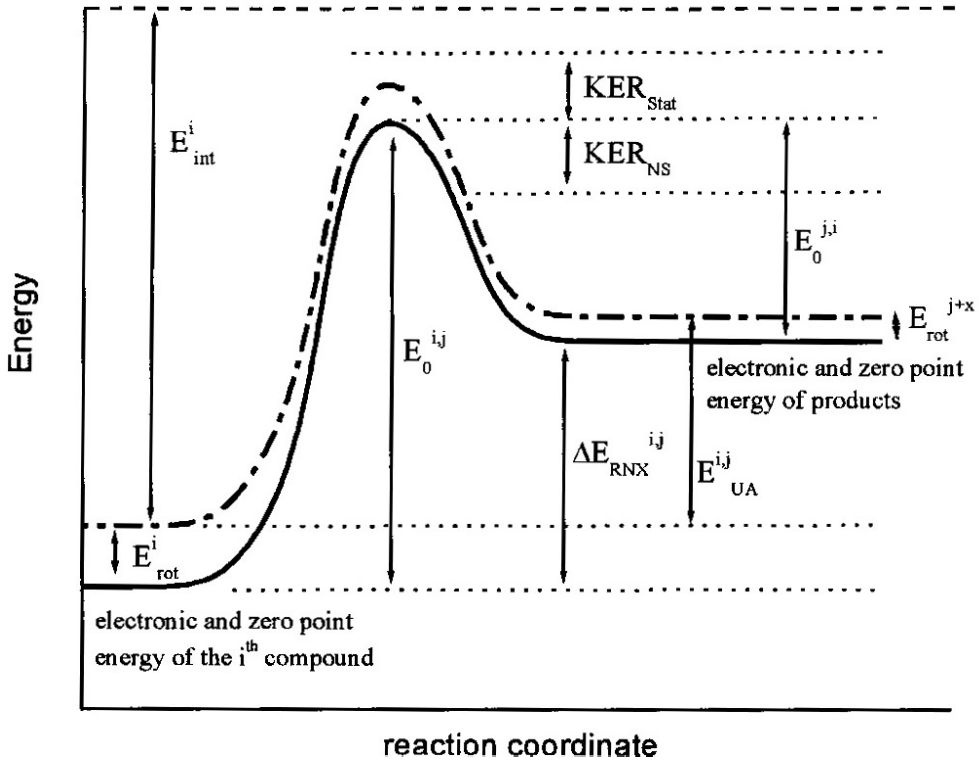

Figure 2. 5: *The energy profile of a reaction, indicating the kinetic energy release. Figure taken from ref. [20].*

During the unimolecular dissociation of an excited ion, some of the excess internal energy of the activated complex is released as the relative kinetic energy of the two fragments. This phenomenon is called the kinetic energy release (KER) and carries important information about the structures of the species involved in the fragmentation, as well as about the energetics and

dynamics of the reaction [94]. While the KER in multiply charged and neutral systems can be studied as well, here it will only be discussed for singly charged ions. The total kinetic energy that is released is divided between the ionic and the neutral fragment, and this total energy can be obtained trivially from the kinetic energy of the ionic fragment using simple momentum conservation [95].

Ions that undergo spontaneous dissociation in the field free region of the mass spectrometers are called metastable ions [64]. They usually occur in the mass spectrum at non-integer masses $M^* = (m_2)^2/m_1$, where m_1 is the mass of the parent ion and m_2 is the mass of the fragment ion. Metastable peaks are also broader than the normal peaks due to the translational energy release and this broadening is directly related to the magnitude of the kinetic energy release [94]. Since the thesis is focused on the theoretical aspects of ion fragmentation, for considerations of the experimental observation of KER, the reader is kindly referred to one of the review articles in this topic [32, 94, 96, 97]. Here, the basic theory of the KER will be discussed in a few words based on *Laskin* and *Lifshitz*'s tutorial paper [94].

Consider the following decomposition of a parent ion of mass m_1, with a kinetic energy of E_1 and $v_1 = (2E_1/m_1)^{1/2}$ velocity in a field-free region:

$$m_1^+ \rightarrow m_2^+ + m_3 \tag{32}$$

As it was defined above, the excess internal energy of the parent ion is distributed among all the internal degrees of freedom, and part of this energy is released in the relative translation of the departing fragments, called kinetic energy release (KER). If u_2 is the vector velocity of the ionic fragment in the center of mass frame, the kinetic energy release, ε, can be derived from the momentum and energy conservation laws:

$$\varepsilon = \frac{m_1 m_2}{2m_3} u_2^2 \tag{33}$$

The corresponding velocity in the center-of-frame and laboratory frame is u_2 and v_2, respectively:

$$u_2 = \sqrt{\frac{2m_3\varepsilon}{2m_1m_2}} \tag{34}$$

and

$$v_2 = v_1 \pm u_2 = v_1 \pm \sqrt{\frac{2m_3\varepsilon}{2m_1m_2}} \tag{35}$$

The kinetic energy of the ionic fragment, E_2, can be derived as:

$$E_2 = \frac{m_2 v_2^2}{2} = \frac{m_2}{2}(v_1 \pm u_2) = \frac{m_2}{2}(v_1^2 + u_2^2 \pm 2v_1u_2) \approx \frac{m_2}{2}(v_1^2 \pm 2v_1u_2)$$

(36)

since the u_2^2 term can be neglected due to the fact that typical KER are between 2 meV and 2 eV, therefore the u_2^2 term represents less than 0.2 % of the energy.

Combining equations 34, and 36:

$$E_2 = \frac{m_2}{2}(v_1^2 \pm 2v_1\sqrt{\frac{2m_3\varepsilon}{2m_3}}) = \frac{m_2}{m_1}E_1(1 \pm \sqrt{\frac{4m_3\varepsilon}{m_2E_1}}) \quad (37)$$

The kinetic energy spread (ΔE) of the ions fragmenting in the FFR of the mass spectrometer caused by the KER is therefore:

$$\Delta E = \sqrt{(\frac{4m_2m_3\varepsilon E_1}{m_1^2})} \quad (38)$$

It can be seen from the equation that the spread of the kinetic energies increases with an increase in the KER, ε, and with an increase in the kinetic energy of the parent ion, E_1. However, the spread in the velocities does not depend on the experimental parameters. Also, it can be shown that the spread in the energy is larger by a factor of m_2v_1 than the spread in the velocity; hence the measurement of the kinetic energy spread is advantageous over the measurement of the velocity spread [94].

Just like the internal energy, the KER is also not a single value, it can rather be described as a distribution, the kinetic energy release distribution (KERD). The KERD can be determined from the shape of the metastable ion peak and the mean value of the KER distribution, <KER>, can be determined from the width of the metastable ion peak [98]. If the shape of the metastable ion peak has a Gaussian distribution, then the KERD will be Maxwell-Boltzmann like, and a temperature can be assigned to it [94].

As mentioned above, KER and KERD are closely related to the structure of the dissociating ion, as well as to the dissociation mechanism, i.e. the potential energy surface of the reaction [94]. In the case of a reaction proceeding through a very loose transition state (no rearrangement), like simple bond cleavages, there is no reverse activation barrier, therefore the excess internal energy, $E^{\#}$, is partitioned among the TS's internal degrees of freedom. Therefore, the KER will be small and reflects the amount of internal excitation of the parent ion. In the case of dissociation with substantial reverse activation barrier, i.e. the TS has a rearranged structure compared to the parent ion, the reverse activation energy is also distributed among the products. Therefore the KER is largely due to the reverse activation barrier, and causes significant widening in the metastable peak.

While the determination of the mean KER (<KER>) requires only simple formalism, the deconvolution of KERD from the peak shape is a more challenging task. There are several theoretical approaches to calculate the KER: the statistical energy partitioning prior to distribution [99], phase space theory (PST) [100], orbiting transition state phase space theory (OTS/PST) [101, 102], finite heat bath theory (FHBT) [42, 103] and the maximum entropy method [104]. The detailed discussion of these theoretical approaches is beyond the scope of this thesis, and the reader is kindly referred to the literature [26, 32, 94, 105, 106]. Of these methods, one of the simplest one is the so-called model free approach of the finite heat bath theory (FHBT) [107] that does not require any knowledge of the potential energy surface of the dissociation. The KERD is calculated with a simple analytical formula:

$$P(\varepsilon) \approx \varepsilon^{l} \exp\left(-\frac{\varepsilon}{k_B T^{\ddagger}}\right) \tag{39}$$

where l is an empirical parameter that ranges from 0 to 1, implying 1 ($l = 0$), 2 ($l = 0.5$) and 3 ($l = 1$) dimensional translation, and $T^{\ddagger}$ is the transition state temperature. These two parameters are optimized when fitting the function to the experimental KERD curves. This form was used in the detailed analysis of the KERD curves of protonated methanol clusters, which is discussed below.

3. Details of the Experiments and the Modeling

The focus of this Ph.D. thesis is on the modeling of the dissociation processes and some of their interesting features; however, the basis of every modeling is the existence of reliable and precise experimental data that it can be compared to. To build models that accurately reproduce experimental data, it is uniquely important to understand the experimental conditions to know of any possible source of errors that the data set might have. The MassKinetics program requires the geometrical parameters of the instrument, the electrostatic potentials on the various lenses and the temperature values to calculate the ion abundances. Therefore, this chapter gives a short description of the experimental work that was done in our group and by collaborations. After introducing the particular experimental setup, each subchapter contains the most important input parameters that were used in the model calculations.

3. 1. Protonated Alkylamine Dimers

Protonated alkylamine dimers were among the first systems studied by MassKinetics [108]. The experimental data was taken from a previous publication by *Norrman* and *McMahon* [88].

A proton-bound dimer of an isotope labeled and an unlabeled amine may lose either an unlabeled or a labeled neutral amine as shown in equations 40 and 41 for the case of methylamine:

$$[CH_3NH_2 \ldots H^+ \ldots CD_3NH_2] \rightarrow CD_3NH_3^+ + CH_3NH_2,\ k_H \quad (40)$$

$$\rightarrow CH_3NH_3^+ + CD_3NH_2,\ k_D \quad (41)$$

These reactions were studied by *Norrman* and *McMahon* using two experimental setups: one on a high-pressure VG 70–70 mass spectrometer, with a B-E instrument configuration [109], the other on a JMS–HX110/HX110A mass spectrometry from JEOL company using a low-pressure chemical ionization.

In the case of VG 70–70 a high-pressure ion source was used by *Norrman* and *McMahon* [88]. It is reasonable to assume that the ions formed in this source have a thermal energy distribution. No temperature dependence of the isotope effects was observed in the 300 – 500K range of source temperatures. As most experiments were performed between 400 and 500 K, an average source temperature of 450 K was used in the modeling. The ions were accelerated to 2900 eV and the protonated dimer was mass-selected by the magnetic field. The metastable fragmentation of this ion was studied by mass analyzed ion kinetic energy spectroscopy (MIKES). From the flight times of the ions given in *Norrman*'s paper, the geometry of VG instrument can be deduced

(length of the flight path up to the field free region (FFR) and the length of the FFR in which fragmentation is observed, to be 1.1 and 0.3 m, respectively). These parameters define the time-scale of the experiments for the ions concerned.

Based on the experimental conditions listed above in the MassKinetics modeling calculations the ions were considered to be formed in the source region at thermal equilibrium (450 K, defining the internal and kinetic energy distributions). Varying the source temperature by 50 K changed the KIE and KER by less than 1 %, in accordance with the experimental findings. The ions are accelerated to 2.9 keV kinetic energy and mass selected in the first part of the instrument. Only the precursor ion (the protonated alkylamine dimer) enters the field free-region, where metastable unimolecular fragmentation takes place. The product distribution at the end of the FFR represents the mass spectrum.

In the JEOL instrument, a low-pressure ionization source was used, from which the ions were accelerated to 10 kV. The instrument geometry was determined from the flight times to be 2.5 m in the FFR and 1.5 m in the FFR. The time-scale was slightly longer on the JEOL compared to the VG instrument. When modeling the experimental results from the low-pressure ionization source, the same input parameter set (distance, potential and temperature values) was used, with slight modification in the accelerating voltage and the flight times.

The fragment ion intensities were measured and the isotope effect, k_H/k_D was determined for each dissociation using the following assumption of the kinetic method as discussed above [82]:

$$\ln\frac{k_H}{k_D} \approx \ln\frac{I_H}{I_D} \approx \frac{\Delta PA}{RT_{eff}} \tag{42}$$

The experimentally determined reaction rate ratios can be found in Table 3. 1 and were used for comparison in our study as it is described in details in the Results and discussion section.

Internal parameters are also needed to describe the molecular ion and the dissociation mechanism when performing reaction kinetics calculations. One of the most important of these is the critical energy of the dissociation, which equals to the reaction enthalpy of the dissociation at 0K. The reaction enthalpies were calculated by *Norrman* and *McMahon* at the MP2/6–31G** level of theory using the Gaussian program package [110]. The vibrational frequencies were scaled with the appropriate scaling factor [111] to account for anharmonicity and inaccuracies of the applied level of theory. The reaction enthalpy (ΔH°) for reaction (40) was calculated to be 26.9 kcal/mol. The reaction enthalpy of (41) can be determined from that of (40) and from the difference of zero point vibrational energies as qualitatively shown in Figure 3. 1. Note that in the calculation only one complex was calculated and rapid interconversion between the two structures was assumed, both because of the much lower isomerization barrier compared to the

dissociation threshold, and because of tunneling involved in the exchange of the hydrogen atom. The ΔH° for reaction (41) is 0.128 kcal/mol (5.56 meV) larger than that for reaction (40). Figure 3. 1 also illustrates that the excess energy ($E^{\#}$) is the difference between the internal energy (E) and the 0 K reaction enthalpy.

Table 3. 1: The *k_H/k_D ratios measured on VG 70–70 and on JMS–HX110/HX110A for dissociation of deuterium labeled metastable proton bound amine dimers. Data were taken from reference [88].*

	k_H/k_D	
B-d_n	VG	JEOL
CD_3NH_2	1.39 ± 0.01	4.1 ± 0.1
CD_3NH-CH_3	1.28 ± 0.01	1.63 ± 0.05
CD_3NH-C_2H_5	1.22 ± 0.01	1.36 ± 0.01
CD_3NH-nC_3H_7	1.19 ± 0.01	1.30 ± 0.01
CD_3NH-n-C_4H_9	1.16 ± 0.02	1.26 ± 0.02
$CH_3CD_2NH_2$	1.16 ± 0.01	1.30 ± 0.01
CH_3CD_2NH-CH_3	1.14 ± 0.01	1.24 ± 0.01
CH_3CD_2NH-C_2H_5	1.12 ± 0.01	1.25 ± 0.01
$CD_3CH_2NH_2$	1.17 ± 0.01	1.18 ± 0.01
CD_3CH_2NH-CH_3	1.15 ± 0.01	1.13 ± 0.01
CD_3CH_2NH-C_2H_5	1.13 ± 0.01	1.13 ± 0.01

For methyl-propylamine and methyl-butylamine, these values were not available, so the critical energies were calculated by an extrapolation based on the other compounds with known reaction enthalpies. The accuracy of these values is estimated to be ± 1 kcal/mol (compared to ± 0.1 kcal/mol accuracy of the ΔH° values quoted in [88]), which means that the calculation results probably does not carry a higher uncertainty that the claimed experimental uncertainty from the mass spectra.

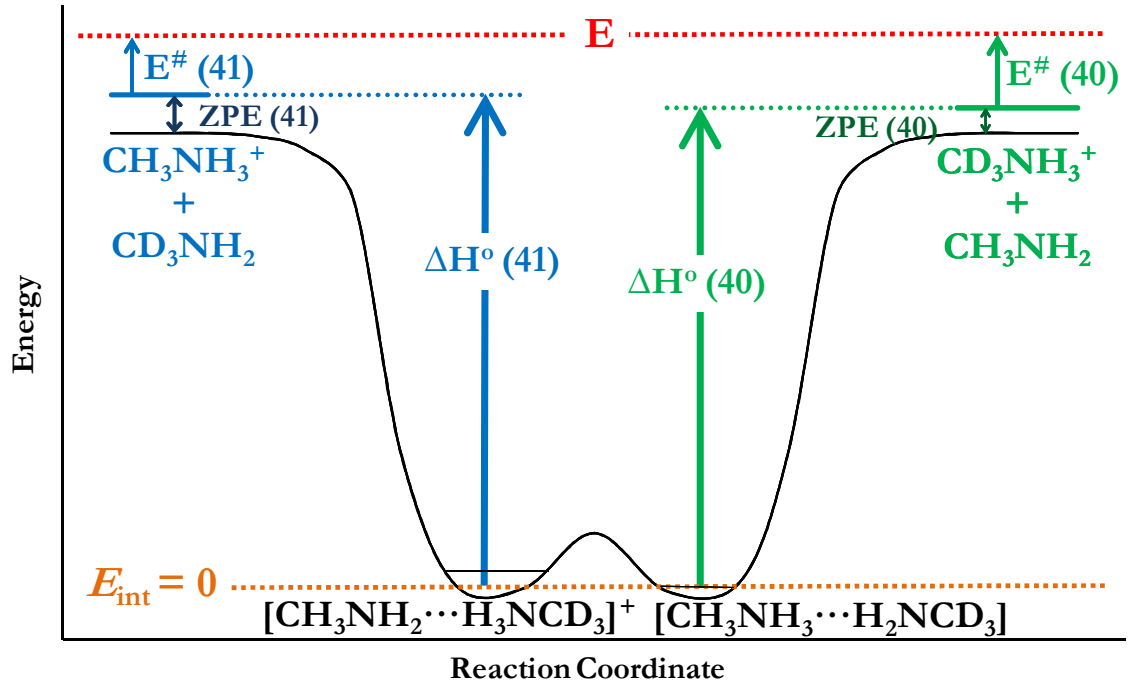

Figure 3. 1: *Schematic potential energy diagram of the fragmentation of protonated methylamine dimers.*

The published effective temperature was determined using equation (42) based on the experimentally measured ion intensities (the reaction rate ratios) and the calculated reaction enthalpy (proton affinity) values. For more specifics on the calculation of the reaction enthalpies and on the details of determining the proton affinity differences, the reader is kindly referred to the original paper [88]. The published effective temperatures can be found in Table 3. 2; these served as a comparison to the effective temperatures that were calculated using MassKinetics.

The next input parameter that is needed is the vibrational frequency set for the molecular ions. Vibrational frequencies of most proton bound amine dimers were also calculated by *Norrman* and *McMahon* at the MP2/6–31G(d,p) level and were kindly provided to us [88]. For the proton-bound dimers of methyl-propylamine, methyl-butylamine, methyl-ethylamine, and diethylamine, these values were determined at the B3LYP/6–31G(d,p) level of theory. For determining ZPEs, the calculated frequencies were scaled using the values suggested in the literature: 0.9608 for MP2/6–31G(d,p) and 0.9806 for B3LYP/6–31G(d,p) [111, 112]. The RRKM calculations and statistical energy partitioning use the molecular ion and product ions vibrational frequencies also, but in these cases, the low frequency modes have a larger influence on the calculated densities of state and, therefore, the scaling factors optimized for low frequency vibrations have been used (1.0229 for MP2/6–31G(d,p) and 1.0013 for B3LYP/6–31G(d,p)) [111].

Table 3. 2: Experimental T_{eff} *(K) for deuterium labeled metastable proton bound amine dimers. Data were taken from reference [88].*

	T_{eff} (K)	
B-d_n	VG	JEOL
CD_3NH_2	194 ± 4	44 ± 1
$CD_3NH\text{-}CH_3$	259 ± 8	128 ± 8
$CD_3NH\text{-}C_2H_5$	285 ± 29	149 ± 7
$CD_3NH\text{-}C_3H_7$	285 + 16	167 ± 5
$CD_3NH\text{-}n\text{-}C_4H_9$	321 ± 12	203 ± 5
$CH_3CD_2NH_2$	367 ± 16	238 ± 7
$CH_3CD_2NH\text{-}CH_3$	431 ± 24	270 ± 17
$CH_3CD_2NH\text{-}C_2H_5$	323 ± 21	204 ± 8
$CD_3CH_2NH_2$	320 ± 18	202 ± 14
$CD_3CH_2NH\text{-}CH_3$	373 ± 27	196 ± 7
$CD_3CH_2NH\text{-}C_2H_5$	366 ± 24	202 ± 14

The next step in setting up the model is to describe the transition state through which the dissociation occurs. Proton-bound dimers and ion–dipole complexes are known to dissociate through loose, product-like transition states [32, 88, 113, 114] and, therefore, can be characterized well by the pre-exponential factor (A) alone. The TS is defined by the molecular frequencies of the products plus five 'cluster modes'. Among them, one corresponds to an internal rotation of the dimer, which is assumed to be unchanged upon dissociation; the frequencies of the other four vibrations are reduced in the TS [99, 115]. Using the value of $\log A = 15$ suggested for proton-bound alcohols, calculations gave good agreement in the case of proton-bound alkylamines, as well [113]. Optimizing the pre-exponential factors of the transition state of reaction (40), the best agreement between the calculated and the measured KIE values was obtained using a $\log A\,(40) = 15.4$. In these optimizations, the value of $\log A$ for reaction 41 is determined simply from $\log A$ (40) and the respective product frequencies, and is not optimized independently. The value of the pre-exponential factor is indicative of a loose transition state [32, 113, 114]. Note that the same $\log A$ (40) was used for all compounds studied in the present paper. To check the influence of this value on the modeling, the calculations were repeated using 10 times larger and 10 times lower pre-exponential factors, as well. As the product frequencies corresponding to the two reaction channels are different, the frequency factors also differ by a small amount. This is an entropy effect and in the case of methylamine, this favors

reaction (40) over (41) by 5.5 %. This is equivalent to a 0.08 $cal \cdot mol^{-1} \cdot K^{-1}$ entropy difference in a thermal system (at 600 K), which agrees reasonably with the 0.1 – 0.2 $cal \cdot mol^{-1} \cdot K^{-1}$ ΔS values that were determined experimentally. Note that the 5.5 % difference in reaction entropy quoted above was calculated for the methylamine-d_3-methylamine dimer, for the other compounds it is slightly different, of course.

The MassKinetics calculations only required data of the instrument geometry, the applied potentials and temperatures, and the *ab initio* critical energies. The published reaction rate ratio values and the effective temperature values were only used in the comparison to the results of the modeling, and therefore they served as a measure of the goodness of the applied model and were not, in any way, part of the optimization process.

3. 2. Protonated Benzylpyridinium Salts and Protonated Esters

The unimolecular dissociation of protonated benzylpyridinium salts and protonated aromatic benzoic esters were studied to examine the internal energy distributions of the molecular and fragment ions at various stages of the fragmentation process. The substituted benzylpyridinium ions include $C_5H_5N^+–CH_2C_6H_4R$ where R = OCH_3, NO_2, CH_3, CN, Cl, F, H CF_3 or I; whereas the protonated substituted aromatic benzoic ester ions are $[C_6H_5COOC_6H_4R]H^+$ where R = CH_3, Cl, OCH_3, Br, H or OH [116].

The fragmentation of benzylpyridinium salts are well characterized and proceed through a simple cleavage of the C-N bond between the substituted benzyl group and the pyridine [71]. The resulting fragments are a substituted benzyl cation and a neutral pyridine; see Figure 3. 2(a). A typical electrospray ionization CID mass spectrum therefore contains two peaks: the molecular ion and the substituted benzyl cation. The intensity ratio of these two peaks was used to calculate the survival yield to study the internal energy distribution of the ions produced by ESI.

In contrast to the fragmentation of the protonated benzylpyridinium ions, the protonated ester ions fragment through a rearrangement reaction, Figure 3. 2(b). Quantum chemical calculations show that the rate-determining step is the formation of the ion-dipole complex, which then decays in a fast dissociation reaction. In ESI, these protonated esters show mainly one fragment ion, $C_6H_5CO^+$ (m/z = 105). However, in some cases, a consecutive fragmentation leading to carbonyl loss (m/z = 77) is also observed for higher cone voltages. In these cases, the sum of these two fragment ions is used for calculating the survival yield values.

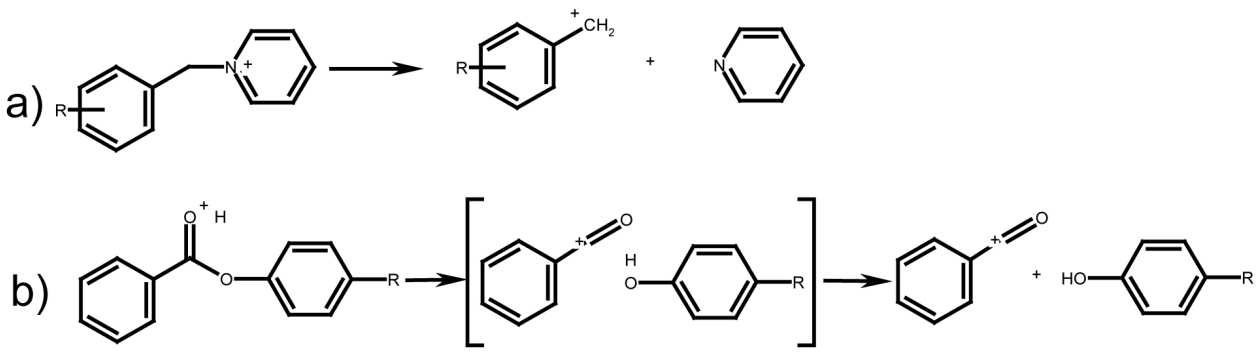

Figure 3. 2: *(a) Dissociation of benzylpyridinium ions involving a direct simple cleavage process. (b) Dissociation of protonated benzyl esters involving a rearrangement process, resulting in the formation of an ion-dipole complex.*

These experimentally determined survival yield curves were used in determining the characteristic temperatures for all the examined pyridinium ions as will be discussed in details in the Results and Discussion chapter: the calculated survival yield values were fitted to the experimentally one to calculate the characteristic temperature.

In our work published in 2005 on protonated benzylpyridinium ions and protonated esters, a Micromass Quattro I triple-quadrupole mass spectrometer was used. The experimental setup consists of an electrospray ionization source, where the sample was sprayed through a metal capillary held at high voltage (4 kV). The ions then passed through the cone and the pre-focusing lenses. Precursor ions were selected in the first quadrupole analyzer followed by an octopole collision cell for the CID experiment. The fragment ions were detected with a transmission quadrupole analyzer.

The geometry parameters of the triple quadrupole (QQQ) setup are discussed below and are also shown in Figure 3. 3: the ions enter the gas phase at point A; and after passing through the 0.10 m long RF-only hexapole, H0, they enter the first quadrupole, Q1, that has a length of 0.25 m. The potential of the cone voltage was either held constant at 35 V or varied in the range 10 – 50 V in the experiments. Note that the exact values of some of the instrumental parameters discussed above influence the results only by a small amount. For example, varying the length of the hexapole from 0.2 to 0.05 m leads to a change of only 5 % in the calculated survival yield. Similarly, changing the voltage on the hexapole from 4 to 10 V, or disregarding the flight time of the ions in the Q1 analyzer, only leads to a less than 5 % change in the calculated survival yield.

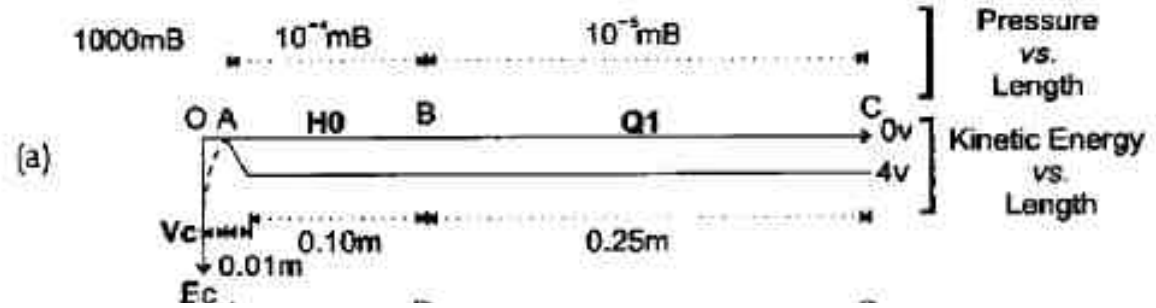

Figure 3. 3: *Schematic geometry of the Micromass Quattro I triple-quadrupole instrument used in the experiments.*

Collision-induced dissociation experiments were performed using N_2 collision gas with an average pressure of $5 \cdot 10^{-3}$ mbar. In this setup, the molecular ions were selected by the first quadrupole and then, as they were passing through the collision cell, they underwent collisions and the resulting fragment ions were scanned by the third quadrupole analyzer. In some cases, where a specific fragmentation channel was monitored, the third quadrupole was set to only allow through the selected fragment ion instead of scanning a whole mass range. This enables higher sensitivity and faster data acquisition. In the case of protonated benzylpyridinium and ester ions, the following parameters were used to model the CID experiment: the pressure of the target gas, N_2, cannot be set accurately in the collision cell, therefore, it was used as an adjustable parameter; the acceleration voltage was varied in the MassKinetics calculations; the cell length was taken as 10 cm; the collisional energy transfer efficiency had an average of 30 % assuming an exponential distribution, and the collisional cross-section was calculated to be 30 $Å^2$ (uniform value for the benzylpyridinium salts and the ester ions).

The above discussed experimental conditions were used as input parameters in the modeling calculations: source temperature, instrument geometry (flight time), cone voltage potential, collision gas type and pressure. The input parameters describing the fragmentation energetics and mechanism were determined by quantum chemical calculations.

In the case of the benzylpyridinium ions, and the aromatic benzoic ester ions, the critical energies were published numerous times, but they were also recalculated at the B3LYP/6–31G* (B3LYP/3–21G* for molecules containing iodine atom) level of theory using the Gaussian program package [117] due to the additional molecules studied. Since the dissociation reactions of the benzylpyridinium ions are characterized by no reverse activation barriers, the critical energies were defined as the difference in the heats of formation of the products and the reactants as shown in Figure 3. 4. These values are listed in Table 4. 1 together with the results of the modeling calculations, for easier comparison. In the case of the protonated ester ions, due to

the significant reverse activation barrier, critical energies are not equal to the difference in the heats of formation, rather they were determined from quantum chemical calculations on the saddle point representing the transition state.

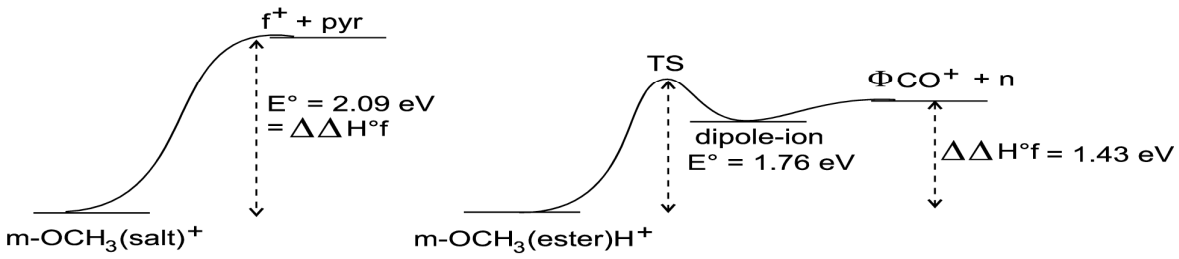

Figure 3. 4: *Fragmentation processes for benzylpyridinium and benzoic ester ions.*

The frequency models of the protonated benzylpyridinium ions and protonated ester ions were calculated at the B3LYP/6–31G* (B3LYP/3–21G* for molecules containing iodine atom) level of theory. The transition states were characterized by pre-exponential factors: in the case of the benzylpyridinium ions, log$A$ = 14 was based on values published in the literature values [21]. Transition states for the fragmentation of the ester ions were determined by quantum chemical calculations at the same level of theory as above, using the gradient techniques implemented in this software.

It is assumed that the initial internal energy distribution of the protonated benzylpyridinium ions is a thermal distribution at the source temperature (353 K), shown in Figure 3. 5 with a mean internal energy of approximately 0.35 eV, which is in accordance with previously published results [25].

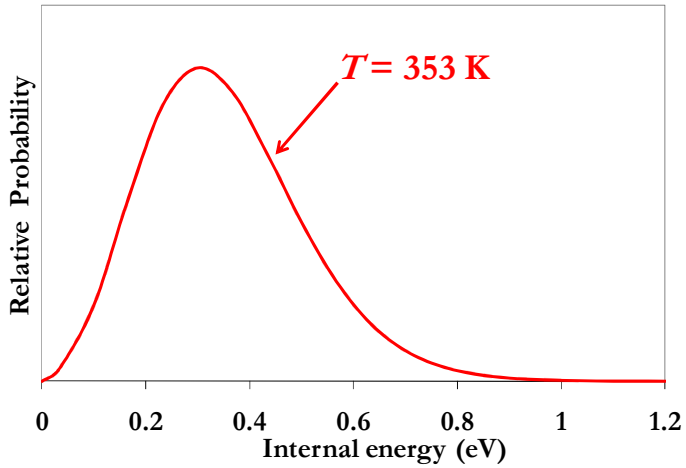

Figure 3. 5: *Initial thermal energy distribution at 353 K.*

3. 3. Protonated Methanol Clusters

Low-Temperature fast atom bombardment (FAB) experiments were performed to study protonated methanol clusters using a VG–ZAB2–SEQ double-focusing mass spectrometer [118]. A 10 μL droplet of methanol was deposited on the stainless-steel probe tip and frozen in liquid nitrogen. The sample, kept in cool nitrogen vapor, was quickly moved into the ion source and was ionized by FAB. Cesium ions of 30 keV kinetic energy were used as the bombarding agent, the nominal mass resolving power was 2000 (10 % valley definition), the accelerating voltage was 8 kV, which was used as the kinetic energy of the ions in the modeling. The flight path in the first field free region plus the magnetic analyzer of the VG–ZAB2–SEQ instrument is 1.0 m; the length of the second field free region is 1.5 m. These distances were taken from the experimental setup and used to calculate the time-frame of experiments. Metastable ion spectra were obtained by the MIKES technique, selecting a given cluster using the magnetic sector, observing fragmentation in the second field free region and determining the fragmentation products by scanning the electrostatic analyzer. To obtain good signal-to-noise ratios, the metastable peak profiles were determined averaging a large number of scans (5 – 10 minutes of overall acquisition time) in a narrow energy-window. All studies were performed under metastable ion conditions; and no collision gas was introduced. The absence of a CID component was carefully checked for, by putting an extra voltage on the collision cell. Analysis of metastable peak profiles was performed using the "META" computer program developed in our laboratory [98].

The low-temperature FAB technique was found to generate large, protonated clusters (up to $n = 15$), as shown in Figure 3. 6 [119, 120]. Methanol clusters (predominantly $(CH_3OH)_nH^+$ ions) show a wide size-distribution: clusters as large as $n = 30$ are observed. At large cluster size ($n > 8$), mixed methanol–water clusters also start to appear [$(CH_3OH)_n(H_2O)H^+$] and, with increasing cluster size these become more abundant. The predominant fragmentation of protonated methanol clusters is the loss of a single methanol molecule:

$$(CH_3OH)_nH^+ \rightarrow (CH_3OH)_{n-1}H^+ + CH_3OH \qquad (43)$$

Metastable fragmentations of all clusters ion between $n = 2$ and $n = 20$ have been detected, and they were examined in detail up to $n = 15$; some selected clusters have also been studied using CID. All of the cluster ions between $n = 3$ and 20 show the loss of a methanol monomer, this being the only metastable process. The only metastable process of the protonated methanol dimer, somewhat surprisingly, is the loss of a water molecule due to an intra-molecular rearrangement (formation of a protonated dimethyl ether) [121]. In CID, consecutive loss of two methanol molecules is also observed. For larger clusters (which have a relatively long high-

internal-energy tail) it was observed that there was loss of a methanol monomer in the first field-free region followed by the loss of another methanol monomer in the second field-free region.

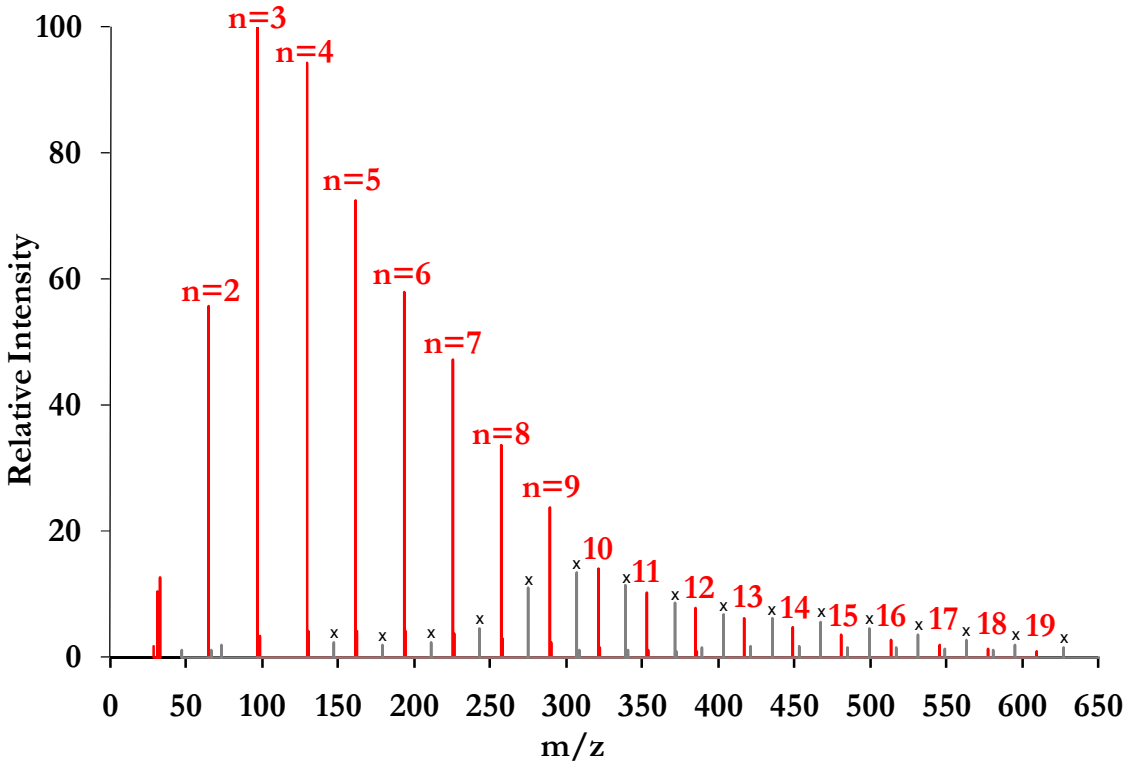

Figure 3. 6: *Low-temperature fast atom bombardment mass spectrum of protonated methanol clusters. The numbered peaks correspond to* $(CH_3OH)_nH^+$ *clusters, the ones labeled with x correspond to mixed water–methanol* $(CH_3OH)_i(H_2O)_jH^+$ *clusters.*

Determination of the mean KER value, in the case of an exactly Gaussian-shaped metastable peak, is fairly straightforward (see the equations discussed in the theory section), requiring only accurate measurement of the peak width. Determination of the KERD is much more demanding, requiring measurement of the metastable peak shape with very good signal-to-noise ratio. Mainly for this reason, KERD curves for larger clusters are difficult to determine experimentally and are rarely published. The abundant clusters produced by low-temperature FAB yielded metastable peaks with high sensitivity, as illustrated for the fragmentation of $(CH_3OH)_{15}H^+$ in Figure 3. 7. The signal-to-noise ratio is sufficiently good to determine the KERD for this fragmentation process from the peak shape (Figure 3. 7). To the best of our knowledge, this is the largest cluster for which a kinetic energy release distribution has been measured.

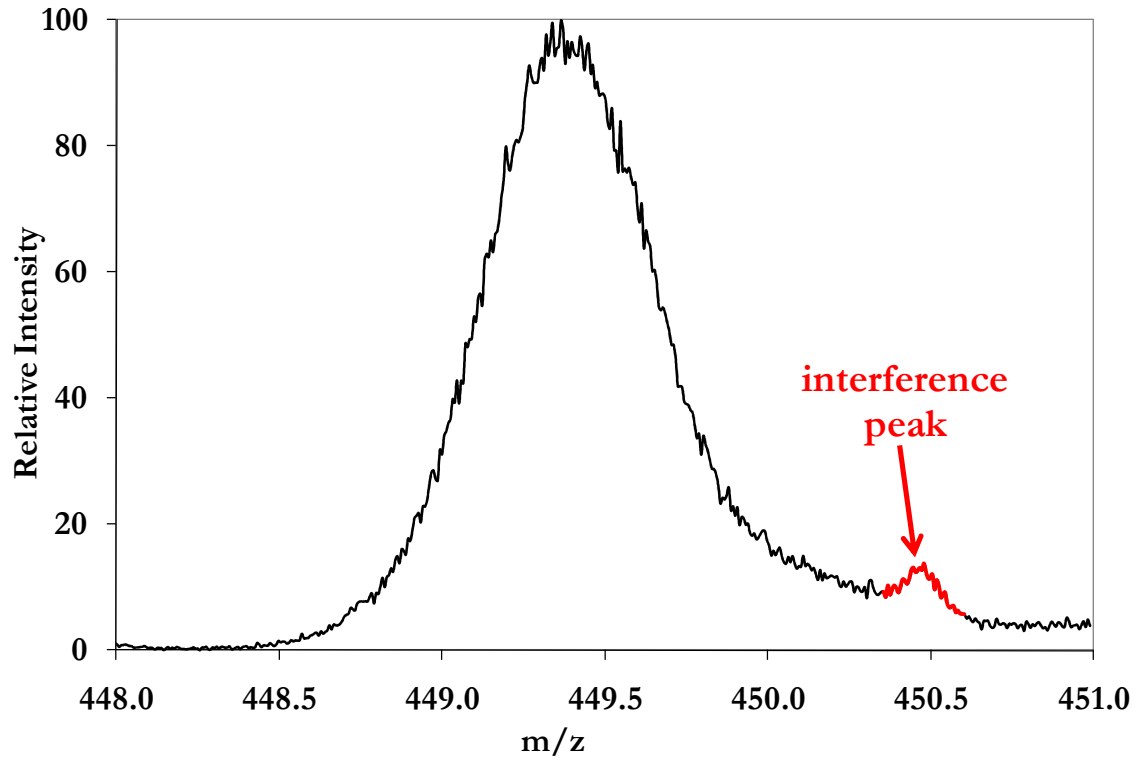

Figure 3. 7: *Metastable peak profile corresponding to methanol loss from $(CH_3OH)_{15}H^+$. The small peak at $m/z = 450.5$ is due to an interference process.*

The critical energies of the dissociation of the various clusters were taken from the literature [122], and were used for the modeling. The vibrational frequencies for the parent and product ions and for the neutral products were calculated at the B3LYP/6–31G* level of theory.

Similarly to the protonated amine dimers (see above), proton-bound molecular clusters are known to dissociate through loose, product-like transition states, which can often be characterized by a single parameter, the Arrhenius-type pre-exponential factor (A). This assumption was employed for the protonated methanol clusters, and the same $\log A$ of 15.4 was used for all clusters, as taken from the literature [108, 123]. It was found that changing A by one order of magnitude had less than 1 % influence on the calculated KER and ion intensity values.

The protonated methanol clusters inside the ion source were also assumed to have a thermal internal energy distribution and the results were calculated as a function of this temperature.

3. 4. Protonated Leucine Enkephalin

There have been seven major attempts by pioneering research groups to determine energetic parameters on the best-studied fragmentation process, the formation of the $\mathbf{b_4}^+$ ion from protonated leucine enkephalin, through the lowest-energy fragmentation channel of the

precursor ion. The various experimental techniques are summarized in Chapter 2; here, I would like to give a short explanation of the published raw experimental data, which were used in the re-analysis [31, 54, 74-79]. In general, whenever it was possible the original ln$k$ vs. $1/T$ data set was used directly from the publication. If this was not available, a conversion procedure described below was done to get the published results in a desired format. Also, a summary of the published Arrhenius-type activation energies (E_a) and pre-exponential factors (listed as log$A$) are discussed and shown in Table 3. 3.

Data in the paper published by *Wysocki* and coworkers were published in the form of ln$k$ vs. $1/T$, therefore, these data could be used to construct the Arrhenius plot without further conversion [80]. Their analysis resulted in a 38.3 kcal/mol (1.66 eV) activation energy and a pre-exponential factor of log$A$ = 15.7. The large pre-exponential factor suggests a very loose transition state.

In the paper by *Vékey* et al., ion intensity ratios were published as a function of collision energy [76]. To get the temperatures from the collision energies, a collision energy transfer efficiency of 17 % were used as indicated in the original paper. The initial average thermal energy was estimated to be 1.72 eV, which corresponds to a temperature of 425 K. The sum of the initial internal energy and the collision energy contributions yields the mean internal energy, which was then converted to a temperature value using a predetermined function. The ion intensity ratios were converted to reaction rate data using the known ion flight times. The RRKM modeling performed by the authors showed that the results could be evaluated with various combinations of critical energies and pre-exponential factors: the activation energy was determined to be 1.56 ± 0.22 eV with various pre-exponential factors of up to 15.5. So far, the results from the two independent methodologies were in excellent agreement.

Williams and coworkers published their BIRD experimental results in the form of ln$k$ as a function of experimental temperature; their numbers were used without any conversion [77]. They have evaluated the results with a conventional Arrhenius plot to yield the activation energy and the pre-exponential factor. For the $\mathbf{b_4}^+$ ion formation, these values are E_a = 1.11 ± 0.06 eV and log$A$ = 10.7 ± 0.6. Besides the b_4^+ ion, another low-energy process, the water loss, has also been studied and yielded a E_a = 0.99 ± 0.07 eV and log$A$ = 8.7 ± 0.8. These experimental results most likely do not contain any serious systematic errors, and up to this point, these results are probably the most reliable results, and are often cited in various comparisons. The pre-exponential factor indicates a tight transition state, which is characteristic of a rearrangement reaction, in good agreement without present understanding of the **b** ion formation mechanism [124, 125].

Like the *Williams* and *Wysocki* groups, *McLuckey* and coworkers published the natural logarithm of the reaction rates as a function of the experimental temperature [75]. Hence these were, again, used without any conversion. The published Arrhenius dissociation parameters were E_a = 1.28 ± 0.08 eV and log$A$ = 12.55 ± 0.87; which are approximately halfway between those of *Wysocki* and *Williams*.

DePauw and coworkers published the ln$k$ data as a function of the effective temperatures [78]. The data for leucine enkephalin have been evaluated in terms of two different fragmentation channels; both lead from MH^+ to the $\mathbf{b_4}^+$ ion. The process that operates at a higher internal energy is characterized by E_a = 0.99 ± 0.04 eV and log$A$ = 9.25 ± 0.4, and the one that predominates at a lower effective temperature by E_a = 0.945 ± 0.01 eV and log$A$ = 9.12 ± 0.09. The possibility of significant systematic errors must be considered due to the above mentioned various assumptions and a calibration process.

Most recently, SID experimental data was published by *Laskin*: fragmentation-efficiency curves were recorded, and internal energy dependent reaction rates were established using RRKM theory [31]. The internal energy was converted to temperature using the above mentioned function and was used in the overall re-analysis work. The RRKM modeling resulted in critical energies, E_0, critical entropies, $\Delta S^{\#}$, and pre-exponential factors for various dissociation channels. Their results for $\mathbf{b_4}^+$ ion formation yields E_0 = 1.14 eV, $\Delta S^{\#}$ = –14.7 eu, and log$A$ = 10.17 calculated at 450 K.

The published Arrhenius dissociation parameters are summarized in Table 3. 3. It clearly shows major controversies among the results: E_a values range from 0.94 to 1.66 eV that is an unexpectedly (and unacceptably) large range. The standard deviation among these values is 0.25 eV, which is in clear contrast to the accuracy/reproducibility of results quoted in most publications. The published pre-exponential factors (which reflect whether the transition state is "loose" or "tight") also span a large range (log$A$ values from 9.1 to 15.7).

For the RRKM modeling, besides the critical energy and pre-exponential factor, other parameters are also needed: (a) for collision cross-section, we took a recently published ion-mobility experimental result [126] of 162 Å^2 as the best available data; (b) for collisional energy transfer efficiency, the previously used value of 12.8 ± 2.1 % was applied in the modeling calculations [127] and an analytical formula adapted from *Armentrout*'s experimentally determined collisional energy distribution was used for calculating the energy distribution after the CID process [57]; (c) the vibrational frequencies were determined at the B3LYP/3–21G* level and the optimized structure corresponds to a low-lying conformer (obtained by full geometry optimization, but without detailed conformation analysis). The accuracy of the listed vibrational

frequencies should be sufficient for these model calculations; (d) the transition state was described by the pre-exponential factor.

Table 3. 3: *Activation energies and pre-exponential factors of the $MH^+ \rightarrow b_4^+$ fragmentation process of leucine enkephalin. Error margins are shown as reported in the original publications. The average of the various results and their standard deviation are also indicated.*

			Experimental values (from the literature)		
Source	**Method**	***n*** [a]	**Activation energy**[b]	**log *A***	T_{exp} [c]
[74]	ESI/Thermal decomposition	13	1.66	15.7	600-680
[76]	SID/RRKM	10	1.56 ± 0.22	15.5[e]	400-450
[77]	Blackbody Infrared Radiative Dissociation (BIRD)	5	1.11 ± 0.06	10.7 ± 0.6	429-476
[75]	Quadrupole ion trap, thermal activation	6	1.28 ± 0.08	12.55 ± 0.87	458-493
[54]	Infrared multiphoton dissociation (IRMPD)		1.12 – 1.46	9 – 16	298-406
[79]	Infrared multiphoton dissociation (IRMPD)	5	1.09	10.74[e]	400-600
[78]	Quadrupole ion trap, resonant activation	4	0.99 ± 0.04	9.25 ± 0.4	365-480
[78]	Quadrupole ion trap, resonant activation	3	0.945 ± 0.01	9.12 ± 0.09	500-600
[31]	Time- and energy-resolved SID/RRKM	25	1.14[d]	10.17	450
	Average and std. deviation of the 9 values listed above		***1.21 ± 0.25***	***11.8 ± 2.5***	***489 ± 74***

[a] *number of experimental points at different temperatures and/or internal energies used in the original publication*
[b] *in eV units*
[c] *in K*
[d] *critical energy*
[e] *estimated or literature value, not determined or optimized*

4. Results and Discussion

4. 1. Energy Distributions

As it was already shown in the beginning of Chapter 2, the internal energy is one of the most important factors influencing the mass spectrum. Therefore, it is of great importance to know this parameter in order to successfully model ion intensities and related processes. Protonated benzylpyridines, protonated ester ions and protonated alkylamine dimers were selected to determine the internal energy and its distributions for ions produced by electrospray ionization.

4. 1. 1. Protonated Benzylpyridinium and Benzoic Ester Ions

Protonated benzylpyridinium ions were used to determine the internal energy and its distribution. After the ion formation, the ions are assumed to have a thermal (Boltzmann) energy distribution at the source temperature (353 K). The corresponding Boltzmann distribution was calculated with MassKinetics, and the resulting curve is shown in Figure 4. 1 (red line), which is the same as earlier, in Figure 3. 5. Note that at this temperature, the mean internal energy is rather small (0.35 eV) and is not enough for dissociation. The ions then undergo collisional activation in a small place behind the cone lens with nitrogen as the collision gas. In the MassKinetics calculations, multiple collisions were taken into account, with an average of 30% collisional energy transfer efficiency. Since the total number of collisions is determined based on the length of the high-pressure region, the pressure, and the assumed collision cross sections together, any one of these three parameters can be chosen for empirical adjustments; in our calculations, the collisional gas pressure was varied. Our MassKinetics calculations show that the collisions in the ionization source increase the internal energy, and broaden the distribution significantly. This effect is demonstrated by calculating the internal energy distribution after 20 and 40 collisions, from which a corresponding temperature can be determined. After 20 collisions, the internal energy distribution is as shown in Figure 4. 1 (green circles), which is very close to the thermal energy distribution at 790 K (sold green line). After 20 more collisions, the internal energy is further increased, as shown by the blue circles in Figure 4. 1. The E_{int} distribution in this case, that is, a thermal energy distribution at 353 K plus the additional internal energy supplied by the collisions, can be fit with a thermal energy distribution, in which the characteristic temperature is found to be 1210 K. This thermal energy distribution is shown by a solid blue line in Figure 4. 1.

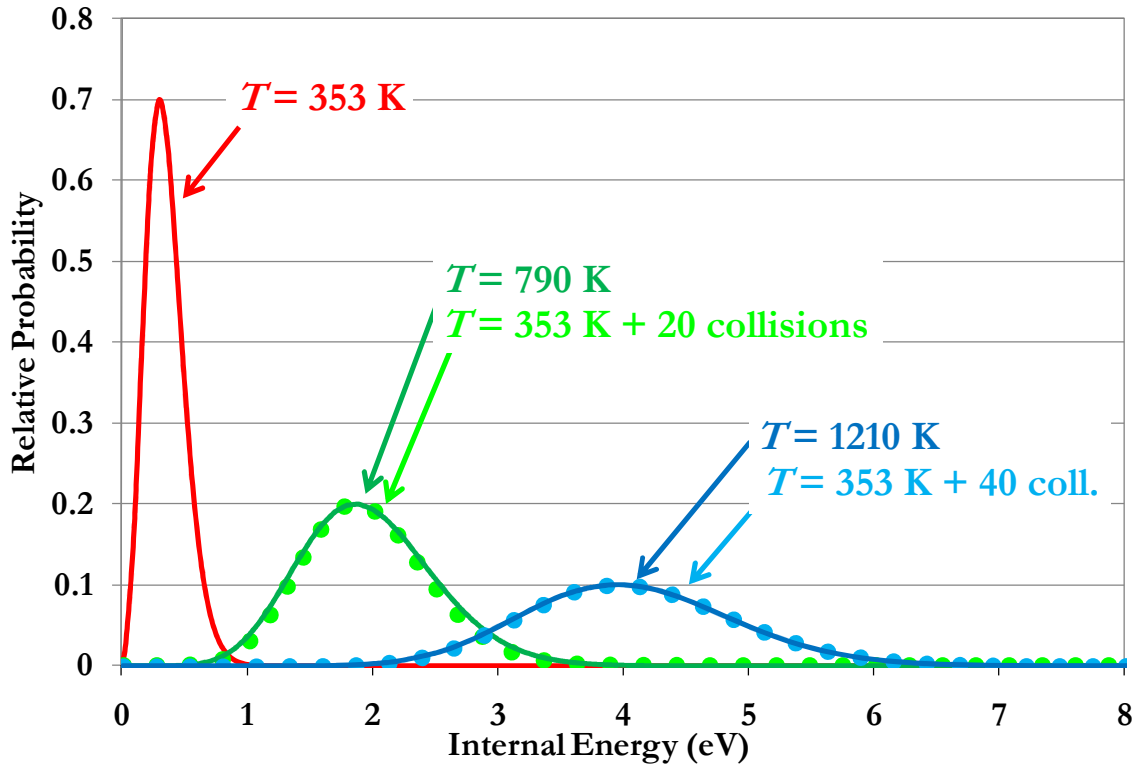

Figure 4. 1: *The initial thermal internal energy distribution (353 K), and the internal energy distributions after different number of collisions. Internal energies assuming a characteristic thermal distribution are also shown with solid lines.*

The most important finding of these model calculations, and the main message of Figure 4. 1 is that the energy distributions observed after a number of collisions in the source closely resemble thermal energy distributions at much higher temperatures. Although the ions in the mass spectrometer are not in a thermal equilibrium, the internal energy distribution can still be characterized by a temperature, which we call the characteristic temperature, T_{char}, of the ions.

Next, representative fragmentation rates were calculated as a function of the internal energy and are shown in Figure 4. 2. The residence time of the ions in the mass spectrometer until the first quadrupole can be calculated from the instrument geometry, and is equal to 58 and 62 μs for methoxy-substituted benzylpyridinium ions and ester ions, respectively. The approximate rate constant necessary to produce abundant fragment ions is in the order of magnitude of the reciprocal of the residence time, $k \approx 2 \cdot 10^4\ s^{-1}$. The internal energy corresponding to this rate constant can be determined from the rate constant curves in Figure 4. 2; this energy is the appearance energy (AE). The appearance energy – as expected – is much larger than the critical energy (ca.1.38 – 3.28 eV); the difference between $E_{app} - E_0$ is one measure of the kinetic shift, as discussed above.

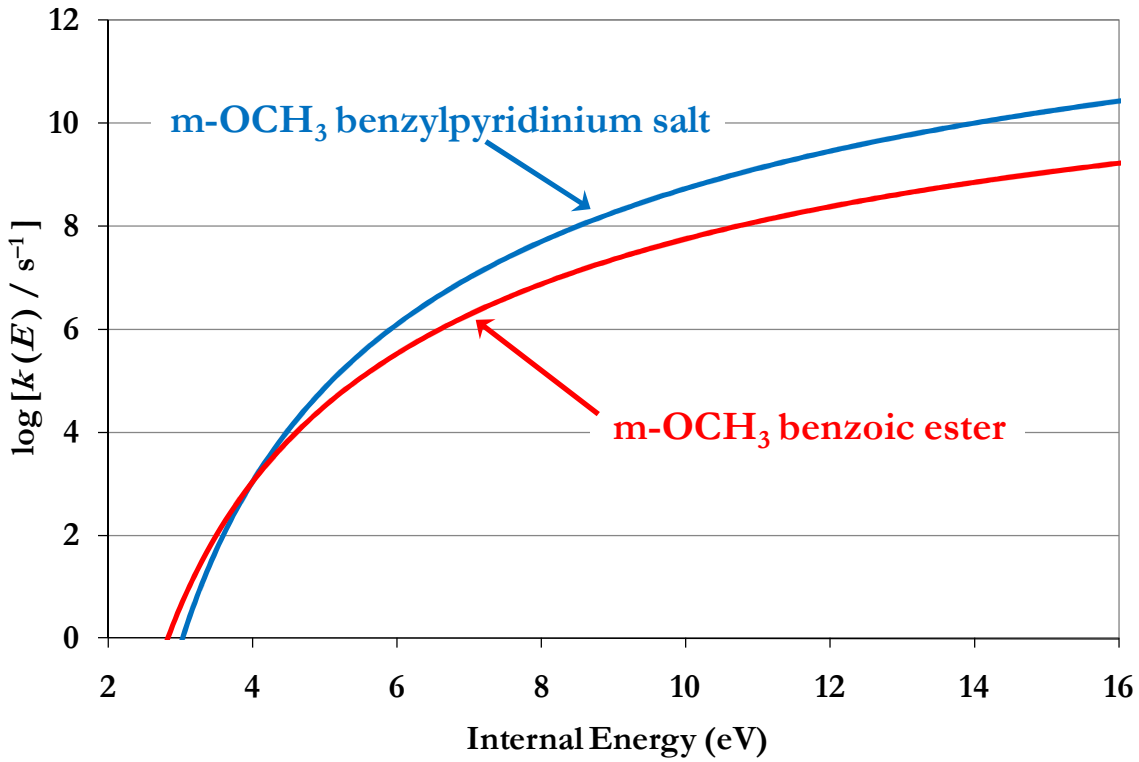

Figure 4. 2: *Calculated dissociation rates curves for the m-methoxy-substituted benzylpyridinium ion and for the m-methoxy-substituted benzoic ester ion.*

In the next step, the characteristic temperatures were determined using MassKinetics program for the benzylpyridinium ions by fitting the calculated survival yields to the experimentally determined values. Two compounds, the *p*-OCH_3 and *p*-NO_2 derivatives, are characterized by the lowest and the highest critical energies (1.55 and 2.55 eV, respectively), and the survival yields are 0.8 % and 54 %, respectively. The determined characteristic temperature values are fairly high, which is an indication of many collisions as discussed above, and are similar for all compounds: the mean value is 1524 K with a standard deviation of 98 K (see Table 4. 1). Note that the *p*-methoxy-substituted benzylpyridinium molecular ion is almost completely decomposed (SY < 2 %) at cone voltages > 30 V, so the characteristic temperature could not be determined accurately in this case.

Table 4. 1: *Number of degrees of freedom, calculated critical energies, ΔH_f of the fragmentation reaction, appearance energies, survival yields, characteristic temperatures and mean internal energies of the precursor ions.*

Compound	**DOF**	E_0 **(eV)**	ΔH_f **(eV)**	**EA (eV)**	**SY (%)**	T_{char} **(K)**	$<E_{int}>$ **(eV)**
p-I salt	69	2.44	2.44	5.07	0.177	1652	5.60
p-Cl salt	69	2.04	2.04	3.93	0.107	1478	4.73
p-F salt	69	2.05	2.05	4.14	0.081	1563	5.12
H salt	69	2.17	2.17	4.27	0.095	1616	5.23
p-CN salt	72	2.38	2.38	5.12	0.292	1542	5.29
p-NO_2 salt	75	2.55	2.55	5.83	0.544	1495	5.42
o-CH_3 salt	78	2.00	2.00	4.07	0.071	1460	5.10
m-CH_3 salt	78	2.08	2.08	4.37	0.111	1482	5.17
p-CH_3 salt	78	2.10	2.10	4.60	0.040	1620	6.00
p-CF_3 salt	78	2.37	2.37	5.57	0.554	1389	5.03
m-OCH_3 salt	81	2.09	2.09	4.60	0.109	1467	5.43
p-OCH_3 salt	81	1.55	1.55	2.93	0.008	-	-
p-Cl ester	72	1.75	1.22	4.31	0.093	1464	5.10
m-Br ester	72	1.75	1.22	4.15	0.054	1480	5.20
H ester	72	1.73	1.35	4.11	0.110	1439	4.80
p-OH ester	75	1.71	1.48	3.81	0.032	1437	5.10
p-CH_3 ester	81	1.71	1.44	4.68	0.265	1329	4.77
m-OCH_3 ester	84	1.76	1.43	4.77	0.186	1347	5.10
p-OCH_3 ester	84	1.70	1.52	3.61	0.086	1273	4.81

Together with determining the characteristic temperatures, the internal energy distributions of the pyridinium molecular ions prior to decomposition were calculated and are shown in Figure 4. 3. The distributions are fairly similar for all benzylpyridines, with the *p*-chloro and *p*-methyl compounds as the two extremes. The mean internal energies, $<E_{int}>$, were found to be close, with an average value of 5.3 eV and a standard deviation of 0.3 eV, and are also listed in Table 4. 1. Note that previous experimental studies [71] on the internal energy distributions produced by electrospray ionization and also, results of MassKinetics modeling discussed above indicate that the ion internal energies are close to thermal distributions.

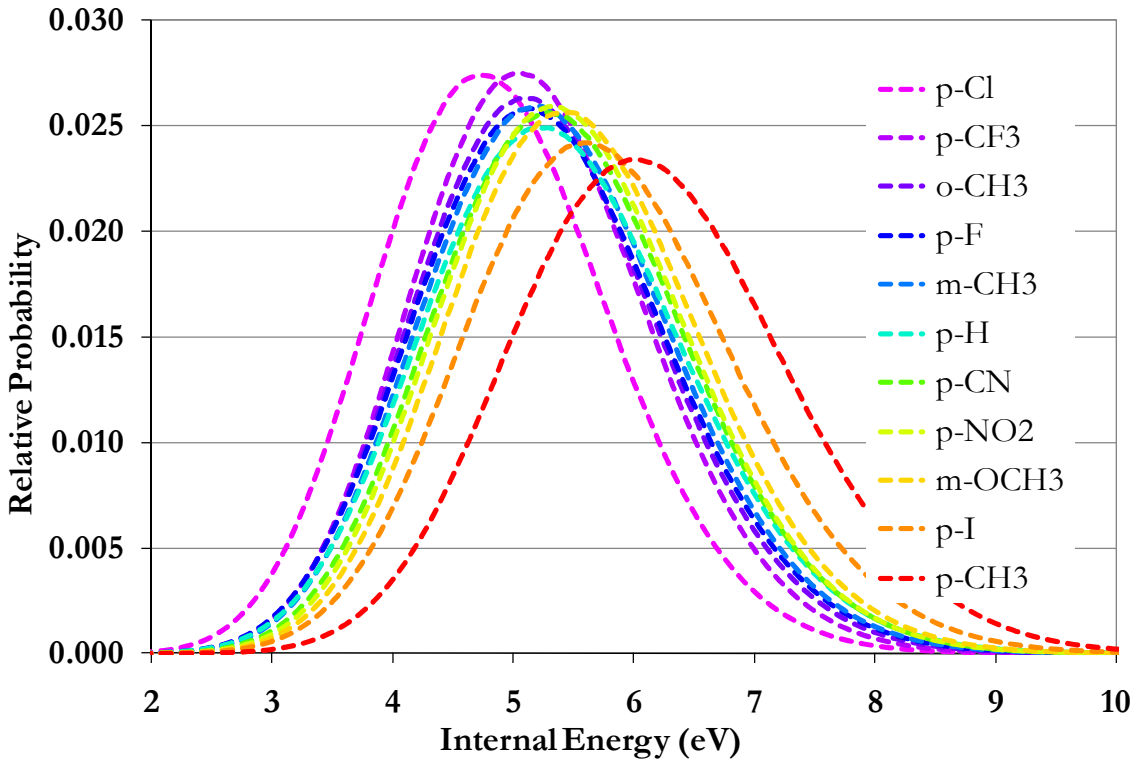

Figure 4. 3: *Internal energy distributions of substituted benzylpyridinium ions*

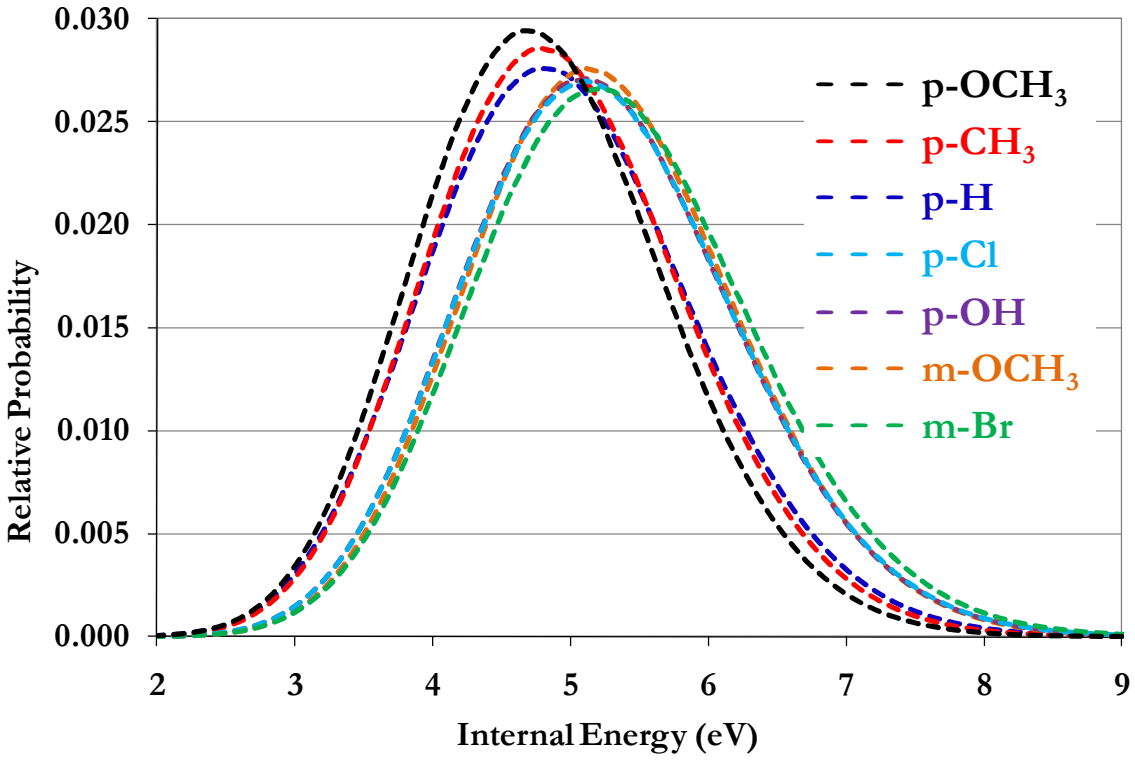

Figure 4. 4: *Internal energy distributions of the protonated benzoic ester ions*

Similarly to the case of the protonated benzylpyridinium ions, the internal energy distributions of the protonated benzoic esters were calculated: those obtained at 35 V cone voltage are shown in Figure 4. 4. For the ester ions, the resulting characteristic temperatures (on average 1400 K) and mean internal energies (5.0 eV) are very close to those determined for the benzylpyridines.

As discussed previously, the internal energy distributions were calculated for the pyridinium and benzoic ester ions. From the individual internal energy distributions the average internal energy distributions for the benzylpyridinium and for the benzoic ester ions were determined and are shown in Figure 4. 5. The average internal energy distributions for the two groups are roughly the same, with less than 0.5 eV difference in the mean internal energy value. This result conformed the previous assumption that the electrospray ion source produces roughly the same initial internal energy distributions for systems with similar degrees of freedom but different dissociation mechanism.

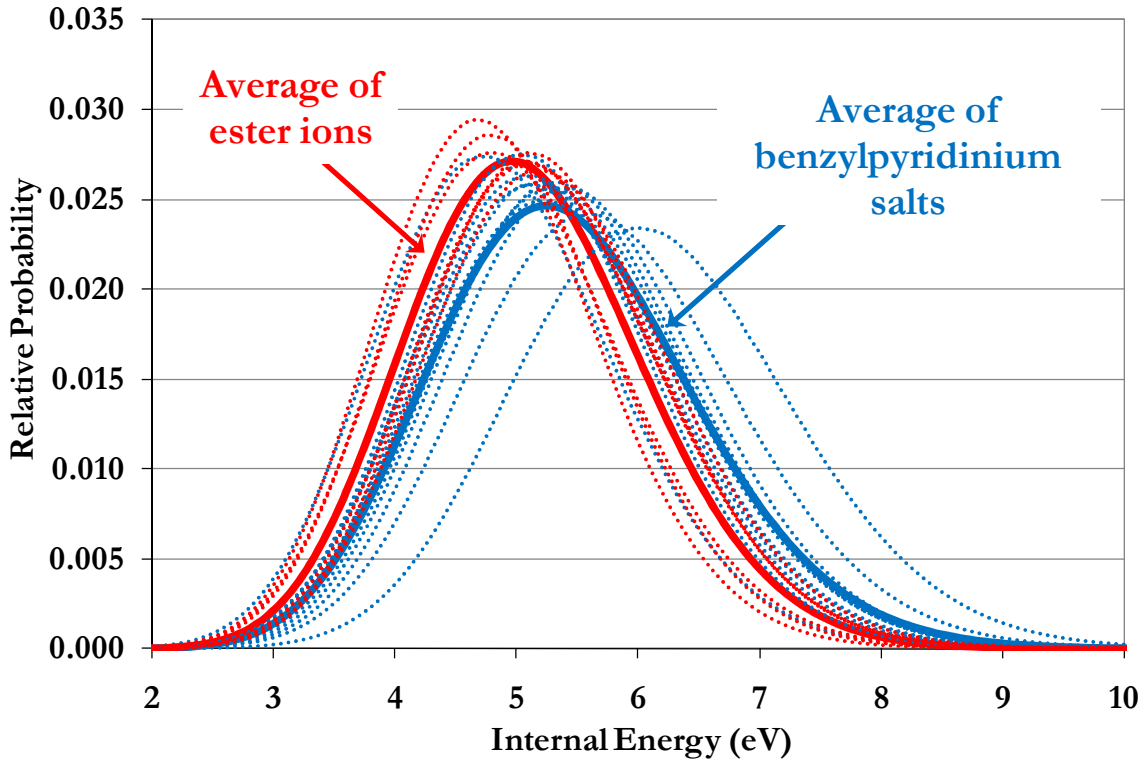

Figure 4. 5: *Internal energy distributions of benzylpyridinium ions, and the esters.*

Note that although the experimentally found survival yields vary significantly for the benzoic esters, the critical energies are in a narrow range (Table 4. 1). This suggests that the different degree of fragmentation is due to the different transition state properties. This statement can be made semi-quantitative by checking the correlation between the survival yields and the critical energies. Because of the form of the Arrhenius equation (as the assumption of a thermal energy

distribution holds) and the integrated form of the first-order rate equation, the logarithm of the SY should be proportional to the logarithm of the critical energy – at the same characteristic temperatures and with similar transition states. Indeed, Figure 4. 6 shows that in the case of the benzylpyridinium salts, there is a much stronger correlation between the experimental survival yields and the critical energies than for the benzoic esters. (In fact, the two outlier points are the p-Me and p-Cl species mentioned earlier.) Therefore, the degree of fragmentation of the different substituted benzylpyridinium salts seems to vary due to the variations in the critical energies, whereas in the case of the esters, it is the different transition states that lead to the different degrees of fragmentation.

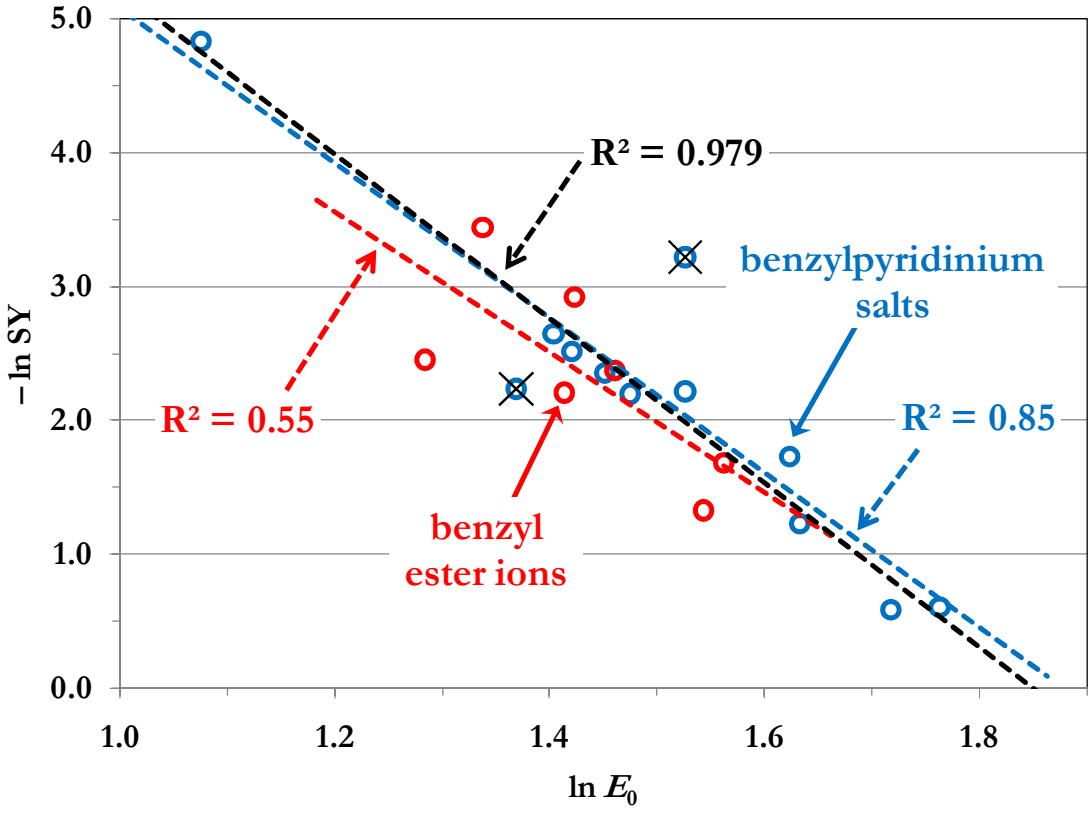

Figure 4. 6: *The logarithm of the survival yield as function of the logarithm of the critical energy for protonated benzylpyridinium (blue) and benzoic ester ions (red). Without the two outliers (black cross), the fit is almost perfect for the benzylpyridinium ions.*

Until this point, all the calculations studying the internal energy distributions were performed at a 353 K source temperature and a 35 V cone voltage. However, because of the many collisions in the source region, the internal energies can vary due to the cone voltage; therefore the effect of the cone voltage on the characteristic temperatures and the mean internal energies was investigated

using our two model systems. The mean internal energies of the protonated benzylpyridinium and the benzoic ester ions as a function of cone voltage are shown in Figure 4. 7.

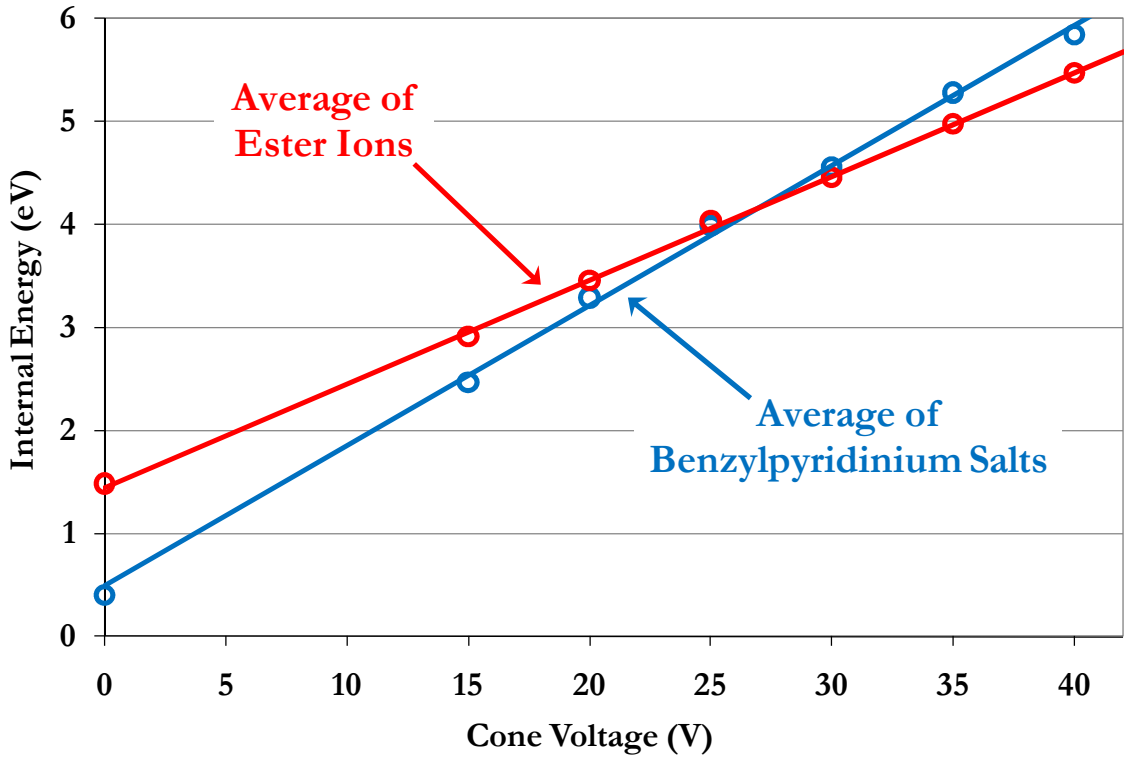

Figure 4. 7: *Average of mean internal energies of benzylpyridinium ions and of ester ions as a function of the cone voltage.*

As expected, the internal energy increases with the cone voltage, due to the higher energy collisions. It is quite interesting that the internal energy is very similar for all of the compounds studied here, and does not seem to depend strongly on the ion structure. Therefore, using fixed source conditions, all the ions have the similar mean internal energies, which are distributed among the various oscillators (DOF). The source does not behave as a thermostatic bath and the ions with different DOF are characterized by different temperatures. This is illustrated in Figure 4. 8, where the DOF, i.e. number of atoms are shown as a function of the characteristic temperature: the linear relationship is clearly noticeable.

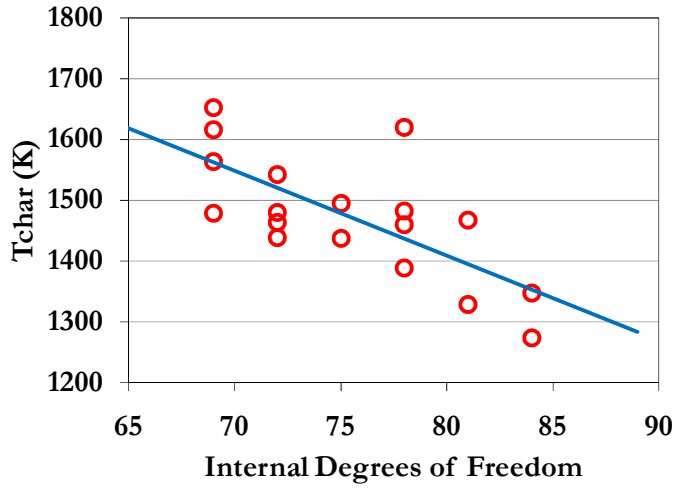

Figure 4. 8: *Number of degrees of freedom as a function of the determined characteristic temperature for protonated benzylpyridinium and benzoic ester ions.*

Another important conclusion from Figure 4. 7 is the apparent linear correlation between internal energy $<E_{int}>$ and the cone voltage, which suggests similar number of collisions – assuming constant collisional energy transfer efficiency – independent of the cone voltage. This linear dependence of the mean internal energy $<E_{int}>$ on the cone voltage was also supported by MassKinetics model calculations, in which the internal energy was determined using the pressure as an adjustable parameter, and the acceleration voltage scanned in the range of 10 – 50 V. A further interesting feature of this diagram is linear extrapolation to zero cone voltage. These values are 1.4 and 0.5 eV for the protonated ester ions and benzylpyridinium ions, respectively. These values are close to the thermal energy of the respective ions at the source temperature of 353 K for benzylpyridinium ions (0.3 eV). For the ester ions, the extrapolated energy value (1.4 eV) is different from the thermal energy (0.3 eV).

The relationship between the experimental cone voltages and the characteristic temperatures from the MassKinetics modeling (Figure 4. 9) again shows a roughly linear dependence, but the fit is significantly worse than in the case of the internal energy.

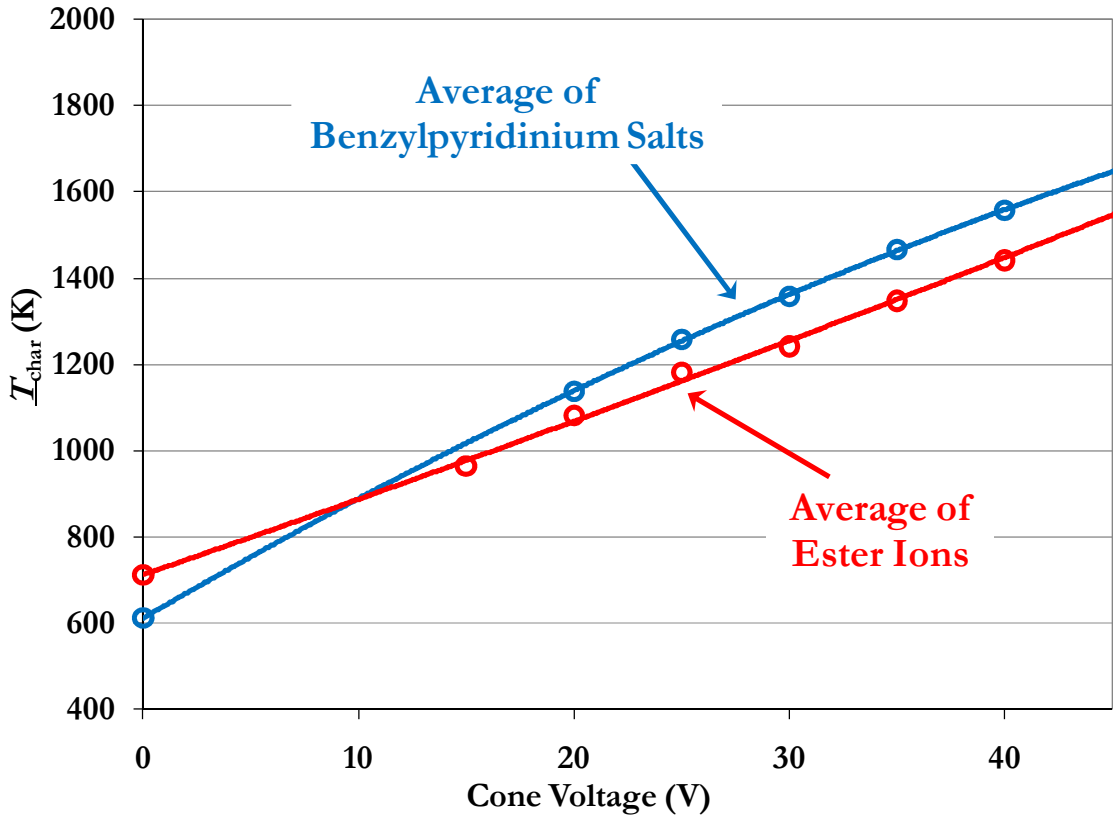

Figure 4. 9: *Characteristic temperatures of the m-methoxybenzyl pyridinium ion, and the m-methoxy benzoic ester as a function of the cone voltage.*

4. 1. 2. Protonated Alkylamine Dimers

In this section, our results on small proton bound alkylamine dimers are presented. In the case of alkylamine dimers, the previously published experimental results consisted of two different sets of data: a data set using high pressure conditions on a VG mass spectrometer and another data set using low pressure conditions on a JEOL instrument as it was described in an earlier chapter along with the parameters used in the modeling calculations. No experimental results were used to fit to in the modeling: only the parameters describing the experimental conditions (such as flight distances/times, potentials, temperatures) and the parameters determined by *ab initio* calculations regarding the dissociation energetics were used.

First, the initial internal energy distributions were confirmed by comparing the calculated ion intensity ratios to the experimentally observed ion ratios. In the case of the high pressure experimental setup, the assumption of an initial thermal internal energy distribution gave excellent results when comparing the calculated ion ratios to the experimentally observed ones. Interestingly, when modeling the results of the low-pressure JEOL experiments, calculations with the assumed thermal distributions did not agree with the experimentally observed ion ratios.

After considerable modeling efforts, it was concluded that the initial internal energy distribution in the low-pressure ion source is not thermal. This possibility was noted by *Norrman* and *McMahon* as well [88].

As the next step, effective temperatures for the alkylamine dimers were determined from the calculated ion intensity ratios using the reaction enthalpy difference, $\Delta\Delta_r H$, between the reaction channels (40) and (41), based on the fundamental equation of the kinetic method, discussed in Chapter 2:

$$\ln \frac{k_{H1}}{k_D} \approx \ln \frac{I_H}{I_D} = \frac{\Delta(\Delta H_0)}{RT_{eff}} \tag{44}$$

This equation was applied for both sets of experimental data, with the high-pressure and the low-pressure ion source. The two experimental setups gave quite different results, suggesting that at least one must be inaccurate. In the case of the high pressure experimental setup, the assumption of an initial thermal internal energy distribution gave excellent results when compared to the experimentally observed effective temperatures. The calculated effective temperatures for the alkylamine dimer systems are reasonably close to the experimentally determined values: it results in an average 179 K effective temperature for the protonated methylamine dimer (range of 134 – 225 K using the error limits as described above), which is close to the 194 K value determined experimentally by *Norrman* and *McMahon*.

The results are listed in Table 4. 2, showing that, in the case of the low pressure experimental setup (JEOL instrument), the experimentally observed effective temperatures are much lower than the modeling results assuming an initial thermal internal energy distribution, indicating that the experiments using a low pressure ion source might not produce thermal distribution for the molecular ions. The reasons behind this phenomenon were examined as discussed in the following paragraphs.

First, let us draw some conclusions based on the experimentally observed ion ratios: if the internal energy distribution of the ions were thermal in the low-pressure ion source, higher I_H/I_D ion ratio would indicate a lower effective temperature. This, in turn, would result a lower degree of fragmentation. In contrast, the experiments show that fragment ion yield is much higher in the JEOL instrument using the low-pressure ion source. (An alternative explanation is that a difference in the time-scale of the two instruments causes the variation in the isotope effect. Model calculations indicate that the difference in the time-scales is small, and have a very small influence on the results. Note that taking the time-scale into account in the MassKinetics modeling is straightforward and accurate.)

This argument can be rephrased: in the low-pressure ion source the internal energy distribution has two characteristics: it leads to higher fragment ion abundance, while the effective temperature is lower than that in the case of the high-pressure ion source. High fragment ion abundance means that a larger fraction of ions have internal energy above the fragmentation threshold, while low effective temperature means that the energy distribution must be narrow above the fragmentation threshold. Note that qualitatively such a non-thermal distribution can be expected based on the ion formation mechanism, assuming that the collisions in the source are sufficient to raise the internal energy of the ions, but happen seldom enough that a thermal equilibrium is not reached, rather like in a carefully carried out threshold collision-induced dissociation (TCID) measurement.

Table 4. 2: *Effective temperatures determined from experimental ion ratios taken from reference [88] and T_{eff} determined with Equation (44) using calculated ion ratios.*

	T_{eff} (K)			
B-d_n	VG		JEOL	
	Experimental	Calculated	Experimental	Calculated
CD_3NH_2	194 ± 4	251.31	44 ± 1	239.57
CD_3NH-CH_3	259 ± 8	336.48	128 ± 8	328.27
CD_3NH-C_2H_5	285 ± 29	305.75	149 ± 7	298.31
CD_3NH-C_3H_7	285 + 16	325.89	167 ± 5	317.49
CD_3NH-n-C_4H_9	321 ± 12	365.73	203 ± 5	358.77
$CH_3CD_2NH_2$	367 ± 16	391.92	238 ± 7	385.83
CH_3CD_2NH-CH_3	431 ± 24	408.02	270 ± 17	402.85
CH_3CD_2NH-C_2H_5	323 ± 21	363.69	204 ± 8	356.68
$CD_3CH_2NH_2$	320 ± 18	348.19	202 ± 14	342.25
CD_3CH_2NH-CH_3	373 ± 27	381.02	196 ± 7	375.2
CD_3CH_2NH-C_2H_5	366 ± 24	405.11	202 ± 14	399.34

Since it was concluded that the difference in the internal energy distribution from the thermal distribution contributed to the observed lower effective temperature, a thorough examination was carried out to understand the reasons behind the observed phenomenon.

When a complex undergoes collisional cooling, the internal energy distribution will change and will become more similar to a thermal distribution. Until true equilibrium is reached, the energy

distribution will be characterized by a higher than thermal fragmentation rate and a lower than thermal effective temperature, as observed experimentally.

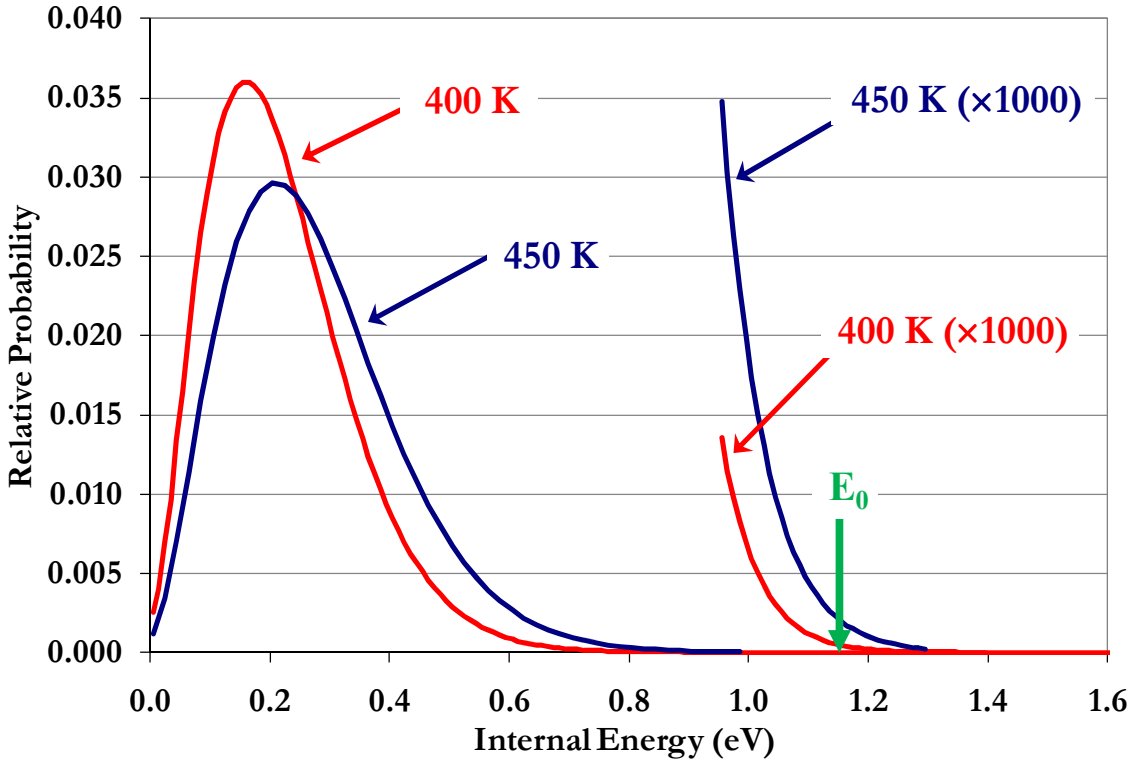

Figure 4. 10: *Thermal internal energy distribution of the protonated methylamine dimer at 400 K (red line) and 450 K (blue line) temperatures. The tails of the distribution are shown on a 1000 times magnified scale.* E_0 *indicates the critical energy of the lower energy channel.*

At this point it may be instructive to discuss the calculated internal energy distributions. Thermal IED of protonated methylamine dimer is shown in Figure 4. 10 at 400 and 450 K. The fragmentation threshold (1.1670 eV) is only slightly above the critical energy (1.1665 eV) of the lower energy channel. (Note that the critical energy is taken from the literature [88], the four decimal units are a consequence of energy conversion from kcal to eV units.) The fragmentation threshold is always higher than the critical energy, the difference is the kinetic shift that was discussed in the theory section, and demonstrated in the case of benzylpyridinium ions. The probability of precursor ions above 1.16 eV of internal energy is very low both at 400 and 450 K, so this part of the distribution is magnified by 1000 times in Figure 4. 10. On one hand, the tails of the distributions are similar, suggesting that the effective temperature and the size of the kinetic isotope effect will not depend on the source temperature significantly (which was also observed experimentally). On the other hand, the tail at lower temperature is smaller, suggesting

that the fragment ion yield will be much reduced at lower source temperatures. (Personal communication from *McMahon* indicates that this was observed experimentally, indeed.)

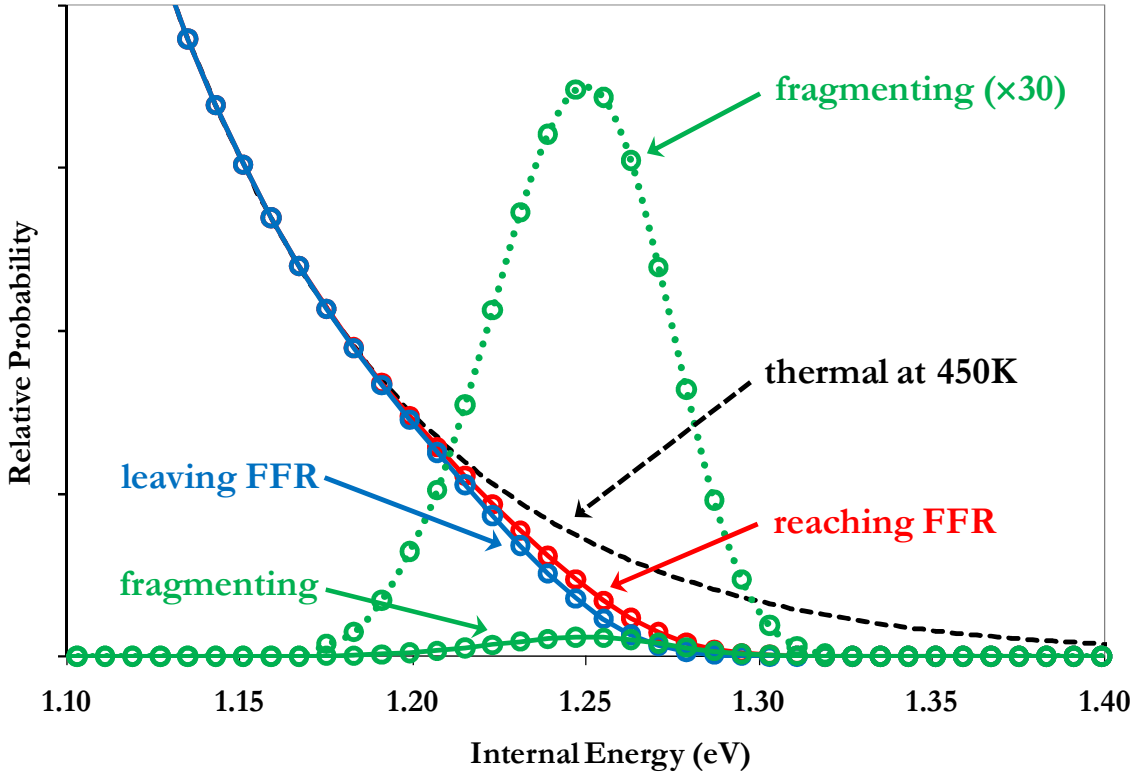

Figure 4. 11: *The high energy tail of the internal energy distribution of the protonated methylamine dimer using the high-pressure ion source at 450 K source temperature. The thermal distribution is shown by the dashed black. Red circles show the energy distribution of ions reaching the FFR, blue circles of those leaving the FFR intact. The difference between these two distributions (shown by green circles) are the ions fragmenting in the FFR, yielding metastable products (also shown by 30× magnification, indicated by the dotted green line). Using Equation (44), and the calculated fragment ion ratio* $T_{eff} = 179K$ *is obtained.*

The tail of the internal energy distribution calculated at 450 K source temperature was analyzed and compared to several internal energy distributions of ions at various stages in the mass spectrometer. Figure 4. 11 shows the IED of various fractions of protonated methylamine dimers in the 1.1 – 1.4 eV range using the VG instrument (high-pressure ion source). Thermal IED at 450K is shown by the dashed black. A significant portion of the high-energy ions will decompose before they reach the FFR. For this reason, the probability of high-energy ions reaching the FFR (red circles in Figure 4. 11) will be significantly reduced compared to that of thermal distribution. The difference between the distribution of ions entering (red circles) and leaving the FFR (blue circles) corresponds to the internal energy distribution of those protonated methylamine dimers that do fragment in the MIKES experiment (indicated by green circles and

also shown enlarged by 30 times indicated by dotted green line). The figure illustrates that metastable ions represent only a small fraction of all parent ions (area under respective curve by green circles) and will have a fairly wide energy distribution. Ions fragmenting through the two competitive reaction channels (40 and 41) have different IEDs, but the difference is so small that it cannot be shown in Figure 4. 11. The effective temperature, determined using Equation (44), characterizes this fragmenting ion population. The experimental ion ratio ($k_H/k_D = 1.39$) corresponds to 194 K, while the calculated value ($k_H/k_D = 1.43$) results in an effective temperature of 179 K.

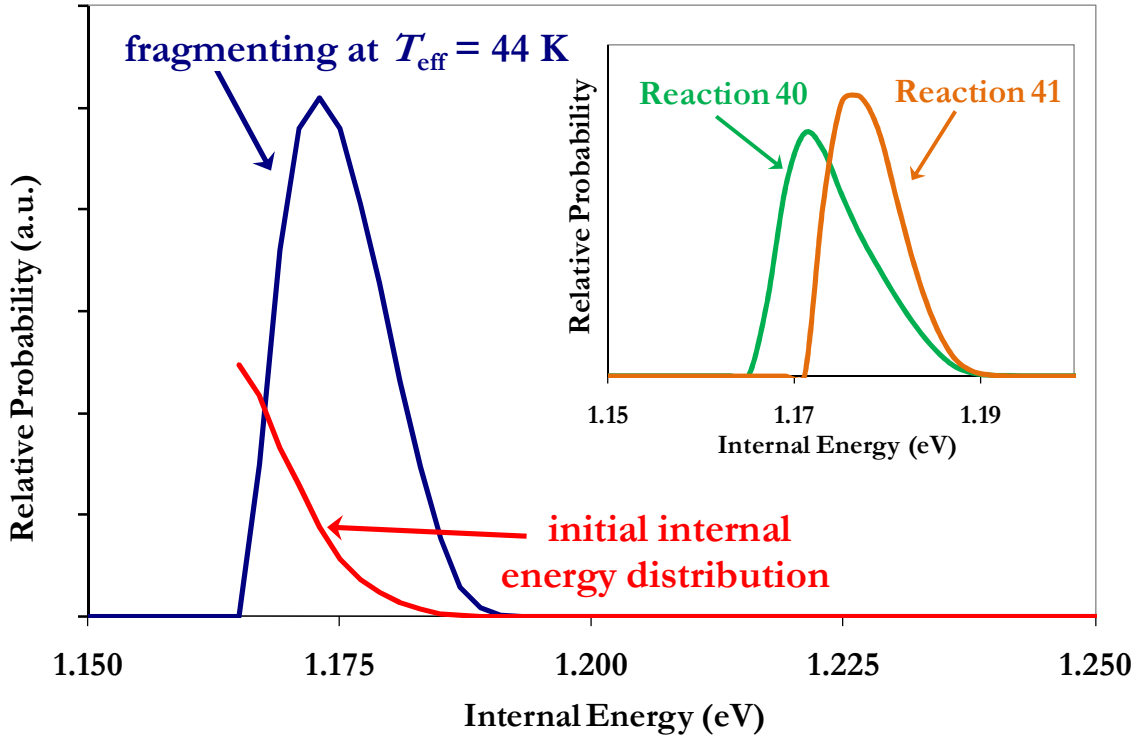

Figure 4. 12: *High-energy tail of the internal energy distribution of protonated methylamine dimers reaching the field free region (red line), and that of ions fragmenting inside the field free region (blue line) on the low-pressure experimental setup. The distribution is empirically obtained to result in a 44 K effective temperature. Note that only the part above the fragmentation threshold (E_0 = 1.167 eV) is significant in this respect. The insert shows the internal energy distributions of ions fragmenting through reactions (40) and (41) (green and brown lines, respectively).*

In the case of modeling the low-pressure ion source results (Figure 4. 12), the initial IED (red line) was determined empirically so that it results in an ion intensity ratio equal to that obtained experimentally (4.10). In other words, the initial internal energy was determined by fitting the calculated ion intensity ratio to the experimentally observed one. As discussed in the

experimental publication, this corresponds to a 44 K effective temperature. The shape of the IED below the fragmentation threshold (1.167 eV) has no relevance to fragmentation. Note that the distribution drops down very fast above the fragmentation threshold and there are practically no ions of internal energy higher than 1.19 eV.

The energy distribution of the ions fragmenting inside the FFR is very narrow, shown by the blue line in Figure 4. 12. We have experimented with several other trial internal energy distributions and all of those capable of yielding T_{eff} = 44 K were fairly similar to that shown in Figure 4. 12, that is the IED of the fragmenting ions was always a narrow peak between E_0 (1.167 eV) and 1.19 eV.

In the next step, let us compare the IED of ions fragmenting in a mass spectrometric experiment to those occurring under thermal (i.e., equilibrium) conditions. The ions produced in a high-pressure source at 450 K source temperature result in a 179 K effective temperature according to model calculations. This is close to the experimentally determined effective temperature (T_{eff} = 194 K). Note that in this case, the source and the effective temperatures are significantly different. The effective temperature in metastable fragmentation should be always lower than the initial temperature of the ion source; this is a consequence of ion fragmentation occurring inside mass spectrometer. The IED of fragmenting ions at 179 K effective temperature (purple line in Figure 4. 13) can be compared to that of decomposing ions in a "real" thermal system (thermodynamic system at high-pressure limit, blue line in Figure 4. 13).

The distributions start at the critical energy (as no ion below the critical energy can decompose) and continues to (in principle infinitely) high internal energy. The ions decomposing in a thermal system (179 K "real" temperature) and in a mass spectrometer (yielding T_{eff} = 179 K) have fairly similar, but not identical distributions. The similarities of such distributions were observed for other alkylamines and other temperatures as well. Figure 4. 13 illustrates the methylamine system at 44 K as well: the green line shows the thermal distribution, the red line the metastable distribution. As thermal and mass spectrometric distributions are not identical is a nice demonstration that the kinetic method is not a thermal experiment. Nevertheless, the roughly similar shape of the curves provides in our opinion qualitative support for the kinetic method (at least in case of metastable ions).

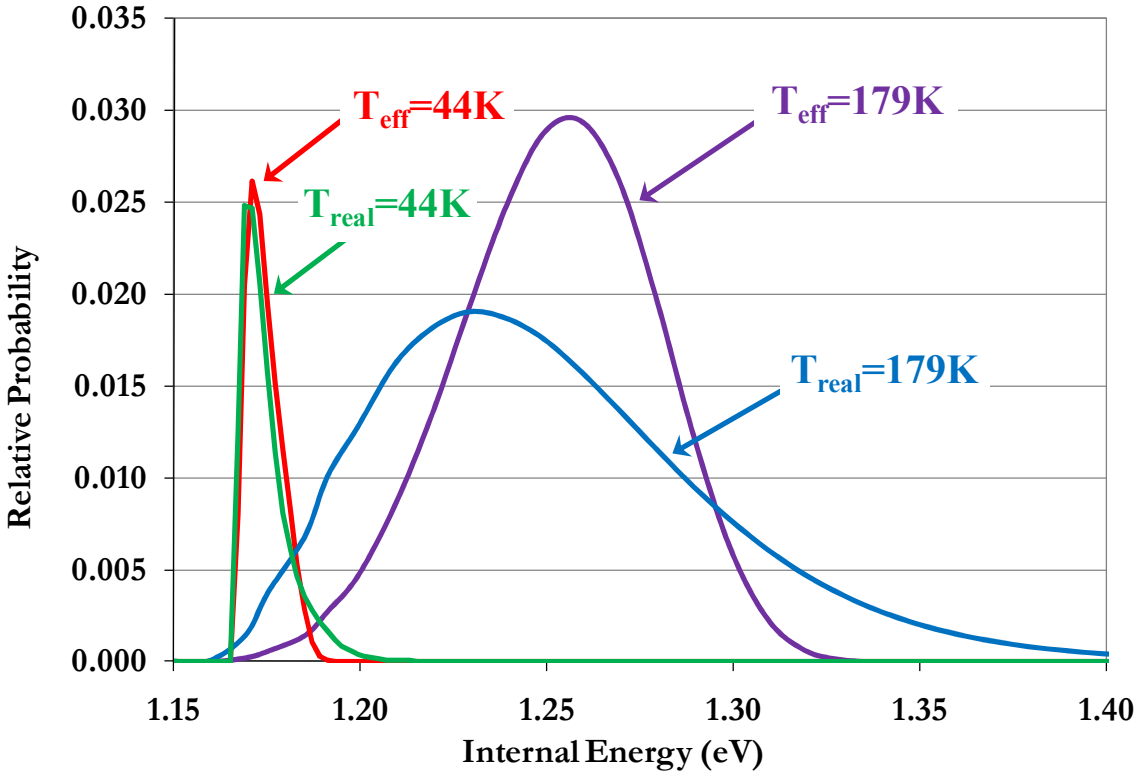

Figure 4. 13: *Comparison of the calculated internal energy distribution of fragmenting protonated methylamine dimers characterized by 179 K (as observed in the high-pressure source) and 44 K (as observed in the low-pressure ion source) effective temperatures (red and purple lines, respectively) with that of ions reacting in a thermal system (at the high-pressure limit) characterized by 179 and 44 K "real" temperatures (green and blue lines, respectively).*

4. 1. 3. Conclusions on Calculating Internal Energy Distributions

It is well known that the internal energy and the internal energy distribution play an important role in shaping the mass spectra in any experiment. Therefore as the first step in our studies the internal energy distribution was examined using model compounds: protonated benzylpyridinium ions, protonated benzoic ester ions in a collision-induced dissociation setup and protonated alkylamine dimers using results from two different experimental setups.

From the experimental ion intensities the survival yield was determined, and the correlation between the critical energies and the transition states were investigated: the logarithm of the SY was found to be proportional to the logarithm of the critical energy in the case of the benzylpyridinium salts, however, for protonated benzoic ester ions, this correlation was much weaker. Therefore, the degree of fragmentation of the different substituted benzylpyridinium ions seems to vary due to the variations in the critical energies, whereas in the case of the esters, it is the different transition states that lead to the different degrees of fragmentation.

The determined survival yields were then used to determine the corresponding characteristic temperatures, T_{char}. Using these characteristic temperatures, the internal energy distributions were calculated and it was found that they are closely resemble thermal energy distributions. It was also found that the shapes of the internal energy distribution of the different substituted benzylpyridinium and benzoic ester ions are similar, and that the average internal energy distributions of the protonated benzylpyridinium and of the benzoic ester ions are similar. Therefore it was concluded that the electrospray source produces roughly the same initial internal energy distribution for systems with similar degrees of freedom.

The effect of the collisions was demonstrated: a thermal distribution at 353 K was calculated with including a number of collisions (20, 40) and it was found that the resulting internal energy distribution can be reproduced by a thermal distribution calculated at a higher temperature (790 K, 1210 K).

Fragmentation reaction rate curves were also calculated as a function of the internal energy and appearance energies were determined to demonstrate the kinetic shift of the modeled experiment.

The mean internal energy was determined for the both sets of precursor ions (protonated benzylpyridines, benzoic esters) as a function of the cone voltage, and an excellent linear relationship was found regardless of the ion structure or the type of the reaction.

In the case of protonated alkylamine dimers, results from two different experimental setups were taken from previous publication – from a high-pressure and a low-pressure ionization source – and modeling calculations were carried out to explain the difference in the experimental results. In the case of the high-pressure experimental setup, the experimental results were successfully modeled assuming thermal internal energy distribution. The effective temperature, T_{eff}, values were determined from the measured intensity ratios (I_H/I_D = KIE) based on the kinetic method. In the case of low-pressure ionization source, the experimental and calculated T_{eff} and the ion ratios were significantly different; hence the assumption of thermal distribution was not supported. Detailed examinations of the internal energy distributions were carried out, and it was concluded from the experimental data that a) there should be a high fraction of high-energy ions, leading to high fragment ion abundances, while at the same time, b) the effective temperature should be low, i.e. the energy distribution must be very narrow above the fragmentation threshold to account for the findings based on the kinetic method.

It was also confirmed that the source temperature should not have a large effect on the observed T_{eff} and KIE, since the tail of the thermal distributions corresponding the source temperature is similar above the fragmentation threshold. However, the lower source temperature results in a

reduced fragment ion yield due to the smaller tail of the distribution that stretches above the fragmentation threshold.

Finally, internal energy distribution of fragmentation portion of the ion population in mass spectrometric conditions was compared to IEDs of ions fragmenting under thermal, equilibrium conditions (high-pressure limit): the two IEDs were found to be similar at many temperatures for many similar systems studied. The roughly similar shape of the calculated IEDs serves a good qualitative support for the kinetic method that has been used in this research.

4. 2. Kinetic Energy Release

4. 2. 1. Protonated Alkylamine Dimers

In the case of protonated alkylamine dimers, the kinetic energy release has been calculated using a microcanonical product energy distribution, as discussed by *Baer* and *Hase* and reviewed earlier, in Chapter 2. This model assumes statistical energy partitioning among the products' vibrational, rotational, and translational degrees of freedom. The KER is then due to the statistically distributed relative translational motion of the two fragments, the fragment ion and the neutral. This formalism will be discussed in the next sub-chapter, 4. 2. 2., when analyzing the results of protonated methanol clusters. One consequence of this model that it predicts a particular KERD that it predicts an almost exactly Gaussian-shaped metastable peak. In the study of *Norrman* and *McMahon*, which forms the experimental basis of the present work, the peak shapes are approximately Gaussian, but their detailed analysis was not performed. Results on the fragmentation of protonated clusters clearly show that in many cases, the metastable peaks indeed do have a Gaussian shape, which converts to a KER distribution described by a three-dimensional translational energy distribution. These results tentatively support the choice of the model used in the present study. As discussed above, the conservation of angular momentum is not considered in our calculations. With the exception of very small molecules, this is often a good assumption for dissociation of ion–molecule complexes. Furthermore, collisional excitations producing ion with high angular momentum states is not likely in the modeled experiments, it is more the case in the TCID excitations.

In Figure 4. 14, the results from the statistical energy partitioning are shown in the case of the protonated diethylamine dimer, under the experimental conditions observed on the VG instrument (high-pressure source).

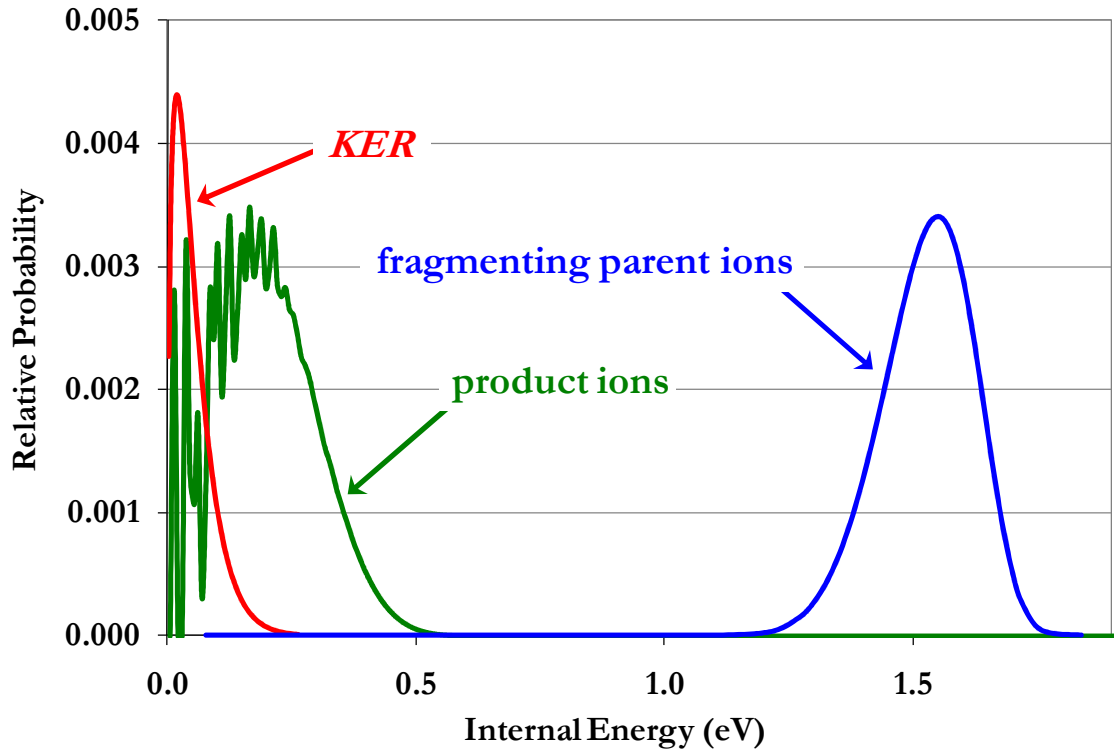

Figure 4. 14: *Calculated energy distributions resulting from statistical energy partitioning in the case of the protonated diethylamine dimer, under experimental conditions observed in the high-pressure experimental setup. Internal energy distributions of the parent ions, and of the fragment ions are shown with blue, and green lines, respectively; while the red line stands for the kinetic energy release distribution of the fragment ions.*

The internal energy distribution of the parent ions fragmenting in the FFR is shown by the blue line; that of the product ion by the green line; the relative translational motion (i.e., the KER distribution) by the red line (the relative rotational energy of the two products and the internal energy of the product neutral is not shown). The shape of the KER is qualitatively fairly similar to a Maxwell–Boltzmann distribution (the kinetic energy distribution of gas molecules in a thermal system). Such distributions will result in approximately Gaussian-shaped metastable peaks. Note that the internal energy distribution of the product ion is not smooth at low energies – a consequence of the quantized nature of the oscillators. (The KER distribution is smooth, as translational energy levels are very close.) The mean excess energy ($E^{\#} = E - E^{\circ}$) in this case is 0.49 eV; in the case of low pressure ionization it is much smaller, 0.20 eV.

It is well established that the mean KER value (<KER>) for a Gaussian-shaped metastable peak can be obtained from that determined at half-height of the metastable peak ($KER_{0.5}$) as [128]:

$$<KER> = 2.16\ KER_{0.5} \qquad (45)$$

KER data in *Norrman* and *McMahon*'s paper has mostly been determined on the JEOL instrument (probably due to its better resolution). Only one example is given using the high-pressure ion source on the VG instrument (Fig. 8 in [88]) corresponding to the fragmentation of protonated diethylamine. From the peak shape given there the $KER_{0.5}$ value is 31 meV; and the peak is approximately of Gaussian shape.

The mean <KER> value is consequently 67 meV. Note that this value is likely to be an upper limit for <KER>, as the influence of peak broadening due to instrumental effects (like the width of the ion beam) was not taken into account. Using the same ± 1 order of magnitude uncertainty in the pre-exponential factor as discussed before, the calculated <KER> value falls into the 47 – 54 meV range. Note that, this calculation uses no empirical parameter beside the pre-exponential factor, so we believe that it is a fair agreement.

Table 4. 3: *Experimental and calculated kinetic energy release data for dissociation reaction of proton-bound dimers B-H+-B-d_n for the low-pressure experimental setup.*

	KER (meV)	
B-d_n	experimental	calculated
CD_3NH_2	5.3	3.6 (3.6 – 4.4)
CD_3NH-CH_3	16.3	17.7 (16.2 – 20.1)
CD_3NH-C_2H_5	24.5	29.2 (27.2 – 31.7)
CD_3NH-C_3H_7	28.4	31.9 (30.5 – 32.5)
CD_3NH-n-C_4H_9	33.2	36.6 (35.2 – 36.9)
$CH_3CD_2NH_2$	19.4	28.3 (25.7 – 31.0)
CH_3CD_2NH-CH_3	24.5	35.5 (32.7 – 38.5)
CH_3CD_2NH-C_2H_5	28.6	31.4 (29.5 – 32.0)
$CD_3CH_2NH_2$	20.2	14.9 (13.4 – 18.3)
CD_3CH_2NH-CH_3	24.6	15.3 (14.2 – 18.3)
CD_3CH_2NH-C_2H_5	29.8	15.0 (15.4 – 16.0)

[a] *Recalculated from data in [88]*

[b] *Calculated using a non-thermal energy distribution for the precursor ion. In the calculation the internal energy distribution was changed from thermal to such a distribution, which yields the KIE experimentally observed on the JEOL instrument (described in detail in the text)*

KER data for other alkylamines are available obtained on the low-pressure ion source (JEOL instrument). It was discussed above, that the IED in this ion source is not thermal; and that was possible to estimate only empirically, based on the experimentally observed ion ratios. Qualitatively, fragmenting ions have a lower internal energy (indicated by the experimentally determined lower effective temperature values) than in the case of high-pressure ion source. Using this empirical IED, the KER can be determined, applying the aforementioned 'prior distribution' model (Table 4. 3). This should result in a lower KER value. Indeed, the KER value determined experimentally for diethylamine is nearly three times lower using a low pressure than using a high-pressure ion source (<KER> = 29 vs. 67 meV, respectively).

In the previous discussions, it was shown that the IEDs for reacting ions in a thermal system and metastable ions characterized by effective temperature are quite similar (Figure 4. 12). It was also shown, that KER values can be well described by a three-dimensional translational energy distribution ($3/2kT$ in a thermal system). Connecting the two features, the KER and the effective temperature should be connected by the simple equation:

$$<\text{KER}> \approx 3/2\ kT_{\text{eff}} \tag{46}$$

Note that the arguments used here are analogous to those of the 'finite heat bath theory' developed by *Klots* to describe fragmentation of cluster ions. Figure 4. 15 shows the correlation according to the equation above, using T_{eff} (determined from experimentally observed ion ratios using Equation (44) [88]) and the <KER> values.

Figure 4. 15 shows both the calculated and the experimentally observed <KER> values (blue and red circles, respectively). There is a good linear correlation between T_{eff} and <KER> and the slope is very close to that described by Eq. (46). This correlation is quite significant, as it suggests that the 'prior distribution' model is a physically reasonable assumption to describe fragmentation of proton-bound alkylamine dimers. It also indicates that (a) KER can be described as a three-dimensional translational motion and suggests that (b) statistical energy partitioning occurs in a late transition state.

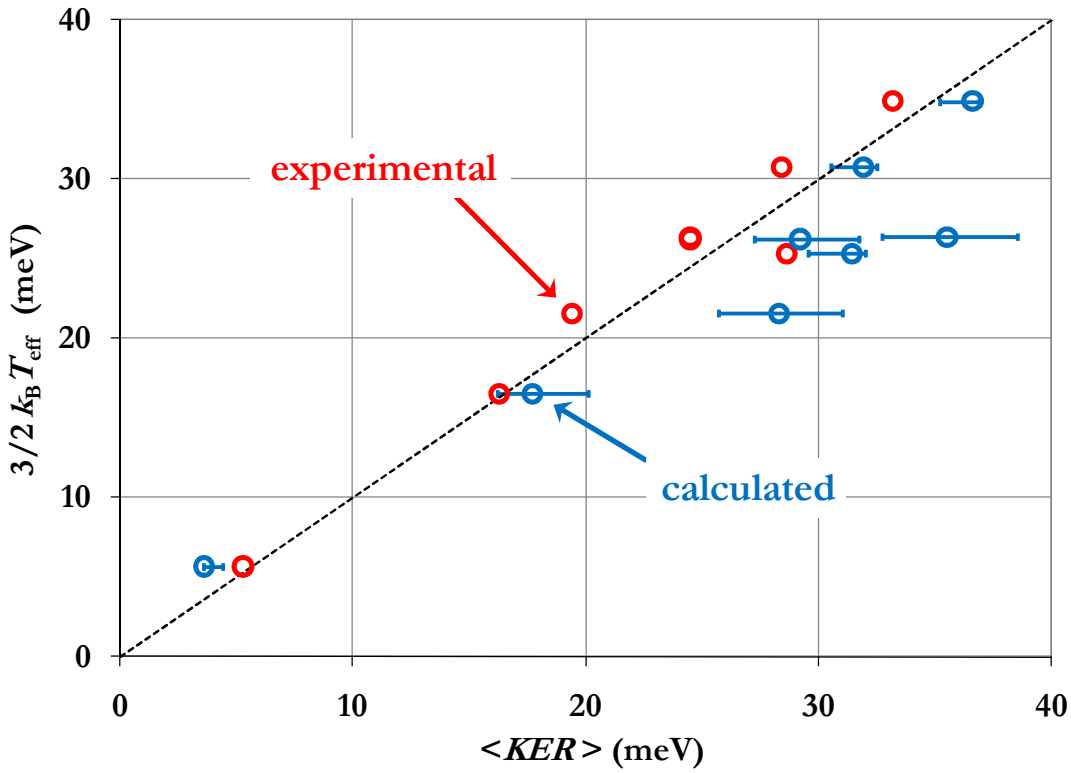

Figure 4. 15: *Correlation between the calculated (blue circles) and experimentally measured (red circles) mean kinetic energy release and the effective temperature, calculated using experimentally observed ion ratios, based on Equation (44). Data are shown for α-D substitution. The expected correlation assuming a three-dimensional translational energy distribution Equation (46) is shown by the broken line (correlation coefficients are 0.979 and 0.952 for experimental and calculated <KER> values, respectively).*

4. 2. 2. Protonated Methanol Clusters

Results on protonated methanol clusters produced by low-temperature FAB experiments were chosen to study kinetic energy release of protonated clusters and to model their behavior in the mass spectrometer and to get an insight of their fragmentation mechanism.

The KERDs were determined from the experimentally measured metastable peak profiles for all clusters between $n = 3$ and 15 using the computer program, META, developed in our lab by *Szilágyi* and *Vékey* [98]. The applied algorithm is based on a numerical approach which uses neither pre-defined analytical functions nor initial assumptions as to the shape of the KER distribution. As examples, the KERD curves determined for the $n = 5$, 11 and 15 methanol clusters are shown in Figure 4. 16. Note that the shapes for all distributions were similar and did not depend on cluster size.

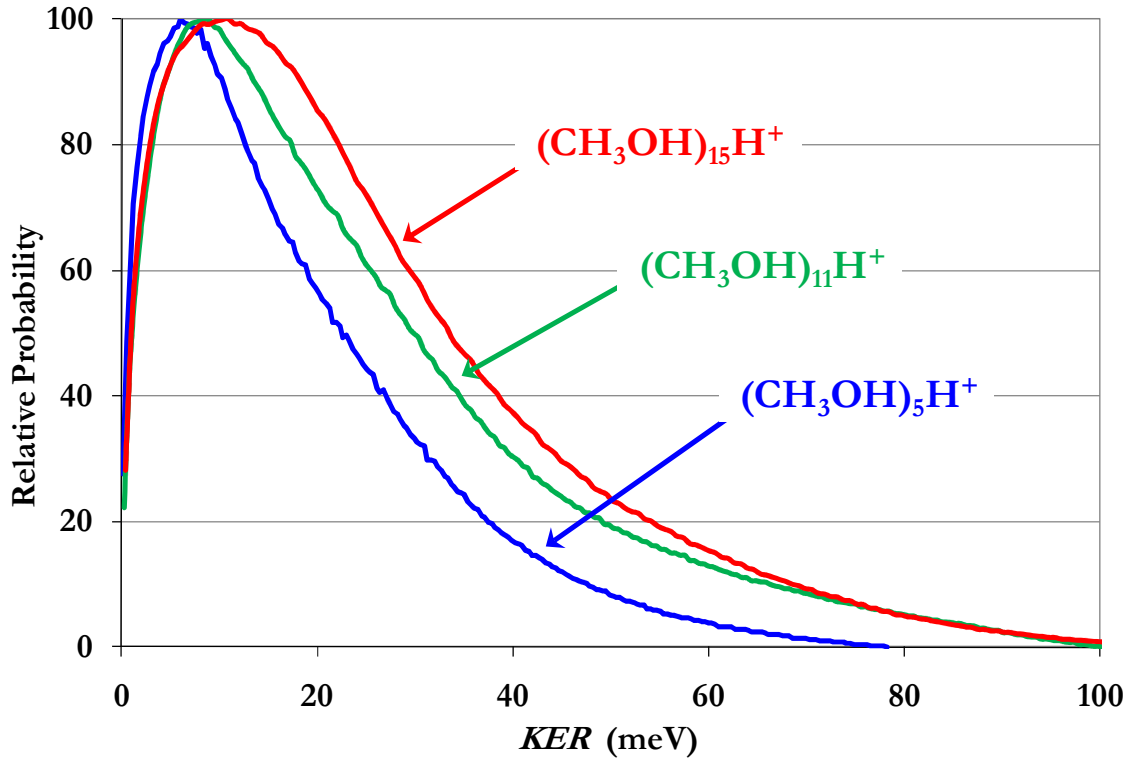

Figure 4. 16: *The experimentally-obtained KERD curves for $(CH_3OH)_nH^+$ clusters (n = 5, 11, and 15) as determined from the metastable peak shapes using the META program.*

Even without a detailed examination it is easy to see the similarity between the KERD shapes shown in Figure 4. 16 and a Maxwell–Boltzmann distribution. The latter describes the kinetic energy of a gas molecule in a thermal system, i.e. corresponds to a three-dimensional translational energy distribution:

$$P(E) = \frac{\Gamma(n+1)}{(k_B T)^{n+1}} E^n e^{-E/k_B T} \tag{47}$$

Here $P(E)$ is the normalized intensity of the curve, k_B is the Boltzmann constant, E is the kinetic energy, n is the parameter which defines the dimension of the distribution (for 3-D: $n = 0.5$, for 2-D: $n = 0$ and for 4-D: $n = 1$), Γ is Euler's gamma function and T is the temperature. The similarity between Maxwell–Boltzmann and KER distributions was modeled quantitatively, fitting a three-dimensional (3-D) translational energy distribution [Equation (47)] on the KERD curves using temperature as the optimized parameter. The results showed very good agreement between experimental KERD and Maxwell–Boltzmann distributions for all clusters. The case of $(CH_3OH)_{15}H^+$ is shown in Figure 4. 17 (dashed black line corresponding to the experiments and the solid red line to the Maxwell–Boltzmann distribution). At this point we would like to note that determination of KERD curves by our algorithm is a purely numerical approach; no

analytical expressions for the KERD curves are used or assumed. This may make the determined KER profiles noisier but there is no danger of distorting the experimental values by a preselected formula.

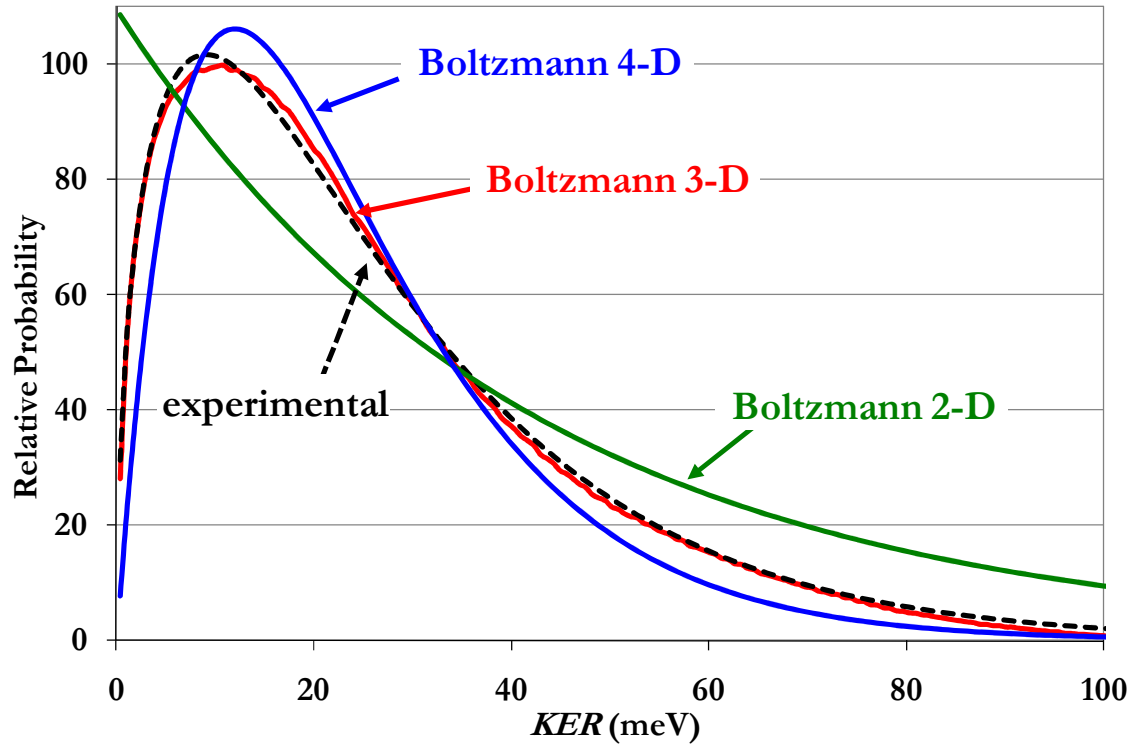

Figure 4. 17: *Experimental (dashed line) and theoretical (solid lines) KERD curves for $(CH_3OH)_{15}H^+$. The theoretical curves were calculated using two-, three- and four-dimensional translational energy distributions using Equation (47).*

The curves shown in Figure 4. 17 clearly suggest that KER distributions corresponding to metastable fragmentation of protonated methanol clusters correspond to a 3-D translational energy distribution. It is well known that the effect of angular momentum conservation may result in KER distributions corresponding to 2-D or 4-D distributions. To check how similar or dissimilar these are, the shapes of two-, three- and four-dimensional translational energy distributions are compared in Figure 4. 17, using Equation (47) (for 2-D $n = 0$ and for 4-D $n = 1$). The Figure clearly shows that the three translational energy distributions are very dissimilar, and that the experimentally-obtained KERD distribution can be described only by 3-D and not by 2-D or 4-D translational energy distributions. These results clearly indicate that the internal energy in the transition state can be well described by a statistical distribution, resulting in a KER corresponding to three translational degrees of freedom. This, in fact, corresponds to the so-called "prior distribution model". This also means that that the necessity of conserving the angular momentum

does not influence energy distributions (and therefore fragmentation) to a significant degree in the case of protonated methanol clusters.

Table 4. 4: *Average kinetic energy release values determined for protonated methanol clusters.*

cluster size (methanol molecules)	KER (meV)	
	experimental	MassKinetics modeling
3	14.6	
4	17.9	
5	18.2	
6	18.7	21.6
7	24.8	20.4
8	24.3	24.7
9	24.5	25.4
10	26.2	25.5
11	24.7	25.1
12	24.9	24.7
13	28.8	25.4
14	27.5	25.7
15	25.9	25.8

The average KER values, <KER>, were determined from the shape of the distributions as a function of the cluster size (Table 4. 4). As in earlier measurements of other clusters, the average KER increases with increasing cluster size. Small to medium size methanol clusters, studied by CID, yield much larger <KER> values in accordance with the higher degree of excitation. The increase is fairly sharp in the beginning but it levels out around the octamer, <KER> being about 25 meV for larger clusters. The reproducibility of the measurements is ± 2 meV. As discussed above, the KER is directly related to the internal energy distribution in the transition state and may be characterized by a 3-D translational energy distribution. The temperature associated with the corresponding Maxwell–Boltzmann distribution [Equation (47)] was determined for each cluster and can be seen in Figure 4. 18.

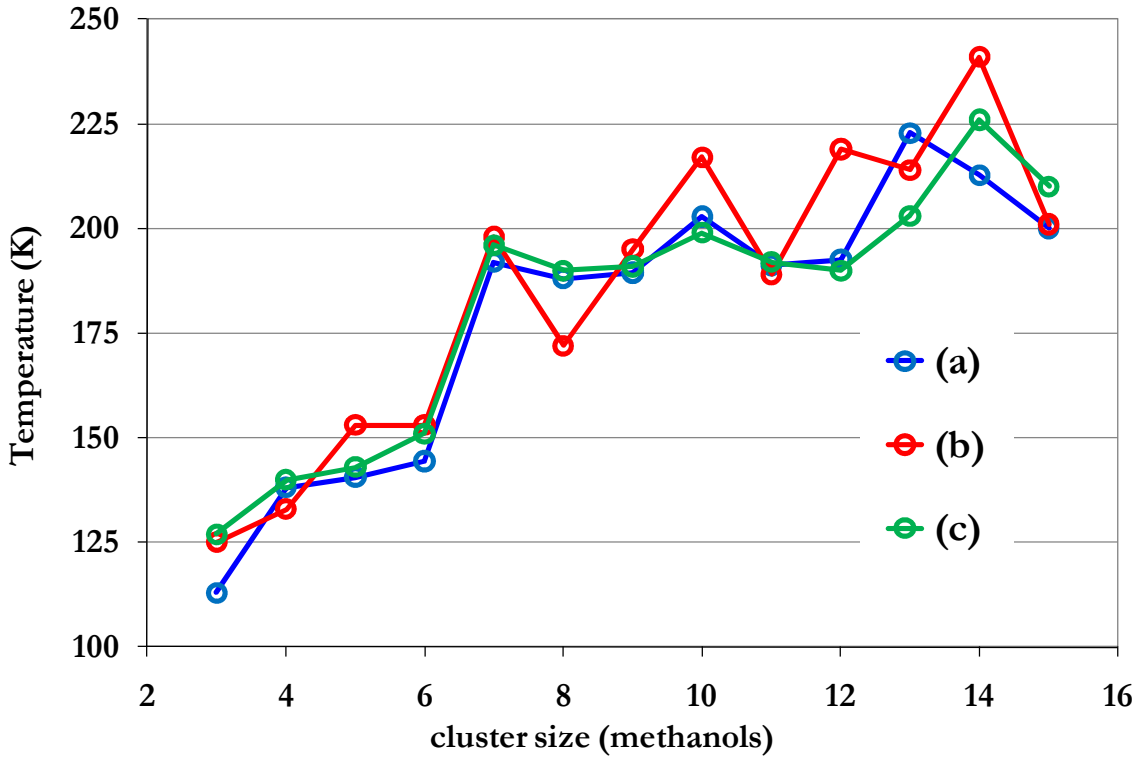

Figure 4. 18: *Transition state temperatures, as determined by various models: (a) determined using Equation (48) from the <KER> values; (b) transitional state temperatures, $T^{\ddagger}$, determined from FHBT using Equation (39) with parameter l being fitted to each KERD curve; (c) the temperature determined using Equation (47) corresponding to a Boltzmann distribution. Note that this is identical to $T^{\ddagger}$ determined using Equation (39), when l is fixed to 0.5. See text for details.*

In an analogous way <KER> may be equated directly with the average kinetic energy in a thermal system,

$$<\mathrm{KER}> = 3/2 k_B T \tag{48}$$

The results are also shown in Figure 4. 18. The temperatures determined in these two different ways are very similar and correspond very closely to the concept of "transition state temperature", developed by *Klots* to characterize internal energy distributions in the transition state and used extensively within the framework of the finite heat bath theory (FHBT) [42, 103]. The FHBT can also be used to evaluate KERD curves, as pioneered by *Laskin* and *Futrell* [103]. In an analogous way, the experimentally-observed KER distributions can be simulated and analyzed by fitting the following analytical formula:

$$P(e) \approx \varepsilon^{l} \exp(-\varepsilon / k_B T^{\ddagger}) \tag{49}$$

Here l is an empirical parameter that ranges from 0 to 1 and $T^{\ddagger}$ is the transition state temperature. Note that a 3-D translational energy distribution corresponds to $l = 0.5$. Using

$l = 0.5$, the optimized $T^{\ddagger}$ values are identical to those determined using Equation (47). When both l and $T^{\ddagger}$ are free parameters, the resulting $T^{\ddagger}$ is slightly higher. The mean value of l (for methanol clusters, $3 \leq n \leq 15$) is 0.4857. Note that the temperature values shown in Figure 4. 18 (subsequently described as transition state temperatures, $T^{\ddagger}$) are quite similar and show an increase with cluster size, the curves slowly flattening above about $n = 7$. In the context of FHBT, as the name implies, the internal energy of a cluster acts as an energy reservoir to supply energy into the reaction coordinate. As the energy flows into the reaction coordinate, the cluster cools down and the transition state temperature is always lower than the real temperature. The larger the molecule, the larger is the energy reservoir. In the case of an infinitely large molecule, the transition state temperature is equal to the real temperature of the cluster. With increasing cluster size, $T^{\ddagger}$ should increase (and does increase as can be seen in Figure 4. 18) and approach the real temperature of the clusters.

A different theoretical model of cluster fragmentation can be developed using the MassKinetics program. In this case, reaction rates are calculated according to RRKM, and statistical energy partitioning is performed according to the "prior distribution" model. As described in the Calculation Details, to apply the model, molecular frequencies and critical energies, basic information about the experimental setup and initial internal energy distribution information are needed. Based on previous results on initial internal energy distribution, it was assumed that the internal energy distributions of molecule ions in the ion source equaled the thermal energy distributions at the source temperature (298 K) for all clusters. MassKinetics was used to calculate <KER> (Table 4. 4) and the KER distribution (shown for $n = 15$ in Figure 4. 19).

The modeled <KER> and KERD showed good agreement with the experimental results. Note that the difference between the theoretically-calculated and experimentally-observed <KER> values was *less* than the uncertainty of the experiments. Agreement between MassKinetics calculations and experimental results was much less satisfactory for small clusters. Note that MassKinetics have been successfully used to model various small ions and clusters. The observed disagreement for small protonated methanol clusters may be due to the presence of a small amount of isomer, in which one methanol molecule is displaced into an outer solvation shell. This may account for higher metastable ion abundances and smaller <KER> than that predicted by theory.

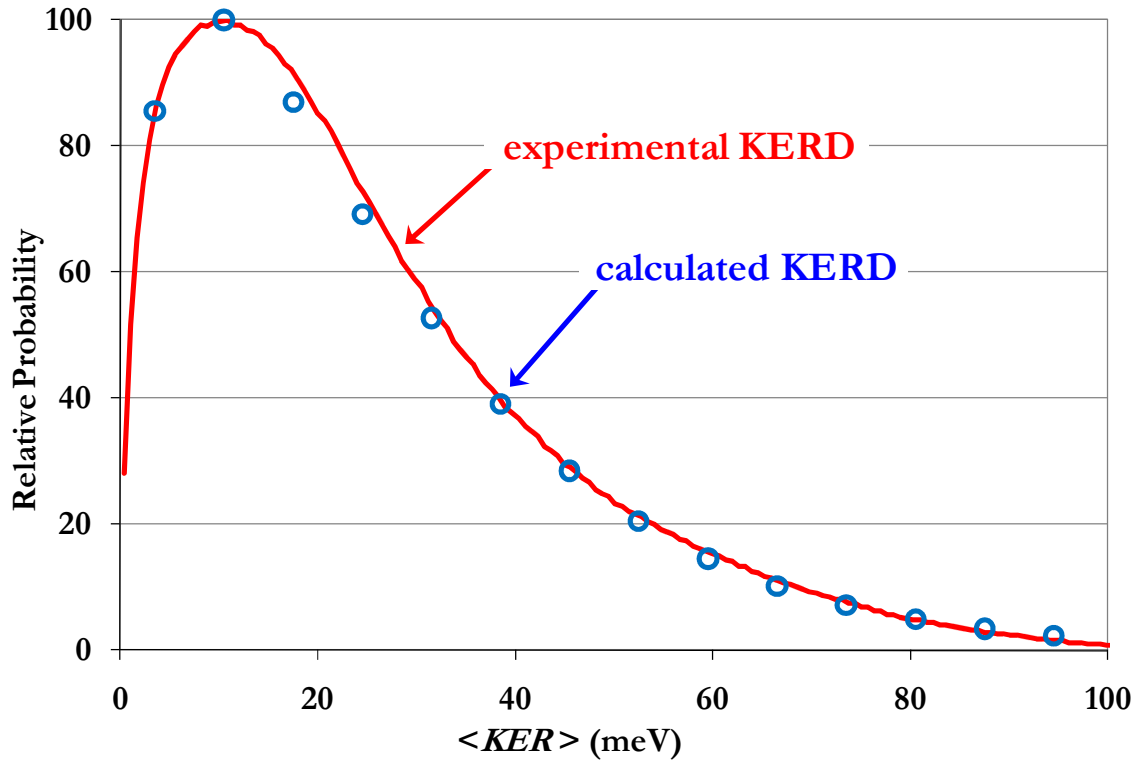

Figure 4. 19: *Experimental KER distribution extracted from the metastable peak shape (red line) and the calculated KERD for* $(CH_3OH)_{15}H^+$ *using MassKinetics (blue circles).*

4. 2. 3. Conclusions on Modeling KER

Result of metastable ion measurements were used to model the kinetic energy release of protonated alkylamine dimers and of protonated methanol clusters.

Statistical energy partitioning was assumed for both examined systems and the modeling results were found to have excellent agreement with the experimental results: modeling calculations showed that KER(D) was found to be similar to Maxwell-Boltzmann 3-D distribution and the metastable peaks showed a Gaussian-shaped curve. This implies the important conclusion that KER is due to a three dimensional translational motion and that the KER can be described by a 3-D distribution, which was debated in the literature.

Based on the results that KERD can be treated three dimensionally, <KER>, determined from the metastable peak, was connected to T_{eff} using the formalism of a three-dimensional translational energy distribution: <KER> ≈ 3/2 $k_B T_{eff}$. Good linear correlation was found that further emphasizes the important finding of the three dimensional KER distribution. It is important to point out that in this calculation, the T_{eff} and the KER came from separate source, the parameters used in the modeling were not connected whatsoever.

In the case of protonated methanol clusters, low-temperature FAB technique was used to produce protonated methanol clusters and KER processes were studied by recording the metastable water loss of the selected clusters. KERD curves were calculated and the shape of the distributions were examined and compared to a 2-D, 3-D and 4-D Boltzmann distribution. Mean KER values, <KER>, were found to increase sharply with increasing cluster size for n = 1 – 7, and level out around the octamer. TS temperatures were determined using equations from three different methods: equation describing Boltzmann distribution; equation describing the <KER> of a thermal system; and equation describing the FHBT. The temperatures determined by the three different ways are very similar and found to increase with cluster size: the maximum value of <KER> was about 25 meV and $T^{\#}$ was about 210 K. This result gives confidence that the transition state and therefore the modeled dissociation can be described statistically applying 3-D model for describing the system. Also, with increasing cluster size the temperature of the transition state becomes approximately equal to the internal temperature of the cluster. This in turn applies that the internal energy of the methanol clusters is very low, approximately 210 K.
KER curves were also studied using MassKinetics: the 3-D -like curves were reproduced again, mean KER values were calculated and showed similar increasing tendencies with increasing the cluster size.

4. 3. Kinetic Isotope Effect (KIE)

The proton-bound deuterium labeled / unlabeled amine dimer may lose either an unlabeled or a deuterium labeled amine neutral as discussed in the Details of the experiment and modeling section. These reactions were examined experimentally and the ratios of the respective reaction rates (k_H/k_D) were found to be larger than unity, indicating a normal secondary isotope effect. This means that the proton affinity of deuterated amines is higher than that of unlabelled amines. Since the KIE yields important information on the structure of the gas phase ions and neutrals and also on reaction mechanism, we have preformed modeling calculations to understand the influencing factors of the KIE. The parameters of the calculations are listed in Chapter 3 and the error limits were determined by repeating the calculations with 10 times larger and lower pre-exponential factors, as well. In the case of methylamine, the isotope effect is calculated to be 1.43 (error limit: 1.33 – 1.61), which is close to the experimentally measured value of 1.39. Fragmentation of the dimers of other α-D substituted alkylamines has also been studied; the KIEs are shown in Table 4. 5. The results indicate good agreement between the calculated and measured KIE values determined using a high-pressure ion source. Correlation between

experimentally observed and theoretically calculated KIEs is also shown in Figure 4. 20. The standard deviation of the experimentally observed and the calculated KIEs (0.020) is only two times larger than the experimental uncertainty of the experimental data (0.010).

Table 4. 5: *Experimental data and results of calculations for dissociation reactions of proton-bound alkylamine dimers B–H^+–B-d_n.*

	VG k_H/k_D		JEOL k_H/k_D	
B-d_n	experimental	calculated[a]	experimental	calculated[a]
CD_3NH_2	1.39	1.43 (1.33 – 1.61)	4.10	1.45 (1.34 – 1.65)
CD_3NH-CH_3	1.28	1.24 (1.20 – 1.29)	1.63	1.20 (1.21 – 1.30)
CD_3NH-C_2H_5	1.22	1.20 (1.18 – 1.25)	1.36	1.18 (1.18 – 1.25)
CD_3NH-C_3H_7	1.19	1.18 (1.16 – 1.20)	1.30	1.16 (1.17 – 1.20)
CD_3NH-n-C_4H_9	1.16	1.17 (1.16 – 1.19)	1.26	1.15 (1.19 – 1.24)
$CH_3CD_2NH_2$	1.16	1.19 (1.16 – 1.23)	1.30	1.15 (1.16 – 1.24)
CH_3CD_2NH-CH_3	1.14	1.17 (1.15 – 1.21)	1.24	1.14 (1.15 – 1.21)
CH_3CD_2NH-C_2H_5	1.12	1.15 (1.13 – 1.16)	1.25	1.13 (1.13 – 1.16)
$CD_3CH_2NH_2$	1.17	1.07 (1.06 – 1.09)	1.18	1.05 (1.06 – 1.09)
CD_3CH_2NH-CH_3	1.15	1.05 (1.04 – 1.06)	1.13	1.04 (1.04 – 1.07)
CD_3CH_2NH-C_2H_5	1.13	1.04 (1.04 – 1.04)	1.13	1.04 (1.04 – 1.04)

[a] *Calculated assuming thermal energy distribution when ions leave the ion source*

The good agreement between the experimentally observed and calculated KIEs rests on three conditions: (1) accurate experiments under well-defined, thermal conditions; (2) accurate calculation of fragment abundances by applying statistical theories; and (3) accurate quantum-chemical calculation of frequency changes due to deuteration. The agreement is good for α-D substitution (red triangles in Figure 4. 20), but it is less satisfactory for the β-D substituted alkylamines (Table 4. 5, and blue circles in Figure 4. 20). As noted by *Norrman* and *McMahon*, α- and β-D substituted alkylamines show experimentally fairly similar KIEs, while the calculated 0-K energy difference is approximately four times lower in the case of β substitution. Our calculations support the previous findings that, the experimentally observed KIEs for β-D substituted amines cannot be explained based on *ab initio* calculated *Δ*ZPE(H/D) values.

Based on the calculated ion ratios, the effective temperatures were determined, as discussed before. In the case of the low-pressure ionization (JEOL instrument) setup, this ion ratio and the

resulted effective temperature were the basis of investigating the initial energy distributions of the fragmenting molecular ions, and helped to conclude that the initial internal energy distribution is in fact not thermal.

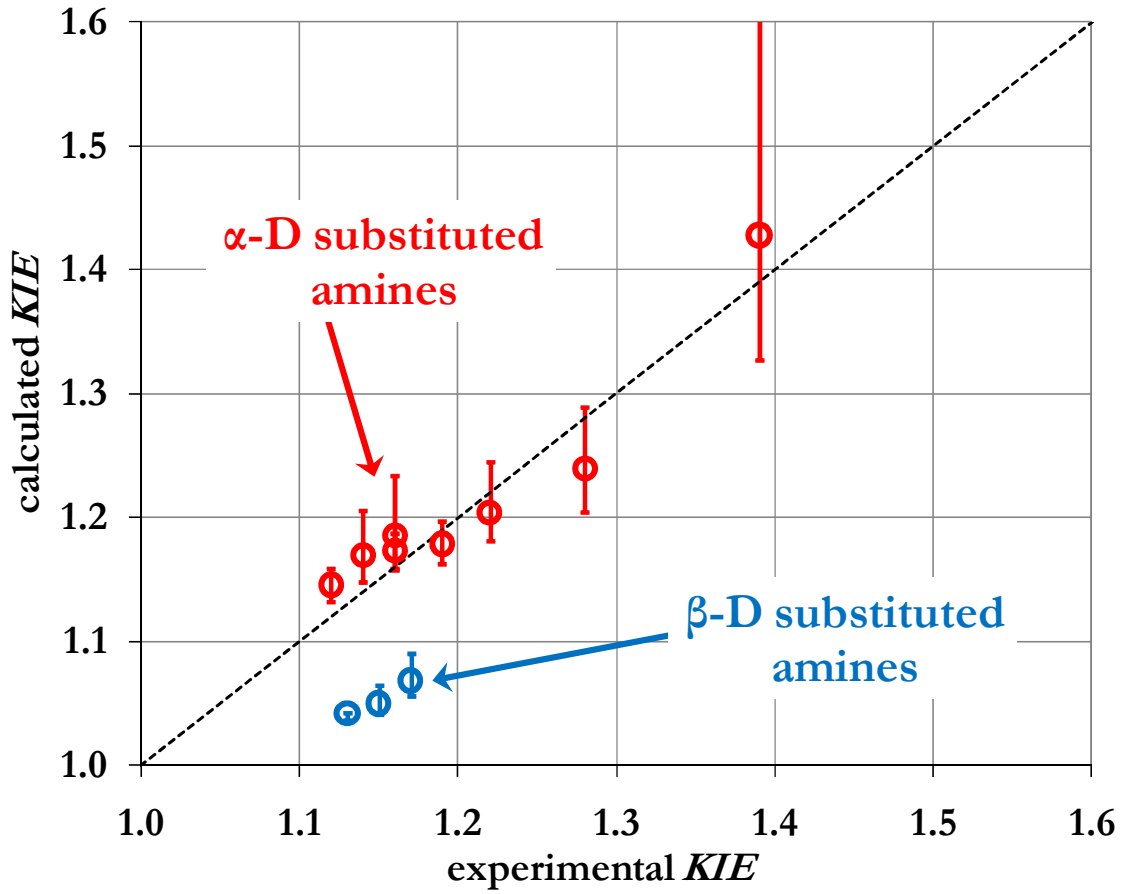

Figure 4. 20: *Correlation between the experimentally measured and modeled KIEs, on the high pressure ionization source VG instrument. The error bars indicate the calculated KIE using 10 times lower and higher pre-exponential factors. Triangles stand for data on the α-D substituted amines (correlation coefficient is 0.953), the circles belong to the β-D substituted amines. The dashed line represents exact agreement between experiments and calculations.*

4. 3. 1. Conclusions on Modeling KIE

A study of the dissociations of protonated alkylamine dimers has been published [88], and the experimentally observed ratio of the respective reaction rates (k_H/k_D) was found to be larger than unity, indicating a normal secondary isotope effect. This kinetic isotope effect was modeled with MassKinetics to have a better insight to the dissociation mechanism. In the case of the high-pressure ionization source, the experimental results were reproduced nicely assuming thermal initial energy distribution for the molecular ions: good agreement between the calculated

and measured KIE values of α-D substituted amines was found. In this case, not only the direction, but also the degree of the – very small – secondary kinetic isotope effect was successfully modeled with excellent correlation. For the β-D substituted alkylamines the calculated kinetic isotope effect values were lower than that of the experimentally observed ones, they were of similar magnitude compared to the α-D substituted amines. This difference between the experimentally observed ones and the calculated KIE values is due to the fact that the zero-Kelvin energy differences, calculated by quantum chemistry, were ca. 4 times lower for the β-D substituted alkylamines than for the α-D alkylamines. Unfortunately, the reason why quantum chemistry did not predict the energy differences correctly could not be determined.

4. 4. A Mass Spectrometry Standard: Protonated Leucine Enkephalin

4. 4. 1. Gibbs Free Energy of Fragmentation

In spite of the significant amount of effort invested, differences among published activation energies and pre-exponential factors for the $MH^+ \rightarrow \mathbf{b_4}^+$ are unacceptably large, as discussed above (Table 3. 3). Some of the results indicate that the reaction proceeds with large positive, according to some other studies with large negative entropy change. This very large uncertainty also implies that the experimental data are not sufficiently accurate to derive information on the temperature dependence of reaction enthalpy and entropy; so we assume these to be constant over the temperature range studied.

It is noted in the literature [129-131] that using the Arrhenius equation often there is a correlation between the determined activation energy and pre-exponential factor. In the present case one can also observe such a strong correlation (Figure 4. 21): When evaluation indicates high activation energy, the resulting transition state is "loose" (high pre-exponential factor). In reverse, low activation energy strongly correlates with a tight (i.e., unfavorable) transition state. The correlation between the measured activation energy and pre-exponential factor suggests, qualitatively, that various experiments might yield a similar value for the Gibbs free energy of fragmentation; but separation of the energy and entropy terms is very inaccurate. Note that the activation energy is equivalent with the activation enthalpy, while the pre-exponential factor corresponds to activation entropy.

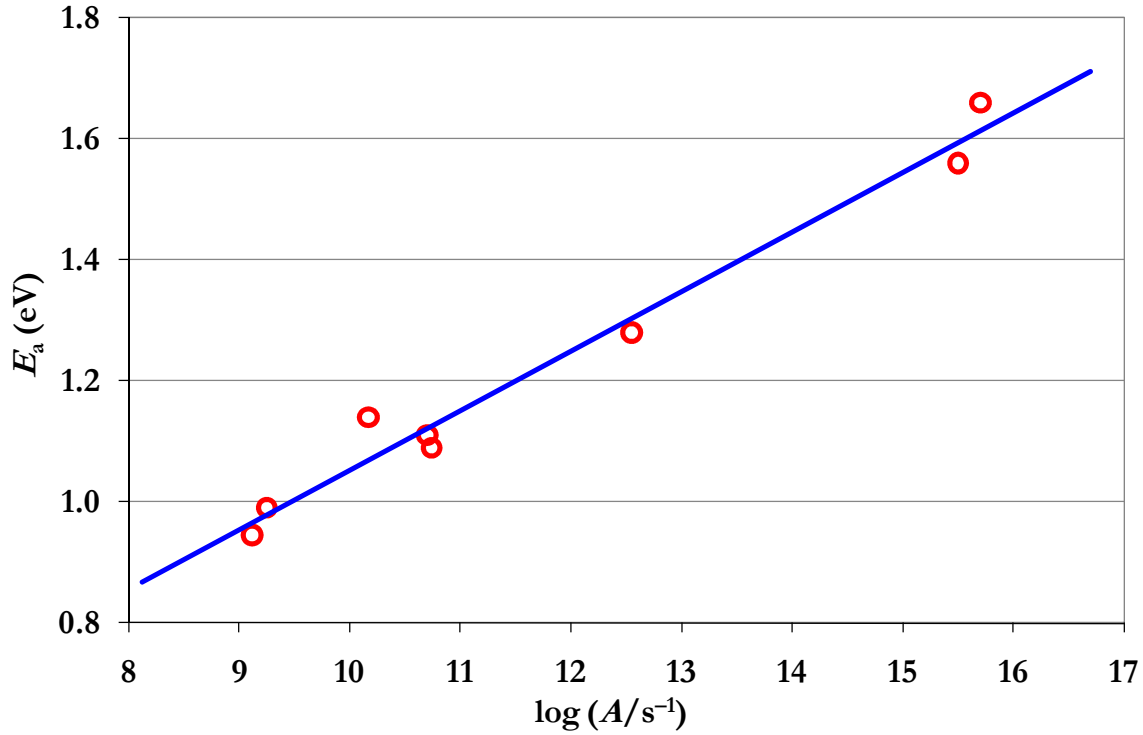

Figure 4. 21: *Correlation between the published activation energies and log A values.*

With these qualitative considerations in mind, we have reviewed the published raw data relating to the $MH^+ \rightarrow \mathbf{b}_4^+$ process. Wherever possible the published original data were used (as measured, evaluated, or estimated by the authors). Although it was not assumed that all experiments were performed under thermal conditions (SID studies are clearly non-thermal), basic thermochemical formulas were applied in order to obtain a better insight into energetics. The pre-exponential factor is closely related to the activation entropy ($\Delta S^{\#}$); the two parameters can be inter-converted using the following equation:

$$A = k_B \cdot T \cdot h^{-1} \cdot \exp(\Delta S^{\#}/R) \qquad (50)$$

We have determined the activation entropy at two different temperatures: at the mean temperature of the given set of experiments, and at the average temperature of all published data (489 K); and both are shown in Table 4. 6. The results show that the activation entropy determined from the pre-exponential factor at the two different experiments differ only slightly ($\pm$ 1 J·mol^{-1}·K^{-1} on average); while the different experiments published yield values which range from –75 to +50 J·mol^{-1}·K^{-1}. This confirms our previous assessment that temperature dependence of $\Delta S^{\#}$ does not need to be considered for discussing data evaluation.

With the activation energy (which is equal to the activation enthalpy) and the activation entropy (calculated as discussed above), the activation Gibbs free energy for the studied reaction can be calculated with the simple equation at any given temperature:

$$\Delta G^{\#} = \Delta H^{\#} - T \cdot \Delta S^{\#} \tag{51}$$

The $\Delta G^{\#}$ values have been calculated with Eq. 51. at the mean temperature of all experiments (489 K) and at the mean temperature of the each individual experiment. The uncertainties of $\Delta G^{\#}$ corresponding to the various published results were calculated using the published uncertainty values of E_a and $\log A$ (wherever was available), using standard formalism; these are also listed in Table 4. 6 All $\Delta G^{\#}$ values fall into a narrow range; those calculated at 498 K have a mean value of 1.35 ± 0.04 eV. Those calculated at the mean temperature of the experiments show an even better agreement, 1.34 ± 0.03 eV. Note that in this derivation only data given in the original publications were used. The results clearly indicate that all seven experiments, based on independent ideas and a wide range of experimental conditions, yield practically the same activation Gibbs free energy for fragmentation of protonated leucine enkephalin to lead to the $\mathbf{b_4}^+$ ion. It is important to note that the same experiments yielded widely different activation energies (E_a), pre-exponential factors and activation entropies ($\Delta S^{\#}$). This behavior indicates that, although experimental measurements might be accurate, the separation of energy and entropy terms in the in the original papers is inadequate. Furthermore without the ability of a satisfactory separation of the $\Delta S^{\#}$ and $\Delta H^{\#}$, any temperature dependence is impossible to determine based on the experimental results.

Some of the experiments discussed above were performed under thermal conditions (those of *Wysocki*'s thermal decomposition, *Williams*' BIRD, and *McLuckey*'s ion-trap results [77, 132, 133], in the case of other experiments, thermal conditions are not, or not necessarily, satisfied (SID results, IRMPD excitation, and some of the ion-trap experiments [78, 133, 134]). Nevertheless, all of these experiments yield practically the same $\Delta G^{\#}$ value. The near agreement among $\Delta G^{\#}$ values determined suggests that $\Delta G^{\#}$ = 1.35 eV (127.7 kJ/mol) might be close to the 'true' thermochemical value at around 489 K. The results suggest, furthermore, that even those mass spectrometric experiments that are performed under non-thermal conditions could yield approximate $\Delta G^{\#}$ values. A final comment to this section is that deriving a single (average and therefore temperature-independent) $\Delta G^{\#}$ value for the $MH^+ \rightarrow \mathbf{b_4}^+$ reaction may be useful, but is a crude approximation; the experimental data can be more accurately described using temperature dependence, and this is discussed in the next section.

Table 4. 6: *Activation energies and pre-exponential factors of the $MH^+ \rightarrow b_4^+$ fragmentation process of leucine enkephalin.*

Publication	Evaluated in the present study (based on the quoted experimental values)		
	$\Delta S^{b,c}$	$\Delta G^{\#\,a,c}$ at 400K	$\Delta G^{\#\,a,d}$ at T_{exp}
[133]	49.30	1.40	1.33
[134]	48.87	1.32	1.35
[77]	–43.54 ± 0.60	1.33 ± 0.06	1.31 ± 0.06
[132]	–8.53 ± 0.17	1.32 ± 0.08	1.32 ± 0.08
[79]	–43.60	1.31	1.32
[78]	–70.73 ± 0.65	1.36 ± 0.04	1.30 ± 0.04
[78]	–75.41 ± 0.15	1.32 ± 0.01	1.37 ± 0.01
[31]	–53.64	1.42	1.39
Average and standard deviation	***–25 ± 50***	***1.35 ± 0.04***	***1.34 ± 0.03***

[a] *in eV units*
[b] *in $J \cdot mol^{-1} \cdot K^{-1}$*
[c] *calculated in this work at 400 K*
[d] *calculated in this work using the average of T_{exp} range*

4. 4. 2. Re-evaluation of the Rate Constants (Arrhenius Plots)

Temperature dependent rate constants are typically evaluated with the Arrhenius equation:

$$k = A\mathrm{e}^{-E_a/RT}$$

or, in logarithmic form:
$$\ln k = \ln A - E_a/RT \qquad (52)$$

where k is the rate constant, A the pre-exponential factor, E_a the activation energy, R the universal gas constant, and T the temperature. Evaluation is usually based on an Arrhenius plot that shows the logarithm of the rate constant as a function of $1/T$. The slope of the plot gives the activation energy and the y-intercept the pre-exponential factor. In the present paper we are re-evaluating results in previous publications on leucine enkephalin with Arrhenius plots. The novel feature is that we shall evaluate all results together; that analysis will hopefully yield much better accuracy.

In some previous publications, rate constants are given as a function of temperature – in some cases, 'real' temperature [77, 132, 133], and in one case the 'effective' temperature [78]. In these cases, the temperature-dependent rate constants were taken from the literature, and were used without any conversion. The data are plotted in Figure 4. 22, in a conventional Arrhenius plot.

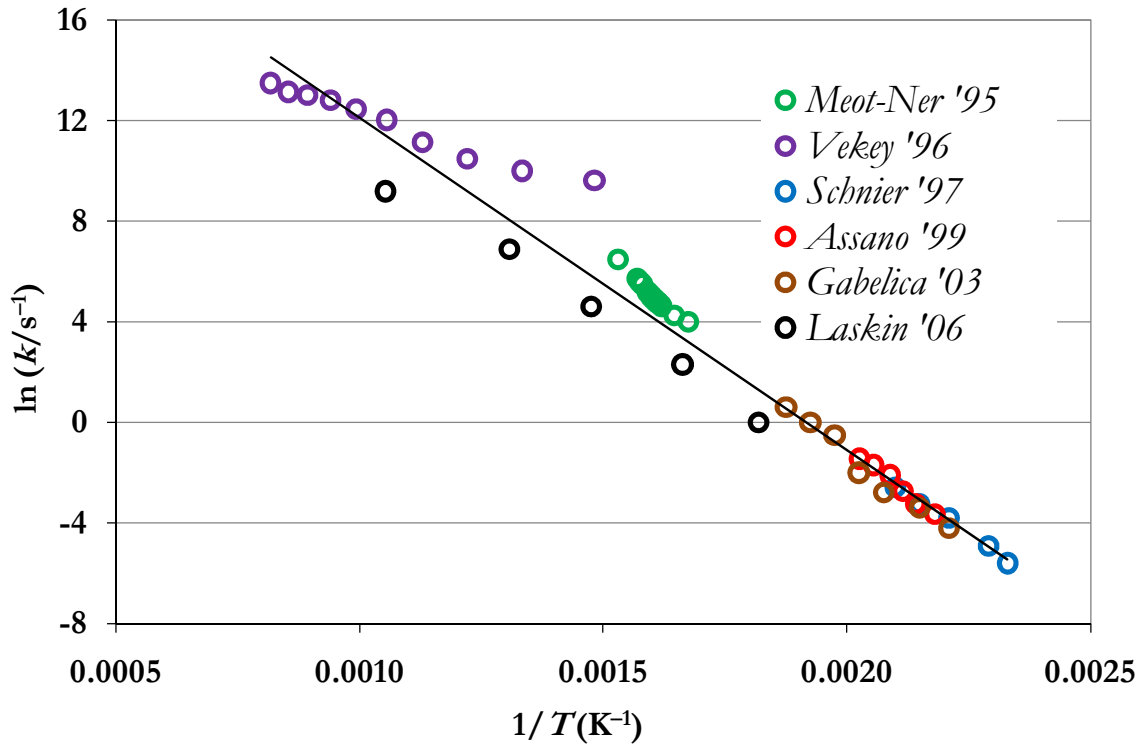

Figure 4. 22: *Arrhenius plot reconstructed from data published in previous papers; see text for details.*

In the case of other papers [31, 134], internal-energy dependent rate constants are given or have been determined from the curves published. To each internal energy, a temperature can be assigned, where the internal energy is equal to the mean thermal energy. In this manner, the internal-energy dependence was converted into approximate temperature dependence; and these values have also been plotted in Figure 4. 22. The mean internal energy of leucine enkephalin at a given temperature can be determined if one knows the vibrational frequencies (see below); the calculations were performed with MassKinetics software [20]. A similar conversion can be done with published approximate analytical formulas [135].

The Arrhenius plot in Figure 4. 22 shows all available temperature- or internal-energy dependent rate constants in the six papers discussed above. Note that in the papers of *Jockusch* et al. and *Paech* et al., no temperature- or internal-energy dependent data were specified, those data could not be included in this analysis. The plot shows a good linear relationship among the data ($R^2 = 0.97$). Furthermore, the data do not show any major deviation – either at the low, or at the high temperature end. The only unconventional feature of this plot is that data are derived from different types of experiments. Using different types of experiments allows a span over an unusually large temperature range; from 400 to 1200 K. Note that data derived from experiments performed under thermal and non-thermal conditions fall on the same line. Largest deviations

(corresponding to a low slope) are shown in the case of SID/RRKM results [134]. These large deviations are most likely due to an incorrect assumption in the original paper, that in the ESI source cold ions (at approximately 425 K) will be formed. Correcting this assumption would decrease deviation from the Arrhenius plot; however, to obtain unbiased results, we have decided not to correct any data given in the original papers. In any event, our calculations indicate that this correction would have only a minor influence on the overall result (less than 0.01 eV in E_a).

A simple linear evaluation yields Arrhenius parameters of $E_a = 1.15 \pm 0.03$ eV and $\log A = 11.2 \pm 0.3$. This evaluation assumes the activation entropy and enthalpy to be temperature independent, as discussed above.

This linear evaluation somewhat biased, because in some papers few, in others more, data points have been given. If we consider that all six publications have the same significance (i.e., they are equally valid), then we have to weight the data in Figure 4. 22 with the inverse of the number of data points given (e.g., in one reference there were 10 data points; therefore these data are weighted by 1/10; in another, there were 6 data points, so these are weighted by 1/6). Weighting yields 'unbiased' results, and the Arrhenius parameters so determined are $E_a = 1.14$ eV and $\log A = 11.0$ at 489 K. Error limits, with 95% confidence interval, indicate a precision of $\pm$ 0.03 eV in E_a, and $\pm$ 0.3 units in the log A value. These precisions are due to the scatter of the data points; i.e., due to random errors in the six experiments discussed.

It is worth discussing the reason for the success of the present evaluation. Using all data points, it was possible to fit a good linear correlation to all the data (Figure 4. 22). The data span over a wide range of temperature and rate constants. This wide range allows the accurate determination of the slope (by interpolation) and the y-intercept (by extrapolation). In this respect, the accuracy of the individual data points is less important than the fact that they span over a large range. (Note that the rate constants in Figure 4. 22 span over 9 orders of magnitude.) This large range is possible only if one uses different experimental techniques; some measure small (e.g., FT-ICR), and some large (e.g., SID), rate constants. On the other hand, the range of measurable rate constants in any instrumental or experimental configuration is usually within a factor of 100 to 1000; that small range makes determination of the slope and intercept very inaccurate. This inaccuracy is illustrated in Figure 4. 23, which shows *Williams*' and *McLuckey*'s results by blue and red circles, respectively (same values as in Figure 4. 22). One can see that the data practically overlap; however, extrapolation (as specified in the original publication and shown by the blue and red trend lines in Figure 4. 23) yields very different results. Note that the large error

connected with extrapolation discussed above is analogous to that discussed in detail by *Ervin* and *Armentrout* with respect to the 'kinetic method' [136].

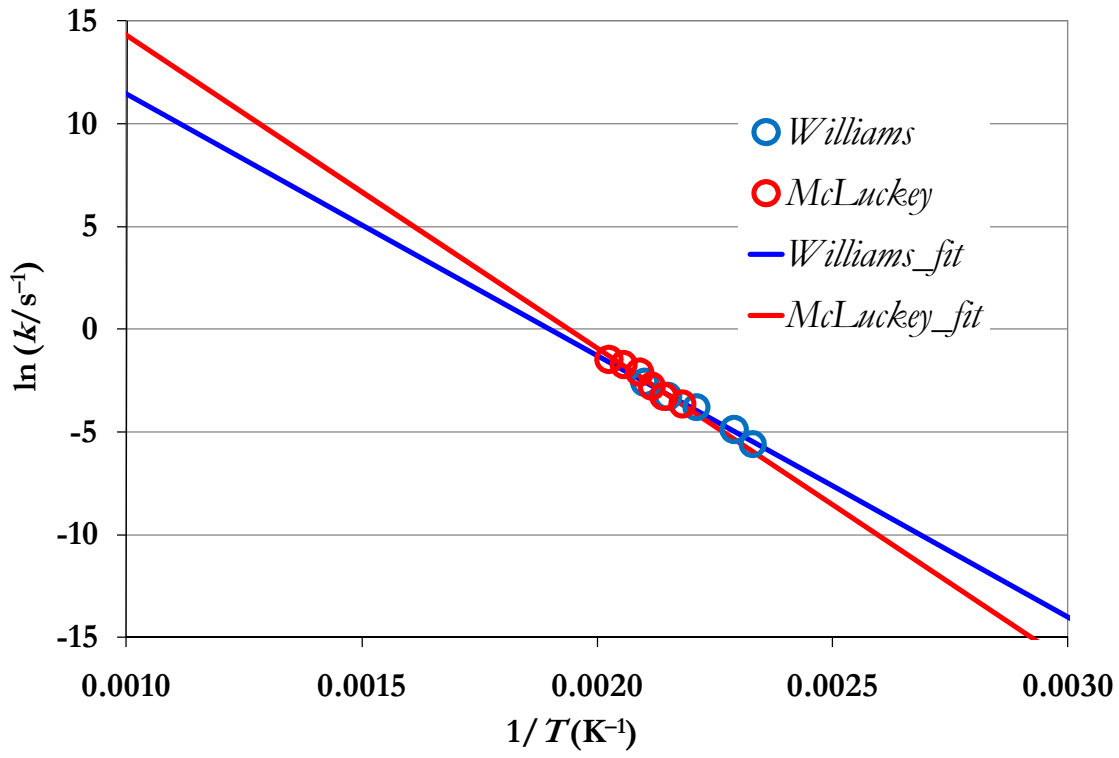

Figure 4. 23: *Arrhenius plot of the experimental points published in Williams' and McLuckey's papers. The difference in the resulted linear fit is illustrated*

The six different data sets were obtained by different groups that used various experimental techniques and different approximations. Because weighting has little influence on the results, considering the relative merits of the six different approaches is not essential to arrive at a consensus value. On the other hand, variation among the results should be a good indication of the overall accuracy – i.e., could be used to estimate systematic errors. This test was performed by leaving out one data set, and by repeating the evaluation with the five remaining data sets. This process was repeated six times by leaving out each different set of data. The six different results were close to each other; the standard deviation of the activation energy was ± 0.015 eV and for log$A$ it was ± 0.17. The largest deviation was observed when *Laskin*'s data were left out; the activation energy shifted up by 0.03 eV and log$A$ up by 0.30 units. The results indicate that systematic errors are comparable to the random errors discussed above. With a 95 % confidence interval (i.e., 2 std. deviations) systematic errors are estimated to be less than 0.03 eV in E_a and 0.3 in log$A$.

Assuming the presence of random and systematic errors, and a 95% confidence interval; the Arrhenius-type activation energy of the $MH^+ \rightarrow \mathbf{b_4}^+$ process of leucine enkephalin is 1.14 ± 0.05 eV; whereas the logarithm of the pre-exponential factor (log*A*) is 11.0 ± 0.5 at 489 K. From the pre-exponential factor the activation entropy can also be determined (with Eq. 50, as above) to yield $\Delta S^{\#} = -38.1\ J \cdot mol^{-1} \cdot K^{-1}$. Accuracy is estimated to be ± 9. 6 $J \cdot mol^{-1} \cdot K^{-1}$.

4. 4. 3. Comparison to the Absolute Rate Theory

The same data have also been evaluated with the absolute-rate theory. We have used the MassKinetics program package [20] to calculate the canonical rate constants as a function of temperature. The calculations used vibrational frequencies and the transition state model described in the next section. The rate calculations used two adjustable parameters: the critical energy (E_0) and the pre-exponential factor (log*A*). These two adjustable parameters have been optimized to give the best fit between the calculated and experimentally determined rate constants.

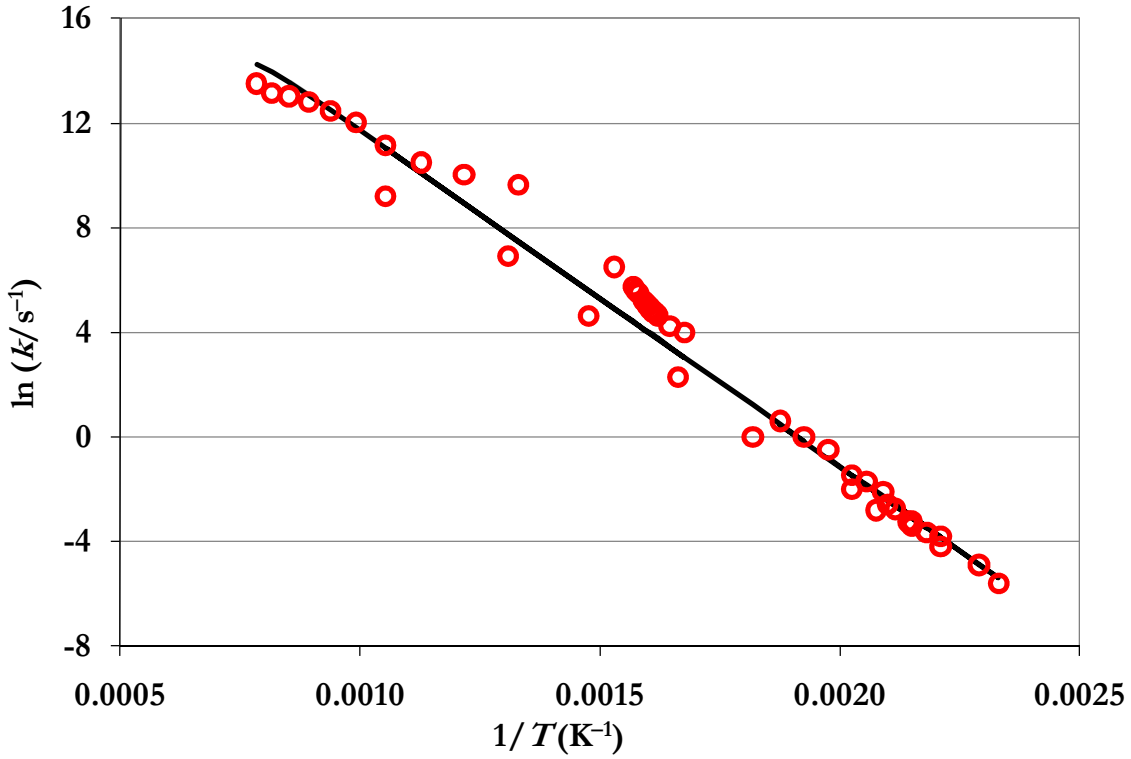

Figure 4. 24: *Arrhenius plot of the best-fit between the experimentally determined rate constants and those calculated with the absolute rate theory.*

The best fit shown in Table 3. 1: has a correlation coefficient of $R^2 = 0.98$. The fit yields a critical energy, E_0, of 1.19 eV, which is 0.05 eV higher than that of the Arrhenius type activation energy,

E_a. This difference agrees well with the calculation of *Jockusch* et al. that showed a 0.07 eV difference [54]. The pre-exponential factor calculated from the transition state model is $10^{10.8}$ s^{-1}. It is noted again that the temperature dependence of the activation entropy and enthalpy has been neglected, as discussed above.

4. 4. 4. Conclusions on Protonated Leucine Enkephalin

The dissociation parameters of leucine enkephalin were chosen for our study due to the fact that this molecule is the most commonly used standard in mass spectrometry. Several paper have been published reporting Arrhenius dissociation parameters for the best studied dissociation process, $MH^+ \rightarrow \mathbf{b_4}^+$ fragmentation reaction of leucine enkephalin: the published data show major controversies among the results: E_a values range from 0.94 to 1.66 eV with a standard deviation of 0.25 eV. The published pre-exponential factors also span a large range (log$A$ values from 9.1 to 15.7).

First, strong correlation between the activation energy and the pre-exponential factor was found, connecting the high activation energy with the loose transition state (high log$A$), and the low activation energy with the tight TS. This suggests that despite the big deviation among the published results for E_a, and log$A$, the experiments might yield similar value for the Gibbs free energy of the studied fragmentation. Because the activation energy is equivalent to the activation enthalpy, while the pre-exponential factor corresponds to activation entropy, the mean $\Delta G^{\#}$ was determined: 1.34 eV and shows only 0.03 eV (5 %) standard deviation. Note, however, that it is a crude approximation and the temperature dependence of $\Delta S^{\#}$ is not considered.

As the next step, the published raw experimental data was taken and an overall Arrhenius plot was constructed to investigate the temperature (or internal energy) dependence. The results show that the data fall on the same line, and that there are no significant deviations from the linear trend-line ($R^2 = 0.97$). The conventional evaluation resulted in an activation energy of 1.14 eV and a pre-exponential factor of $10^{11.0}$ s^{-1}. These values correspond to the mean temperature of the experiments (489 K). The pre-exponential factor corresponds to an activation entropy of –38.1 $J \cdot mol^{-1} \cdot K^{-1}$. The degree of possible systematic errors was evaluated by including or excluding various data sets from evaluation. This evaluation shows that systematic errors are modest, and are similar to the influence statistical errors. Overall accuracy of the results (with a 95% confidence limits) are $\Delta H = 1.14 \pm 0.05$ eV; log$A = 11.0 \pm 0.5$, $\Delta S^{\#} = -38.1 \pm 9.6$ $J \cdot mol^{-1} \cdot K^{-1}$, and in our opinion this is the best available data set for the $\mathbf{b_4}^+$ dissociation channel of protonated leucine enkephalin.

This study also gives an important message for future reference: it was demonstrated that determining dissociation parameter values, using two or more different mass spectrometers may allow one to have a wider temperature range and therefore to determine more accurate and precise dissociation parameters from the Arrhenius plot.

5. Summary

Understanding the mechanism of ion dissociation and the major processes that influence the ion intensities observed in mass spectrometry is fundamental to advance many fields of chemistry. During my Ph.D. research, I investigated several systems to determine the fundamental properties of dissociating ions, such as the initial internal energy distribution, and the effective temperature that describe the initial state of the molecular ion. These parameters, and a carefully constructed framework to describe how they change in the mass spec experiments allows an accurate calculation of the basic features of the mass spectrum, such as ion intensities, and – in the case of metastable decays – peak widths. For this latter, my aim was also to model the kinetic energy release (KER) and kinetic isotope effect (KIE) in the dissociation of protonated dimers and clusters.

All of these carefully chosen model simulations also helped to improve our RRKM-based program package, MassKinetics so that, in the immediate future, it can be used to model a wide variety of systems with close-to-experimental accuracy.

The studied systems can be categorized into four groups: the dissociation of a) protonated alkylamines; b) protonated benzylpyridines, and protonated aromatic benzoic esters; c) protonated methanol clusters; and d) the most commonly used protonated oligopeptide, leucine enkephalin was investigated. The experimental results were taken either from previous publications or were obtained in our research group. As the principal theme of my graduate research was the modeling of mass spectra, this thesis was structured from the modeling point of view: the results were categorized into four subchapters: a) modeling ion energy distributions at different stages of the dissociation processes of various model systems; b) modeling the kinetic energy release for protonated alkylamine and protonated methanol cluster systems; c) calculation of the kinetic isotope effect for protonated alkylamine systems; d) re-evaluation of the previously published experimental data of protonated leucine enkephalin.

5. 1. Conclusions on Calculating Internal Energy Distributions

It is widely accepted that the internal energy and its distribution play an important role in shaping the spectrum in any mass spectrometry experiment. Therefore, as the first step in my studies, the internal energy distribution was examined using model compounds: protonated benzylpyridinium and protonated benzoic ester ions in an electrospray ionization source. These molecules are often used to determine the energy profile of a mass spectrometer because they

readily yield very accurate experimental data for the modeling calculations, and for this reason they were chosen for our MassKinetics studies. In my thesis work, I have modeled the internal energy distributions of the protonated alkylamine dimers from two different experimental setups. These ions dissociate through a loose transition state and the intensity ratio of the two possible fragment ions can be used to determine the dissociation energetics. The experimental ion intensities were used to determine the survival yield (SY), and the correlation between the critical energies and the transition states was investigated: the logarithm of the SY was found to be proportional to the logarithm of the critical energy in the case of the benzylpyridinium salts. However, the correlation was less pronounced for the protonated benzoic ester ions. Therefore, the degree of fragmentation of the different substituted benzylpyridinium ions varies due to changes in the critical energies, whereas in the case of the protonated ester ions, it is the different transition states that lead to the different degrees of fragmentation.

The survival yields were then used to determine the corresponding characteristic temperatures. Using these, the internal energy distributions were calculated and it was found that they closely resemble thermal energy distributions. My calculations gave very similar internal energy distributions for the various substituted benzylpyridinium and benzoic ester ions, and there was no significant difference between the average internal energy distribution of the protonated benzylpyridinium ions and that of the benzoic esters, either. These results conformed the previous assumption that the electrospray ion source produces roughly the same initial internal energy distributions for systems with similar degrees of freedom.

The effect of the collisions was demonstrated by calculating the thermal energy distributions at an initial 353 K temperature plus either 20 or 40 collisions in the source and it was found that the internal energy distribution can be reproduced by a thermal distribution calculated at higher temperatures (790 K, and 1210 K, respectively). The effect of the cone voltage on the mean internal energy was also studied for both sets of the precursor ions, and an excellent linear relationship was found regardless of the ion structure.

Dissociation rate curves were calculated as a function of the internal energy and the appearance energies were determined to demonstrate the kinetic shift in the modeled experiment.

In the case of the protonated alkylamine dimers, results from two different experimental setups were taken from the literature – using a high-pressure and a low-pressure ionization source – and MassKinetics calculations were carried out to explain the significant difference in the experimental results. In the case of the high-pressure experimental setup, the experimental results were successfully modeled assuming thermal internal energy distribution. The effective temperatures (T_{eff}) were determined from the measured ion intensity ratios (I_H/I_D = KIE) based

on the kinetic method. In the case of low-pressure ionization source, the experimental and calculated T_{eff} and the ion ratios were significantly different; hence the assumption of the thermal distribution of the internal energy was refuted. The internal energy distributions were examined in detail, and, based on the experimental data, it was concluded that a) there is a high fraction of high-energy ions, leading to high fragment ion abundances, while at the same time, b) the effective temperature is low, i.e. the energy distribution are very narrow above the fragmentation threshold to account for the findings with help of the kinetic method.

It was also confirmed that the source temperature does not have a large effect on the observed T_{eff} and KIE, because the tail of the thermal distributions corresponding to the source temperature is similar above the fragmentation threshold. However, a lower source temperature results in a reduced fragment ion yield due to the smaller tail of the distribution that stretches above the fragmentation threshold.

Finally, the internal energy distribution of the fragmenting ion population under mass spectrometric conditions was compared to the internal energy distributions of ions fragmenting under thermal, equilibrium conditions (high-pressure limit). The two internal energy distributions were found to be similar at many temperatures for many of the studied systems. The roughly similar shape of the calculated internal energy distributions serves a good qualitative support for the kinetic method that was used in this research.

5. 2. Conclusions on Modeling KER

Results from metastable ion measurements were used to model the kinetic energy release of protonated alkylamine dimers and protonated methanol clusters.

Statistical energy partitioning was assumed for both examined systems and the modeling results were found to be in excellent agreement with the experimental results, which show that the metastable peaks can be fitted with a single Gaussian function. The model calculations showed that KER(D) is similar to a Maxwell-Boltzmann 3-D distribution that is, the KER is due to a three dimensional translational motion, which is still a matter of debate in the literature.

Based on the results that the KERD is three dimensional, the mean kinetic energy release, <KER> was determined both from the metastable peak, and was connected to T_{eff} using the simple relationship of $\langle KER \rangle \approx 3/2\ k_B T_{eff}$. The observed agreement between the experimental kinetic energy release and $3/2\ k_B T_{eff}$ yields further proof of the three dimensional KER distribution. It is important to point out that in this calculation the T_{eff} and the KER data came

from separate studies, the parameters used in the modeling were measured and calculated independently.

In the case of the protonated methanol clusters, low-temperature FAB technique was used to produce protonated methanol clusters and the KER processes were studied by recording the metastable water loss of the selected clusters. KERD curves were calculated and the distribution shapes were examined and compared to 2-D, 3-D and 4-D Boltzmann distributions. Mean KER values, <KER>, were found to increase sharply with increasing cluster size for n = 1 – 7, and level out around octamer size. Transition state temperatures were determined using equations from three different methods: an equation describing Boltzmann distribution; an equation describing the <KER> of a thermal system; and an equation describing the FHBT. The temperatures determined by the three different ways are very similar and found to increase with cluster size: the maximum value of <KER> was about 25 meV, with a $T^{\#}$ of 210 K. These results assert that the product energy distribution can be described statistically with 3-D translation. Also, with increasing cluster size, the temperature of the transition state becomes approximately equal to the internal temperature of the cluster. This in turn applies that the internal energy of the methanol clusters is rather low, at 210 K.

KER curves were also studied using MassKinetics, reproducing the 3-D curves; and the calculated mean KER values showed similar increasing tendencies with increasing cluster size.

5. 3. Conclusions on Modeling KIE

The dissociation of protonated alkylamine dimers were studied by *Norrman* and *McMahon* [88], and the experimentally observed ratio of the reaction rates in non-deuterated vs. deuterated ions (k_H/k_D) was found to be larger than unity, indicating a normal secondary isotope effect. In my thesis work, this kinetic isotope effect was modeled with MassKinetics. In the case of the high-pressure ionization source, the experimental results were reproduced very well assuming thermal initial energy distribution for the molecular ions: very good agreement between the calculated and the measured KIE values of the α-D substituted amines was found. In this case, not only the direction, but also the degree of the – very small – secondary kinetic isotope effect was successfully modeled with good accuracy. For the β-D substituted alkylamines, the experimentally observed KIEs were found to be of similar magnitude compared to the α-D substituted amines. However, the zero-point energy differences from quantum chemical methods were approximately four times smaller than for the α-D alkylamines leading to a calculated kinetic isotope effect that was much lower than the experimental values.

5. 4. Conclusions on the Protonated Leucine Enkephalin Study

Leucine enkephalin was chosen for my studies because this molecule is one of the most commonly used standards in mass spectrometry. Several papers have been published reporting the Arrhenius dissociation parameters for the best studied dissociation process, the $MH^+ \rightarrow \mathbf{b_4}^+$ fragmentation reaction, however, major discrepancies can be found in the published data. The measured E_a values range from 0.94 to 1.66 eV with a standard deviation of 0.25 eV. The published pre-exponential factors also span a large range ($\log A$ values from 9.1 to 15.7).

First, we found a strong correlation between the activation energy and the pre-exponential factor, connecting a high activation energy with a loose transition state (high $\log A$), and a low activation energy with a tight TS. This suggests that despite the large deviation among the published results for E_a, and $\log A$, the experiments might yield similar values for the Gibbs free energy of the fragmentation reaction. From the activation enthalpy, and the pre-exponential factor – which corresponds to the activation entropy –, the $<\Delta G^{\#}>$ could be determined to be 1.34 eV with a standard deviation of only 0.03 eV (5 %). Note, however, that in this approximation, the temperature dependence of $\Delta S^{\#}$ was not taken into account.

As the next step, the published raw experimental data were used to construct an overall Arrhenius plot to investigate the temperature (or internal energy) dependence. The results show that the data are consistent, and that there are no significant deviations from a linear trend ($R^2 = 0.97$). The Arrhenius-type evaluation resulted in an activation energy of 1.14 eV and a pre-exponential factor of $10^{11.0}$ s^{-1} at the mean temperature of the experiments (489 K). The pre-exponential factor corresponds to an activation entropy of –38.1 $J \cdot mol^{-1} \cdot K^{-1}$. The effect of possible systematic errors was evaluated by including or excluding data sets from the evaluation. This shows that systematic errors are modest, and are similar to the influence of random errors. The final results (with a 95% confidence limits) are $\Delta_r H = 1.14 \pm 0.05$ eV; $\log A = 11.0 \pm 0.5$, $\Delta S^{\#} = -38.1 \pm 9.6$ $J \cdot mol^{-1} \cdot K^{-1}$, and so far represent the best available data set for the $\mathbf{b_4}^+$ dissociation channel of protonated leucine enkephalin.

This study also gives an important message for future reference: it was demonstrated that determining dissociation parameters using two or more different mass spectrometers allows one to use data from a wider temperature range and, therefore, to determine more accurate and more precise dissociation parameters from the Arrhenius plot.

6. References

1. Nibbering, N.M.M., *Four decades of joy in mass spectrometry*. Mass Spectrometry Reviews, 2006. **25**(6): p. 962.
2. Pitteri, S.J. and McLuckey, S.A., *Recent developments in the ion/ion chemistry of high-mass multiply charged ions*. Mass Spectrometry Reviews, 2005. **24**(6): p. 931.
3. Laskin, J. and Futrell, J.H., *Collisional activation of peptide ions in FT-ICR mass spectrometry*. Mass Spectrometry Reviews, 2003. **22**(3): p. 158.
4. McLuckey, S.A., *Principles of Collisional Activation in Analytical Mass Spectrometry*. Journal of the American Society for Mass Spectrometry, 1992. **3**: p. 599.
5. Fricker, L.D., *Minireview: Neuropeptidomics to study peptide processing in animal models of obesity*. Endocrinology, 2007. **148**(9): p. 4185.
6. Wells, J.M. and McLuckey, S.A., *Collision-induced dissociation (CID) of peptides and proteins*, in *Biological Mass Spectrometry*. 2005, Elsevier Academic Press Inc: San Diego. p. 148.
7. Rompp, A., et al., *Examples of Fourier transform ion cyclotron resonance mass spectrometry developments: from ion physics to remote access biochemical mass spectrometry*. European Journal of Mass Spectrometry, 2005. **11**(5): p. 443.
8. Pajzs, B. and Suhai, S., *Fragmentation pathways of protonated peptides*. Mass Spectrometry Reviews, 2005. **24**(4): p. 508.
9. Bogdanov, B. and Smith, R.D., *Proteomics by FTICR mass spectrometry: Top down and bottom up*. Mass Spectrometry Reviews, 2005. **24**(2): p. 168.
10. Laskin, J., *Energy and entropy effects in gas-phase dissociation of peptides and proteins*. Principles of Mass Spectrometry Applied to Biomolecules, ed. J.L. Laskin, Chava. 2006: John Wiley & Sons, Inc. 619.
11. Armentrout, P.B., *Threshold collision-induced dissociations for the determination of accurate gas-phase binding energies and reaction barriers*, in *Modern Mass Spectrometry*. 2003, Springer-Verlag Berlin: Berlin. p. 233.
12. Armentrout, P.B. and Baer, T., *Gas-phase ion dynamics and chemistry*. Journal of Physical Chemistry, 1996. **100**(31): p. 12866.
13. Ervin, K.M., *Experimental techniques in gas-phase ion thermochemistry*. Chemical Reviews, 2001. **101**(2): p. 391.
14. Ervin, K.M., *Experimental techniques in gas-phase ion thermochemistry. (vol 101, pg 391, 2001)*. Chemical Reviews, 2002. **102**(3): p. 855.

15. Dunbar, R.C., *BIRD (blackbody infrared radiative dissociation): Evolution, principles, and applications.* Mass Spectrometry Reviews, 2004. **23**(2): p. 127.
16. Klagkou, K., et al., *Approaches towards the automated interpretation and prediction of electrospray tandem mass spectra of non-peptidic combinatorial compounds.* Rapid Communications in Mass Spectrometry, 2003. **17**(11): p. 1163.
17. Eddes, J.S., et al., *CHOMPER: A bioinformatic tool for rapid validation of tandem mass spectrometry search results associated with high- throughput proteomic strategies.* Proteomics, 2002. **2**(9): p. 1097.
18. Wilson, J. and Vachet, R.W., *Multiplexed MS/MS in a Quadrupole Ion Trap Mass Spectrometer.* Analytical Chemistry, 2004. **76**(24): p. 7346.
19. Fernandez, F.M., et al., *Protein identification via surface-induced dissociation in an FT-ICR mass spectrometer and a patchwork sequencing approach.* Journal of the American Society for Mass Spectrometry, 2006. **17**(5): p. 700.
20. Drahos, L. and Vékey, K., *MassKinetics: a theoretical model of mass spectra incorporating physical processes, reaction kinetics and mathematical descriptions.* Journal of Mass Spectrometry, 2001. **36**: p. 237.
21. Vékey, K., *Internal energy effects in mass spectrometry.* Journal of Mass Spectrometry, 1996. **31**(5): p. 445.
22. Wysocki, V.H., et al., *Internal energy distributions of isolated ions after activation by various methods.* International Journal of Mass Spectrometry and Ion Processes, 1987. **75**(2): p. 181.
23. Vékey, K., *Role of internal energy in mass spectormetric fragmentation*, in *Selected Topics and Mass Spectrometry in the Biomolecular Sciences*, R.M. Caprioli, et al., Editors. 1997, Kluwer Academic Publisher: Kluwer. p. 129.
24. Gabelica, V. and De Pauw, E., *Internal energy and fragmentation of ions produced in electrospray sources.* Mass Spectrometry Reviews, 2005. **24**(4): p. 566.
25. Drahos, L., et al., *Thermal energy distribution observed in electrospray ionization.* Journal of Mass Spectrometry, 1999. **34**(12): p. 1373.
26. Robinson, P.J. and Holbrook, K.A., *Unimolecular Reactions.* 1972, Bristol: John Wiley & Sons Ltd.
27. Levsen, K., *Fundamental Aspects of Organic Mass Spectrometry.* Vol. 4. 1978, New York: Verlag Chemie.
28. Arrhenius, S., *Über die Reaktionsgeschwindigkeit bei der Inversion von Rohrzucker in Säuren.* Zeitschrift fur Physikalische Chemie, 1889. **4**: p. 226.

29. Laider, K.J., *The development of the Arrhenius equation*. Journal of Chemical Education, 1984. **61**: p. 494.
30. Tolman, R.C., *Statistical mechanics applied to chemical kinetics*. Journal of the American Chemical Society, 1920. **42**: p. 2506.
31. Laskin, J., *Energetics and Dynamics of Fragmentation of Protonated Leucine Enkephalin from Time- and Energy-Resolved Surface-Induced Dissociation Studies*. Journal of Physical Chemistry A, 2006. **110**(27): p. 8554.
32. Baer, T. and Hase, W.L., *Unimolecular reaction dynamics*. 1996, New York: Oxford University Press.
33. Gilbert, R.G. and Smith, S.C., *Theory of Unimolecular and Recombination Reactions*. 1990, Oxford, UK: Blackwell Scientific Publication.
34. Giddings, J.C. and Eyring, H., *Equilibrium Theory of Unimolecular Reactions*. Journal of Chemical Physics, 1954. **22**(3): p. 538.
35. Lindemann, F.A., Journal of the Chemical Society, Faraday Transactions, 1922. **17**: p. 598.
36. Rice, O.K. and Ramsperger, H.C., Journal of the American Chemical Society, 1927. **49**: p. 1617.
37. Kassel, L.S., Journal of Physical Chemistry, 1928. **32**: p. 1065.
38. Marcus, R.A. and Rice, O.K., J Phys. Colloid Chem., 1951. **55**: p. 894.
39. Marcus, R.A., Journal of Chemical Physics, 1952. **20**: p. 359.
40. Rosenstock, H.M., et al., Proceedings of the National Academy of Sciences, 1952. **38**: p. 667.
41. Wigner, E., Journal of Chemical Physics, 1937. **5**: p. 720.
42. Klots, C.E., *Thermal Kinetics in Small Systems*. Journal of Chemical Physics, 1989. **90**(8): p. 4470.
43. Norrman, K. and McMahon, T.B., *Relation between effective temperature of thermalized ions and ion source temperature*. International Journal of Mass Spectrometry, 1998. **176**: p. 87.
44. Baer, T., *The Dissociation Dynamics of Energy-selected Ions*, in *Advances in Chemical Physics*. 1986. p. 111.
45. McQuarrie, D.A. and Simon, J.D., *Molecular Thermodynamics*. 1999, Sausalito, CA: University Science Books.
46. Bene, J.E.D., et al., *Ab Initio Computation of the Enthalpies of Some Gas-Phase Hydration Reactions*. Journal of Physical Chemistry, 1983. **87**: p. 3279.

47. Gaskell, S., et al., *Sequential mass spectrometry applied to the study of the formation of "internal" fragment ions of protonated peptides.* International Journal of Mass Spectrometry and Ion Processes, 1991. **111**: p. 173.
48. Lifshitz, C., *Kinetic shifts.* European Journal of Mass Spectrometry, 2002. **8**(2): p. 85.
49. Laskin, J. and Futrell, J.H., *Activation of large ions in FT-ICR mass spectrometry.* Mass Spectrometry Reviews, 2005. **24**(2): p. 135.
50. Evan, R.W., et al., *Surface-Induced Dissociation of Peptide Ions in Fourier-Transform Mass Spectrometry.* Journal of the American Society for Mass Spectrometry, 1990. **1**(5): p. 413.
51. Vékey, K., *Multiply charged ions.* Mass Spectrometry Reviews, 1995. **14**(3): p. 195.
52. Shukla, A.K. and Futrell, J.H., *Collisional activation and dissociation of polyatomic ions.* Mass Spectrometry Reviews, 1993. **12**: p. 211.
53. Oppenheim, I., et al., *Stochastic Processes in Chemical Physic: The Master Equation.* 1977, Cambridge: M.I.T. Press.
54. Jockusch, R.A., et al., *Energetics from Slow Infrared Multiphoton Dissociation of Biomolecules.* Journal of Physical Chemistry A, 2000. **104**(14): p. 3188.
55. Drahos, L. and Vékey, K., *MassKinetics: a theoretical model of mass spectra incorporating physical processes, reaction kinetics and mathematical descriptions.* Journal of Mass Spectrometry, 2001. **36**(3): p. 237.
56. Laskin, J. and Futrell, J.H., *On the efficiency of energy transfer in collisional activation of small peptides.* Journal of Chemical Physics, 2002. **116**(10): p. 4302.
57. Muntean, F. and Armentrout, P.B., *Guided ion beam study of collision-induced dissociation dynamics: integral and differential cross sections.* Journal of Chemical Physics, 2001. **115**: p. 1213.
58. Meroueh, O. and Hase, W.L., *Energy transfer pathways in the collisional activation of peptides.* International Journal of Mass Spectrometry, 2000. **201**(1-3): p. 233.
59. Oref, I. and Tardy, D.C., *Energy Transfer in Highly Excited Large Poliatomic Molecules.* Chemical Reviews, 1990. **90**: p. 1407.
60. Bernshtein, V. and Oref, I., *Energy transfer between polyatomic molecules. 1. Gateway modes, energy transfer quantities and energy transfer probability density functions in benzene-benzene and Ar-benzene collisions.* Journal of Physical Chemistry B, 2005. **109**(17): p. 8310.
61. Meroueh, O. and Hase, W.L., *Collisional activation of small peptides.* Journal of Physical Chemistry A, 1999. **103**(20): p. 3981.
62. Heeren, R.M.A. and Vékey, K., *Novel Method to Determine Collisional Energy Transfer Efficiency by Fourier Transform Ion Cyclotron Resonance Mass Spectrometry.* Rapid Communications in Mass Spectrometry, 1998. **12**: p. 1175.

63. Drahos, L., *Belsőenergia szerepe a tömegspektrometriában*, in *MTA, KKKI*. 1999, ELTE: Budapest, Hungary. p. 1.
64. Cooks, R.G., et al., *Metastable Ions*. 1973, Amsterdam: Elsevier.
65. Vékey, K., et al., *Internal Energy Distribution of Benzene Molecular Ions in Surface-induced Dissociation*. Journal of Mass Spectrometry, 1995. **30**: p. 212.
66. Vékey, K., et al., *Electron-Capture Induced Decomposition of the Benzene C6h6(2+)Ion*. Journal of Physical Chemistry, 1986. **90**(16): p. 3569.
67. Collette, C., et al., *Comparison of the Internal Energy Distributions of ions Produced by Different Electrospray Sources*. Rapid Communications in Mass Spectrometry, 1998. **12**: p. 1673.
68. Derwa, F., et al., *New Basis for a Method for the Estimation of Secondary Ion Internal Energy Distribution in "Soft" Inonization Techniques*. Organic Mass Spectrometry, 1991. **26**: p. 117.
69. Williams, D.H. and Naylor, S., *The Internal Energy Distribution in Fast Atom Bombardment/Liquid Secondary Ion Mass Spectra*. Journal of the Chemical Society, Chemical Communication, 1987. **???**: p. 1408.
70. Collette, C. and De Pauw, E., *Calibration of the internal energy distribution of ions produced by electrospray*. Rapid Communications in Mass Spectrometry, 1998. **12**(4): p. 165.
71. Collette, C., et al., *Comparison of the internal energy distributions of ions produced by different electrospray sources*. Rapid Communications in Mass Spectrometry, 1998. **12**(22): p. 1673.
72. Baer, T., et al., *Threshold photoelectron photoion coincidence studies of parallel and sequential dissociation reactions*. Physical Chemistry Chemical Physics, 2005. **7**: p. 1507
73. Sztaray, J., et al., *Leucine enkephalin - a mass spectrometry standard*. Mass Spectrometry Reviews, 2009.
74. Meot-Near (Mautner), M., et al., *Thermal decomposition kinetics of protonated peptides and peptide dimers, and comparison with surface-induced dissociation*. Rapid Communications in Mass Spectrometry, 1995. **9**(9): p. 829.
75. Asano, K.G., et al., *Thermal dissociation in the quaprupole ion trap: ions derived from leucine enkephalin*. International Journal of Mass Spectrometry, 1999. **185/186/187**: p. 207.
76. Vékey, K., et al., *Average activation energies of low energy fragmentation processes of protonated peptides determined by a new approach*. Rapid Commun. Mass Spectrom., 1996. **10**: p. 911.
77. Schnier, P.D., et al., *Dissociation energetics and mechanisms of leucine enkephalin (M+H)(+) and (2M+X)(+) ions (X=H, Li, Na, K, and Rb) measured by blackbody infrared radiative dissociation*. Journal of the American Society for Mass Spectrometry, 1997. **8**(8): p. 771.
78. Gabelica, V., et al., *Calibration of Ion Effective Temperatures Achieved by Resonant Activation in a Quadrupole Ion Trap*. Analytical Chemistry, 2003. **75**(19): p. 5152.

79. Paech, K., et al., *Slow Infrared Laser Dissociation of Molecules in the Rapid Energy Exchange Limit.* Journal of Physical Chemistry A, 2002. **106**(42): p. 9761.
80. Meotner, M., et al., *Thermal-Decomposition Kinetics of Protonated Peptides and Peptide Dimers, and Comparison with Surface-Induced Dissociation.* Rapid Communications in Mass Spectrometry, 1995. **9**(9): p. 829.
81. Cooks, R.G. and Wong, P.S.H., Accounts of Chemical Research, 1998. **31**: p. 379.
82. Cooks, R.G., et al., *Thermochemical determinations by the kinetic method.* Mass Spectrometry Reviews, 1994. **13**(4): p. 287.
83. Cooks, R.G. and Kruger, T.L., *Intrinsic Basicity Determination Using Metastable Ions.* Journal of the American Chemical Society, 1977. **99**: p. 1279.
84. Jasinkim, J.M. and Braumann, J.I., Journal of the American Chemical Society, 1980. **102**: p. 2906.
85. Derrick, P.J. and Donchi, K.F., in *Comrehensive Chemical Kinetics*, C.H. Bamford and Tipper, C.F.H., Editors. 1983, Elsevier. p. 53.
86. Derrick, P.J., Mass Spectrometry Reviews, 1982. **2**: p. 285.
87. Haas, M.J. and Harrison, A.G., *The fragmentation of proton-bound cluster ions and the gas-phase acidities of alcohols.* International Journal of Mass Spectrometry and Ion Processes, 1993. **124**: p. 115.
88. Norrman, K. and McMahon, T.B., *Isotope Effects in dissociation reactions of proton bound amine dimers in the gas phase.* International Journal of Mass Spectrometry, 1999. **182/183**: p. 381.
89. Gozzo, F.C. and Eberlin, M.N., *Primary and Secondary Isotope effects in proton (H+/D+) and chloronium ion (35Cl+/37Cl+) affinities.* Journal of Mass Spectrometry, 2001. **36**: p. 1140.
90. Schroder, D., et al., *Equilibrium isotope effects in cationic transition-metal(I) ethene complexes M(C2X4)(+) with M = Cu, Ag, Au and X = H, D.* Organometallics, 2000. **19**(13): p. 2608.
91. O'Hair, R.A.J., et al., Organic Mass Spectrometry, 1994. **29**: p. 151.
92. Dang, T.T., et al., International Journal of Mass Spectrometry and Ion Processes, 1993. **123**: p. 171.
93. Nourse, B.D. and Cooks, R.G., International Journal of Mass Spectrometry and Ion Processes, 1991. **106**: p. 249.
94. Laskin, J. and Lifshitz, C., *Kinetic Energy Release Distributions in Mass Spectrometry.* Journal of Mass Spectrometry, 2001. **36**: p. 459.
95. Klots, C.E., et al., *Role of Angular-Momentum in Unimolecular Kinetics - Kinetic- Energy Release in Fragmentation of C4h6+.* Journal of Chemical Physics, 1977. **66**(11): p. 5100.

96. Lifshitz, C. and Louage, F., *Theoretical Interpretation for magic nembers in kinetic energy releases.* International Journal of Mass Spectrometry and Ion Processes, 1990. **101**: p. 101.
97. Hache, J.J., et al., *Relative proton affinities from kinetic energy release distributions for dissociation of proton-bound dimers.* Journal of Physical Chemistry A, 2002. **106**(50): p. 12051.
98. Szilágyi, Z. and Vékey, K., *A simple algorithm for the calculation of kinetic energy release distributions.* European Mass Spectrometry, 1995. **1**: p. 507.
99. Rodgers, M.T., et al., *Statistical Modeling of Collision-Induced Dissociation Thresholds.* Journal of Chemical Physics, 1997. **106**: p. 4499.
100. Klots, C.E., Naturforsch., 1972. **27a**: p. 553.
101. Chesnavich, W.J. and Bowers, M.T., *Statistical Phase Space Theory of Polyatomic Systems - Application to Unimolecular Reactions C6h5cn.+- C6h4.++Hcn and C4h6.+- C3h3++.Ch3.* Journal of the American Chemical Society, 1977. **99**(6): p. 1705.
102. Chesnavich, W.J. and Bowers, M.T., *Statistical Phase Space Theory of Polyatomic Systems - Rigorous Energy and Angular-Momentum Conservation in Reactions Involving Symmetric Polyatomic Species.* Journal of Chemical Physics, 1977. **66**(6): p. 2306.
103. Laskin, J. and Futrell, J., *The Theoretical Basis of the Kinetic Method from the Point of View of Fitine Heat Bath Theory.* Journal of Physical Chemistry A, 2000. **104**(38): p. 8829.
104. Lorquet, J.C., *Unimolecular reaction dynamic from kinetic energy release distributions. VI. Energy-selected ions.* International Journal of Mass Spectrometry, 2000. **201**: p. 59.
105. Lorquet, J.C., *Landmarks in the theory of mass spectra.* International Journal of Mass Spectrometry, 2000. **200**(1-3): p. 43.
106. Holbrook, K.A., et al., *Unimolecular Reactions.* 1996: John Wiley & Sons.
107. Klots, C.E., *Kinetic Methods for Quantifying Magic.* Zeitschrift Fur Physik D-Atoms Molecules and Clusters, 1991. **21**(4): p. 335.
108. Drahos, L., et al., *Theoretical calculation of isotope effects, kinetic energy release and effective temperatures for alkylamines.* International Journal of Mass Spectrometry, 2003. **225**(3): p. 233.
109. Szulejko, J.E. and McMahon, T.B., International Journal of Mass Spectrometry and Ion Processes, 1991. **109**: p. 279.
110. Frisch, M.J., et al., *Gaussian 94, Revision B.1.* 1995, Gaussian, Inc: Pittsburgh PA.
111. Scott, A.P. and Radom, L., *Harmonic Vibrational Frequences: An Evaluation of Hartree-Fock, Moller-Plesset, Quadratic configuration Interaction, Denisty Functional Theory, and Semiempirical Scale Factors.* Journal of Physical Chemistry, 1996. **100**: p. 16502.

112. Rauhut, G. and Pulay, P., *Transferable Scaling Factors for Density Functional Derived Vibrational Force Fields.* 99, 1995. **99**: p. 3093.

113. Holmes, J.L., et al., *Proton Affinities of Primary Alkanols: An Appraisal of the Kinetic Method.* Journal of Physical Chemistry A, 1999. **103**: p. 705.

114. Thomas, P.D., et al., *Comments on "Proton Affinities of Primary Alkanols: An Appraisal of the Kinetic Method".* Journal of Physical Chemistry A, 2000. **104**: p. 1359.

115. Drahos, L. and Vékey, K., *How Closely Related are the Effective and the Real Temperature.* Journal of Mass Spectrometry, 1999. **34**: p. 79.

116. Naban-Maillet, J., et al., *Internal energy distribution in electrospray ionization.* Journal of Mass Spectrometry, 2005. **40**(1): p. 1.

117. Frisch, M.J., et al., *Gaussian 98 (Revision A).* 1998, Gaussian Inc.: Pittsburgh PA.

118. Gomory, A., et al., *Kinetic energy release of protonated methanol clusters using the low-temperature fast-atom bombardment: experiment and theory combined.* European Journal of Mass Spectrometry, 2004. **10**(2): p. 213.

119. Kosevich, M.V., et al., *Temperature Dependences of Ion Currents of Alcohol Clusters Under Low-temperature Secondary Ion Mass Spectrometric Conditions.* Journal of Mass Spectrometry, 1998. **33**: p. 843.

120. Boryak, O.A., et al., *On some peculiarities of the low temperature fast atom bombardment mass spectra of ethanol.* International Journal of Mass Spectrometry and Ion Processes, 1997. **163**(3): p. 177.

121. Fridgen, T.D. and McMahon, T.B., *Binding Energies of Prototn -Bound Ether/Alcohol Mixed Dimers Determined by FTICR Radiative Association Kinetics Measurements.* Journal of Physical Chemistry A, 2002. **106**: p. 1576.

122. El-Shall, M.S., et al., *Reactions and Thermochemistry of Protonated Methanol Clustes Produced by Electron Impact Ionization.* Journal of Physical Chemistry, 1992. **96**: p. 2045.

123. Vékey, K., *Internal Energy Effects in Mass Spectrometry.* Journal of Mass Spectrometry, 1996. **31**: p. 445.

124. Yalcin, T., et al., *Why are B ions stable species in peptide spectra?* Journal of the American Society for Mass Spectrometry, 1995. **6**(12): p. 1165.

125. Yalcin, T., et al., *The structure and fragmentation of B-n (n>=3) ions in peptide spectra.* Journal of the American Society for Mass Spectrometry, 1996. **7**(3): p. 233.

126. Polfer, N.C., et al., *On the Dynamics of Fragment Isomerization in Collision-Induced Dissociation of Peptides.* Journal of Physical Chemistry A, 2008. **112**(6): p. 1286.

127. Peltz, C., et al., *SORI Excitation: Collisional and Radiative Processes.* Journal of the American Society for Mass Spectrometry, 2007. **18**: p. 2119.

128. Holmes, J.L. and Terlouw, J.K., *The Scope of Metastable Peak Observations.* Organic Mass Spectrometry, 1980. **15**: p. 383.

129. Laskin, J. and Lifshitz, C., *Principles of mass spectrometry applied to biomolecules*. 2006: John Wiley & Sons, Inc.

130. Philibert, J., *Some Thoughts and/or Questions about Activation Energy and Pre-Exponential Factor.* Defect and Diffusion Forum, 2006. **249**: p. 61.

131. Oba, M., et al., *Determination of activation energy and pre-exponential factor for individual compounds on release from kerogen by a laboratory heating experiment.* Geochemical Journal, 2002. **36**(1): p. 51.

132. Asano, K.G., et al., *Thermal dissociation in the quadrupole ion trap: ions derived from leucine enkephalin.* International Journal of Mass Spectrometry, 1999. **185/186/187**: p. 207.

133. Meot-Ner (Mautner), M., et al., *Thermal decomposition kinetics of protonated peptides and peptide dimers, and comparison with surface-induced dissociation.* Rapid Communications in Mass Spectrometry, 1995. **9**(9): p. 829.

134. Vékey, K., et al., *Average Activation Energies of Low-energy Fragmentation Processes of Protonated Peptides Determined by a New Approach.* Rapid Communications in Mass Spectrometry, 1996. **10**(8): p. 911.

135. Drahos, L. and Vékey, K., *Determination of the thermal energy and its distribution in peptides.* Journal of the American Society for Mass Spectrometry, 1999. **10**(4): p. 323.

136. Ervin, K.M. and Armentrout, P.B., *Systematic and random errors in ion affinities and activation entropies from the extended kinetic method.* Journal of Mass Spectrometry, 2004. **39**(9): p. 1004.

7. Publications

7. 1. Publications Related to the Ph.D. Thesis

1. **J. Sztáray**, A. Memboeuf, L. Drahos, K. Vékey; Leucine Enkephalin – a mass spectrometry standard. Mass Spectrometry Reviews, 2009 accepted on 10/31/2009.
2. J. Naban-Maillet, D. Lesage, A. Bossee, Y. Gimbert, **J. Sztáray**, K. Vékey and J.C. Tabet; Internal energy distribution in electrospray ionization. Journal of Mass Spectrometry, 2005, 40(1), 1-8.
3. Á. Gömöry, P. Végh, **J. Sztáray**, L. Drahos and K. Vékey; Kinetic energy release of protonated methanol clusters using low-temperature fat-atom bombardment: experiment and theory combined. European Journal of Mass Spectrometry, 2004, 10 (2), 213-220.
4. L. Drahos, **J. Sztáray**, K. Vékey; Theoretical calculation of isotope effects, kinetic energy release and effective temperatures for alkylamines. International Journal of Mass Spectrometry, 2003, 225(3), 233-248.

7. 2. Publications Not Related to the Ph.D. Thesis

1. A.A. Tolun, H. Zhang, D. Il'yasova, **J. Sztáray**, S.P. Young, D.S. Millington; Allantoin in Human Urine Quantified by UPLC-MS/MS. Analytical Biochemistry, submitted on 10/26/2009.
2. H. Zhang, D. Il'yasova, **J. Sztáray**, S.P. Young, F. Wang, D.S. Millington; Quantification of the Oxidative Damage Biomarker 2,3-Dinor-8-Isoprostaglandin-F2α in Human Urine Using Liquid Chromatography-Tandem Mass Spectrometry. Analytical Biochemistry, submitted on 10/12/2009.
3. F. Pollreisz, Á. Gömöry**, J. Sztáray**, P. Végh, L. Drahos, A. Kiss, K. Vékey; Very high critical energy fragmentation observed in CID. International Journal of Mass Spectrometry, 243(1), 2005, 41-47
4. W.K. Lewis, B.E. Applegate, **J. Sztáray**, B. Sztáray, T. Baer, R.J. Bemish, R.E. Miller; Electron impact ionization in helium nanodroplets: Controlling fragmentation by active cooling of molecular ions. Journal of the American Chemical Society, 126 (36), 2004, 11283-11292

5. I. Bagyi, B. Balogh, A. Czajlik, O. Elias, Z. Gaspari, V. Gergely, I. Hudaky, P. Hudaky, A. Kalaszi, L. Karolyhazy, K. Keseru, R. Kiss, G. Krajsovszky, B. Lang, T. Nagy, A. Racz, A. Szentesi, T. Tabi, P. Tapolcsanyi, **J. Vaik**, J.C.P. Koo, G.A. Chass, O. Farkas, A. Perczel, P. Matyus; Generation and analysis of the conformational potential energy surfaces of N-acetyl-N-methyl-L-alanine-N'-methylamide. An exploratory ab initio study. Journal of Molecular Structure – Theochem 625(1), 2003, 121-136

8. Abstract

Mass spectrometry is one of the most important analytical methods when it comes to fundamental as well as bioanalytical or proteomics research. In order to automate the interpretation of mass spectra, we need to understand what happens inside the mass spectrometer, such as the ionization and fragmentation processes. This can only be accomplished by a joint effort of careful experiments and accurate modeling.

In my graduate research, there were three main goals to achieve: (1) Gain a better understanding of the fundamental properties of dissociating ions and the influence of these on what is happening to the ions during the processes in the mass spectrometer. This will then allow accurate calculations of the basic features of the mass spectrum, such as ion intensities, and – in the case of metastable decays – peak widths. (2) Model interesting features, such as kinetic energy release and the kinetic isotope effect of a few chosen systems to get a better handle on these processes. (3) Working on these fundamental problems and models systems, test and further develop the MassKinetics program.

The studied systems can be categorized into four groups: a) The dissociation of protonated alkylamines was modeled and the internal energy distributions were determined in two different experimental conditions. The results helped to understand what effects the experimental conditions have on the results, and to study the theoretical aspects of kinetic energy release and the kinetic isotope effect. b) Protonated benzlypyridines and protonated aromatic benzoic esters are often used to determine the energy profile of a mass spectrometer. Therefore, these systems were studied to characterize their dissociation processes, and of the dependence of the internal energy distribution on the instrumental parameters. c) Kinetic energy release data from low-temperature measurements of protonated methanol clusters were modeled, and the translational energy distribution was shown to be three dimensional. d) Finally, several recent publications on the most commonly used protonated oligopeptide, leucine enkephalin were re-analyzed to address the discrepancies of the published dissociation parameters of the most studied fragmentation pathway, leading to the $\mathbf{b_4}^+$ ion. The reasons behind the deviations were determined, and a consistent set of Arrhenius dissociation parameters were found with an acceptable confidence interval.

Overall, my results show that with the knowledge of a few basic parameters and the experimental setup, the fate of the ions can be modeled and accurate ion intensities as well as other features of their dissociation can be predicted. These results bring the possibility of the automatic evaluation of any mass spectra into the near future.

9. Összefoglaló

A tömegspektrometria az analítika és a szerkezetkutatás egyik legfontosabb módszere, mind az alap-, mind pedig az alkalmazott bioanalitikai és proteomikai kutatásokban. A mért tömegspektrumok automatikus kiértékeléséhez szükség van a tömegspektrométerben lejátszódó folyamatok – például az ionizáció és fragmentáció – alapos és kvantitatív megértésére. Ezt a kísérleti és a modellezési eredmények együttes felhasználásával lehet csak elérni.

Doktori munkámnak három kitűzött célja volt: (1) A disszociáló ionok legfontosabb tulajdonságainak vizsgálata, valamint ezeknek a tömegspektrométerben letjátszódó folyamatokra való hatásának feltérképezése. Ez teszi lehetővé a tömegspektrum legfontosabb paramétereinek, mint pélául az ion intenzitásoknak vagy – metastabilis bomlások esetén – a csúcsalakoknak a pontos elméleti meghatározását. (2) Néhány kiválasztott rendszer (protonált dimerek és oldószer-klaszterek) unimolekuláris disszociációja során észlelhető érdekességek, mint például a kinetikusenergia-felszabadulás (KER) illetve a kinetikus izotópeffektus (KIE) modellezése. (3) Ezen vizsgálatok közben a MassKinetics program tesztelése és továbbfejlesztése.

Az általam vizsgált rendszerek négy csoportba oszthatók: a) Modelleztem a protonált alkil-aminok disszociációját, és meghatároztam a belsőenergia-eloszlást két különböző kísérleti adatsorra. Ezek az eredmények segítettek megérteni, hogy a kísérleti körülményeknek milyen hatása van az eredményekre. Tanulmányoztam továbbá a kinetikusenergia-felszabadulás valamint a kinetikus izotópeffektus elméleti vonatkozásait is. b) A protonált benzil-piridineket és a protonált aromás benzol-észtereket gyakran használják a tömegspektrométerek energiaprofiljának meghatározására. Tanulmányoztam ezen rendszerek disszociációját, valamint a kísérleti paramétereknek az ionok belsőenergia-eloszlására tett hatását. c) Modelleztem protonált metanol-klaszterek alacsony hőmérsékletű kísérletekből meghatározott kinetikusenergia-felszabadulását annak érdekében, hogy meghatározzuk a transzlációs szabadsági fok dimenzionalitását. d) Végezetül a tömegspektrometriában leggyakrabban használt oligopeptid, a leucin-enkefalin legtöbbet vizsgált fragmentációs folyamatát, a $\mathbf{b_4}^+$ ion képződését vizsgáltam részletesen. Az irodalomban számos publikáció közölt disszociációs paramétereket erre a bomlásra, azonban ezek az adatok egymással nem mutattak jó egyezést. Munkám során feldolgoztam az irodalomban közölt adatokat, modellezés segítségével megértettem az eltérések okait, majd ennek eredményeképpen meghatároztam az új, elfogadható hibahatárral rendelkező Arrhenius-féle disszociációs paramétereket.

Összefoglalva, kutatásaim megmutatták, hogy néhány alapvető elméleti és kísérleti paraméter ismeretében az ionok sorsa modellezhető, és pontos ion intenzitások, és más tömegspektometriai adatok pontosan megjósolhatóak. Ezen eredmények segítségül szolgálnak majd a tömegspektrumok jövőbeni automatikus kiértékeléséhez.